THE UNIVERSITY OF MICHIGAN

COLLEGE OF ENGINEERING
Department of Chemical and Metallurgical Engineering

Progress Report

EFFECT OF ULTRASONIC WAVES ON BIOLOGICAL MASS TRANSPORT

H. Scott Fogler

ORA Project 01319

supported by:

U. S. PUBLIC HEALTH SERVICE
DEPARTMENT OF HEALTH, EDUCATION, AND WELFARE
NATIONAL INSTITUTES OF HEALTH
GRANT NO. HE-10549-02
BETHESDA, MARYLAND 20014

administered through:

OFFICE OF RESEARCH ADMINISTRATION ANN ARBOR

September 1970

Enoch
UMR
1501

TABLE OF CONTENTS

SECTION I

Summary

by

H. S. Fogler

SUMMARY PAGE

Grant Number: HE 10549-02 Effect of Ultrasonic Waves on Biological Mass Transport

Principal Investigator: Hugh Scott Fogler

Sponsoring Institution: Department of Chemical and Metallurgical Engineering
University of Michigan, Ann Arbor, Michigan 48104

Period Covered: Sept. 1, 1967 - June 31, 1970

Date of Report: Sept. 1, 1970

Summary

The following reports describe the preliminary results of the effect of ultrasonic waves on mass transfer. The mass transfer studies conducted under NIH Grant No. HE 10549 were in two areas: (1) gas absorption and (2) membrane transport.

The studies on gas absorption were divided into two areas: large scale bulk streaming and our recent findings on high speed streaming in thin films. In bulk streaming experiments, increases in the gas absorption rate of up to 800% were observed in the ultrasonic runs over the runs in which no ultrasonics were applied. However, one of the most interesting and potentially useful things we found in our study was that of the small scale streaming. This streaming was extremely rapid and was induced in thin films which were fractions of a centimeter in height. The fluid velocities in this film were far greater than any previously reported streaming velocities which were either experimentally observed or theoretically predicted. These intense streaming currents will bring about an even greater increase in the mass transfer rate than was observed in the bulk streaming experiment mentioned above.

In the membrane transport area, both theoretical and experimental investigations were also undertaken to determine the effect of ultrasonic waves on mass transfer.

In the theoretical analysis by Fogler and Lund, first results show that significant increases in the rate of mass transport through membrane ducts

should be found with the application of ultrasonics. Experimental studies do indeed reveal that ultrasonic waves do increase the rate of transport through membranes. Steady flow experiments utilizing Amicon PM-30 and XM-100 membranes showed increases in mass transfer rates of 300% and 400% respectively, when ultrasonic waves were applied to the system.

In our studies in ultrafiltration type membrane transport, we have observed increases of up to 1700% in the rate of transport across the membrane with the application of ultrasonics. In all cases, standardization runs were made after ultrasonic waves have been applied to the membrane in order to check for a breakage or degradation of the membrane. We found no evidence of any change in membrane properties. Consequently, we are assured that these extremely large increases in transport rates result solely from the ultrasonic wave motion and not from changes in the membrane properties.

With the application of ultrasonics to biological systems, one must take care that the wave conditions are properly adjusted so as not to induce any harmful side effects to the tissue and body fluids by acoustic cavitation. Since it is known that various biological fluids behave as viscoelastic liquids, a brief and preliminary investigation was undertaken on cavitation in viscoelastic fluids to determine whether the degrading effects of cavitation could be accelerated or retarded in this fluid type. Preliminary results show that the elasticity can significantly retard the collapse process and certain situations produce damped oscillatory motion of the cavity rather than the usual damaging catastrophic collapse observed in purely viscous liquids. This suggests that under proper control, the damaging effects of cavitation could be minimized in biological fluids, and possibly bring about an additional enhancement in the transport rates as a result of the stirring produced by the oscillatory bubble motion.

There was no cavitation present in either the membrane or gas absorption experiments reported above, as the systems in which we observed increases in mass transport were operated below the cavitation threshold.

SECTION II

Ultrasonic Gas Absorption

This section represents a portion of the work by Mr. M. L. Cadwell and Prof. H. S. Fogler relating to the enhancement of gas absorption in liquids. Following this report is a copy of the paper which has been accepted for publication in the Chemical Engineering Progress Symposium Series. This work was presented at the 67th National A.I.Ch.E. meeting in May.

ULTRASONIC GAS ABSORPTION

M. L. Cadwell and H. S. Fogler
Division of Chemical Engineering
University of Michigan
Ann Arbor, Michigan 48104

I. Introduction

The intent of this research was to study the influence of ultrasonics on the absorption of a gas contacted directly with a liquid. It was originally anticipated that ultrasonically induced "acoustic streaming" or "microstreaming" currents would be the primary mechanisms enhancing the mass transport process.

A brief derivation and review of the equations governing acoustic streaming is presented in the first part of this phase of this report, and solutions to the streaming equations are presented for a few simple geometries.

Initial results on the enhancement of gas-liquid mass transport are presented for streaming occurring in a cylindrical tube in which a high frequency (800 kHZ) ultrasonic transducer was aimed perpendicular to the liquid surface, thereby inducing gross circular streaming patterns within the liquid.

The final phase of this investigation involved visual observations of acoustically induced convection in various geometrical configurations at frequencies of 800, 175, and 20 kHZ. Emphasis in this study was on how the convective patterns established might enhance absorption rates at the gas liquid interface. It is believed that the results of these observations fall into two distinct categories. At high frequency (800 kHZ) bulk acoustic streaming occurred which was similar to that observed

by Ghabrial and Richardson (1954) and described mathematically by Piercy and Lamb (1954), Nyborg (1964), and Eckart (1949). At low frequency (20 kHZ), when the liquid depth between the transducer and gas-liquid interface was much smaller than the sonic wavelength, high intensity vortex patterns were observed. These patterns apparently can not be explained in terms of simplified acoustic streaming theory, since the velocities observed were an order of magnitude greater than that predicted from purely elementary considerations.

The Equations Governing Acoustic Streaming

The following is an abbreviated development of the equations describing ultrasonic streaming in a fluid. Starting with the 3 basic equations of fluid mechanics

Equation of Continuity

$$\frac{\partial \rho}{\partial t} + \nabla(\rho \underset{\sim}{U}) = 0 \tag{1}$$

Equation of Motion

$$\rho\left[\frac{\rho \underset{\sim}{U}}{\partial t} + (\underset{\sim}{U}\cdot\nabla)\underset{\sim}{U}\right] = -\nabla\rho + \left(\frac{4}{3}\mu + K\right)\nabla(\nabla \underset{\sim}{U}) - \mu\nabla\times\nabla\times\underset{\sim}{U} \tag{2}$$

Equation of State

$$\nabla\rho = C^2\nabla\rho + R\nabla\frac{\partial \rho}{\partial t} \tag{3}$$

Markham (1952) has shown that the inclusion of the term

$R\frac{\partial \rho}{\partial t}$ in the above equation can adequately account for heat transfer effects in many situations.

It is assumed that the fluid is being perturbed ultrasonically with an angular frequency $\omega = 2\pi f$, and that there is no movement of the fluid by any other external forces. As usual, we assume that the velocity, pressure and density can be represented by

$$\underset{\sim}{U} = \underset{\sim}{U}_0 + \underset{\sim}{U}_1 + \underset{\sim}{U}_2 + \cdots \tag{4}$$

$$P = P_0 + P_1 + P_2 + \cdots \tag{5}$$

$$\rho = \rho_0 + \rho_1 + \rho_2 + \cdots \tag{6}$$

where $\underset{\sim}{U}_i = \sigma(\varepsilon)\ \underset{\sim}{U}_{i-1}$, $P_i = \sigma(\varepsilon)\ P_{i-1}$ and $\rho_i = \sigma(\varepsilon)\ \rho_{i-1}$. Substituting the above expressions into equations (1), (2), and (3) and collecting terms of like orders of magnitude, noting that $\underset{\sim}{U}_0 = 0$ since there are no applied external forces other than ultrasonic perturbations, one arrives at the zero, first, and second order perturbation equations:

Zero Order

$$\underset{\sim}{U}_0 = 0 \tag{7}$$

$$\nabla P_0 = 0 \tag{8}$$

$$\nabla \rho_0 = 0 \tag{9}$$

First Order

$$\frac{\partial \rho_1}{\partial t} + \rho_0 (\nabla \underset{\sim}{U}_1) = 0 \tag{10}$$

$$\rho_0 \frac{\partial \underset{\sim}{U}_1}{\partial t} = -\nabla P_1 + \left(\frac{4}{3}\mu + K\right) \nabla (\nabla \cdot \underset{\sim}{U}_1) - \mu \nabla \times \nabla \times \underset{\sim}{U}_1 \tag{11}$$

$$\nabla P_1 = C^2 \nabla \rho_1 + R \frac{\partial \rho_1}{\partial t} \tag{12}$$

Second Order

$$\frac{\partial \rho_2}{\partial t} + \nabla \cdot \rho_1 \underset{\sim}{U}_1 + \rho_0 \nabla \cdot \underset{\sim}{U}_2 = 0 \tag{13}$$

$$\rho_0 \left[\frac{\partial \underset{\sim}{U}_2}{\partial t} + (\underset{\sim}{U}_1 \cdot \nabla) \underset{\sim}{U}_1\right] + \rho_1 \frac{\partial \underset{\sim}{U}_1}{\partial t} = -\nabla P_2 + \left(\frac{4}{3}\mu + K\right) \nabla (\nabla \cdot \underset{\sim}{U}_2)$$

$$- \mu \nabla \times \nabla \times \underset{\sim}{U}_2 \tag{14}$$

$$\nabla P_2 = C^2 \nabla \rho_2 + R \nabla \frac{\partial \rho_2}{\partial t} \tag{15}$$

Both pressure and density may be eliminated from equation (11) to yield

$$\rho_0 \frac{\partial^2 \underset{\sim}{U}_1}{\partial t^2} = \rho_0 C^2 \nabla (\nabla \cdot \underset{\sim}{U}_1) + \left(\frac{4}{3}\mu + K + R\rho_0\right) \nabla \left(\nabla \cdot \frac{\partial \underset{\sim}{U}_1}{\partial t}\right) - \mu \nabla \times \nabla \times \underset{\sim}{U}_1 \tag{16}$$

Multiplying equation (10) by $\underset{\sim}{U}_1$, and adding it to equation (14):

$$\rho_0 \frac{\partial \underset{\sim}{U}_2}{\partial t} + \rho_0 \{\underline{(\underset{\sim}{U}_1 \cdot \nabla) \underset{\sim}{U}_1 + \underset{\sim}{U}_1 (\nabla \cdot \underset{\sim}{U}_1)}\} + \underline{\frac{\partial}{\partial t} (\rho_1 \underset{\sim}{U}_1)} \tag{17}$$

$$= - \nabla P_2 + \left(\frac{4}{3}\mu+K\right)\nabla(\nabla\cdot\underset{\sim}{U}_2) - \mu\nabla\times\nabla\times\underset{\sim}{U}_2$$

Equations (16) and (17) in more simplified form provide the basis for ultrasonic acoustic streaming. Since $\underset{\sim}{U}_1$ represents the velocity due to sonic perturbations, it is sinusoidal with respect to time; it can therefore be represented by:

$$\underset{\sim}{U}_1 = \underset{\sim}{U}_1(r)e^{j\omega t} \tag{18}$$

where $\underset{\sim}{U}_1(r)$ is a velocity vector dependent only on spacial position. Because equations 10, 11, 12, which relate ρ_1 and P_1 to $\underset{\sim}{U}_1$ are linear, it is seen that ρ_1 and P_1 also vary sinusoidally with time. Substitution of equation (18) into (16), and dividing by $\omega^2\rho_0/2$

$$\left[\frac{2C^2}{\omega^2} + \frac{2j}{\omega\rho_0}\left(\frac{4}{3}\mu+K+\rho_0 R\right)\right]\nabla(\nabla\cdot\underset{\sim}{U}_1) + 2\underset{\sim}{U}_1 = \frac{2j\mu}{\rho_0\omega}\nabla\times\nabla\times\underset{\sim}{U}_1 \tag{19}$$

The following parameters frequently appear in the literature on ultrasonics: $k = \omega/C$, defined as the wave number; $\alpha = \frac{\mu\omega^2}{\rho_0 C}\left|\frac{4}{3} + \frac{K}{\mu} + \frac{R\rho_0}{\mu}\right|$, defined as the attenuation coefficient; and $\beta = \sqrt{\omega\rho_0/2\mu}$, recognized as the reciprocal of the acoustic boundary layer thickness. Substitution of these terms into equation (20)

$$\left[\frac{2}{k^2} + \frac{j}{\beta^2}\left(\frac{4}{3} + \frac{K}{\mu} + \frac{R\rho_0}{\mu}\right)\right]\nabla(\nabla\cdot\underset{\sim}{U}_1) + 2\underset{\sim}{U}_1 = \frac{j}{\beta^2}\nabla\times\nabla\times\underset{\sim}{U}_1$$

Because, under most conditions $\alpha << k << \beta$:

$$\frac{2}{k^2} + \frac{j}{\beta^2}\left[\frac{4}{3} + \frac{K}{\mu} + \frac{R\rho_0}{\mu}\right] \simeq \frac{2}{(k-j\alpha)^2}$$

Therefore, equation (21) takes the form

$$\frac{2}{(k-j\alpha)^2}\nabla(\nabla\cdot\underset{\sim}{U}_1) + 2\underset{\sim}{U}_1 = \frac{j}{\beta^2}\nabla\times\nabla\times\underset{\sim}{U}_1 \qquad (21)$$

The above solution can be divided into two terms, (Eckart, 1948)

$U_1 = U_{1C} + U_{1R}$ such that

$$\nabla\times\underset{\sim}{U}_{1r} = 0 \quad \text{and} \quad \nabla^2\underset{\sim}{U}_{1r} = -(k-j\alpha)^2 U_{1r} \qquad (21a)$$

$$\nabla\cdot\underset{\sim}{U}_{1C} = 0 \quad \text{and} \quad \nabla^2\underset{\sim}{U}_{1C} = 2j\beta^2 U_{1C} \qquad (21b)$$

Procedures suggested for solving equation (21) or equations similar to them have been reviewed extensively (Nyborg, 1964, Rayleigh, 1945, Schlicting, 1960, and Eckart, 1948).

Once $\underset{\sim}{U}_1$ is obtained, ρ_1 and P_1 can be obtained from equations (7) and (8); one can then proceed to solve Equation (19) for $\underset{\sim}{U}_2$. In practice, this is a formidable task, for the underlined terms in equation (17) are nonlinear. A simplified approach to the solution of equation (19) is to time average each individual term over a few sonic cycles. The nonlinear nature of the term $(\underset{\sim}{U}_1\cdot\nabla)\underset{\sim}{U}_1 + \underset{\sim}{U}_1(\nabla\cdot\underset{\sim}{U}_1)$ suggest that a solution to $\underset{\sim}{U}_2$ is of the form

$$\underset{\sim}{U}_2 = \underset{\sim}{U}_2(r)\ e^{2j\omega t} + \overline{\underset{\sim}{U}}_2(\underset{\sim}{r}) \tag{22}$$

where $\underset{\sim}{U}_2(\underset{\sim}{r})$ and $\overline{\underset{\sim}{U}}_2(r)$ are dependent only on spacial position. Substituting the above expression into Equation (19) and performing the necessary time averaging (indicated by an overbar)

$$\rho_0\{\overline{(\underset{\sim}{U}_1\cdot\nabla)\underset{\sim}{U}_1 + \underset{\sim}{U}_1(\nabla\cdot\underset{\sim}{U}_1)}\} + \overline{\frac{\partial}{\partial t}(\rho_1\underset{\sim}{U}_1)}$$

$$= \overline{\nabla P}_2 + \left(\frac{4}{3} + K\right)\nabla(\nabla\cdot\overline{\underset{\sim}{U}}_2) - \mu\nabla\times\nabla\times\overline{\underset{\sim}{U}}_2 \tag{22}$$

From the solutions to the first order equations, it can be shown that

$$\overline{\frac{\partial}{\partial t}(\rho_1\underset{\sim}{U}_1)} = 0$$

and it has been shown that $\nabla(\nabla\cdot\overline{\underset{\sim}{U}}_2) = (\nabla^2\overline{\underset{\sim}{U}}_2)\ O\left(\frac{2\mu\omega}{\rho_0 C}\right)$ (Rayleigh, 1945); thus, for most systems:

$$\nabla(\nabla\cdot\overline{\underset{\sim}{U}}_2) <<< \nabla^2\overline{\underset{\sim}{U}}_2$$

Therefore equation (22) becomes

$$\rho_0\{\overline{(\underset{\sim}{U}_1\cdot\nabla)\underset{\sim}{U}_1 + \underset{\sim}{U}_1(\nabla\cdot\underset{\sim}{U}_1)}\} = -\overline{\nabla P}_2 + \mu\nabla^2\overline{\underset{\sim}{U}}_2 \tag{23}$$

This equation is known as the basic streaming equation. Several examples from the literature will be reviewed here to

illustrate the types of solutions which can result upon application of equations (23) and (21).

In the first example, an ultrasonic beam of radius R_b is propagated along the axis of a very long circular cylinder whose length is L and radius R. The solution to equation (21) is assumed to be irrotational. Thus,

$$\nabla^2 U_1 = -(k-j\alpha)^2 U_1$$

If the length of the cylinder is sufficiently long, $\alpha L >> 1$, and the first order solution is:

$$U_1 = Ae^{-2\alpha x}\cos(\omega t - kx) \qquad r < R_b$$

$$U_1 = 0 \qquad R_b < r < R_0$$

The discontinuity in first order velocity profile arises from the assumption that $\underset{\sim}{U}_1$ is irrotational. The streaming equation becomes, for radial symmetry:

$$\mu\left[\frac{\partial^2 \bar{U}_2}{\partial r^2} + \frac{1}{r}\frac{\partial \bar{U}_2}{\partial r}\right] = -\frac{\partial P}{\partial Z} + \frac{\rho_0 \alpha A^2}{2} \qquad r < R_b$$

$$\mu\left[\frac{\partial^2 \bar{U}_2}{\partial r^2} + \frac{1}{r}\frac{\partial \bar{U}_2}{\partial r}\right] = -\frac{\partial P}{\partial Z} + \qquad R_b < r < R_0$$

The boundary conditions are that

$$\bar{U}_2 = 0 \qquad \text{at } r = R_0$$

$$\frac{\partial \bar{U}_2}{\partial r} = 0 \qquad \text{at } r = 0$$

and if the ends are capped so that there is no net bulk flow across any cylindrical cross section,

$$\int_0^{R_0} \bar{U}_2 \, r dr = 0$$

The solution is:

$$\bar{U}_2 = \frac{\alpha \rho_0 A^2 R_b^{\,2}}{2\mu} \left\{ - \ell n \frac{R_b}{R_0} + \tfrac{1}{2}\left[1-\left(\frac{r}{R_b}\right)^2\right] - \left[1-\left(\frac{r}{R_0}\right)^2\right]\left[1-\tfrac{1}{2}\left(\frac{R_b}{R_0}\right)^2\right] \right\}$$

$$\text{for } r < R_b$$

and

$$\bar{U}_2 = \frac{\rho_0 \alpha A^2 R_b^{\,2}}{\mu} \left\{ - \ell n\left(\frac{r}{R_0}\right) - \left[1-\left(\frac{r}{R_0}\right)^2\right]\left[1-\tfrac{1}{2}\left(\frac{R_b}{R_0}\right)^2\right] \right\}$$

$$\text{for } R_b < r < R_0$$

This solution was derived by Piercy and Lamb (1954), and represents a slight variation from that originally derived by Eckart (1948). Nyborg (1964) presents an analogous solution for the case of propagation of a beam of sound with Z_b, between two parallel plates separated by a distance h. Defining Z = 0 at the edge of the lower plate, his solution is:

$$\bar{U}_2 = \frac{\rho_0 \alpha A^2}{2\mu} e^{-2\alpha x} \left[(h-Z_b)Z + \frac{Z(Z-h)}{2} \left[2-3\left(\frac{Z_b}{h}\right)^2 + \left(\frac{Z_b}{h}\right)^3 \right] \right]$$

$$\text{for } Z_b/2 < Z < h/2$$

These solutions are characterized by a bulk, non-circular (except at the ends, $x = 0$ and $x = \ell$) fluid motion. A somewhat different pattern results, however, if the first order solution along the plane mid-way between the plates is that of a standing wave,

$$U_1 = A \cos\omega t \cos kx$$

and if the sound beam propagates along the entire distance between the plates. Under these conditions, both a horizontal and vertical velocity exists:

$$U_2 = -\frac{U_0^2 \sin 2kx}{8\beta C} \left[e^{-\beta y} (4 \sin\beta y + 2 \cos\beta y + e^{-\beta y}) + \frac{3}{2} - \frac{9}{2} \left[1 - \left(\frac{y}{h}\right) \right]^2 \right]$$

$$V_2 = -\frac{2kU_0^2 \cos 2kx}{8\beta C} \left[e^{-\beta y} (\sin\beta y + 3\cos\beta y + \frac{e^{-\beta y}}{2}) + \frac{3}{2} \beta(h-y) - \frac{3}{2} \beta h \left[1 - \frac{y}{h} \right]^3 \right]$$

The fluid patterns are circular, and repeat themselves at integral ½-wavelengths. This solution was originally derived by Rayleigh.

List of Symbols Used in Equations Governing Acoustic Streaming

A	Amplitude of velocity wave
C	Speed of sound
K	Ditational viscosity
L	Length of cylinder
P	Pressure
P_0	Zero order pressure
P_1	First order pressure
P_2	Second order pressure
R	Radius of cylinder
R_b	Radius of transducer
$\underset{\sim}{U}$	Velocity vector
$\underset{\sim}{U}_0$	Zero order velocity vector
$\underset{\sim}{U}_1$	First order velocity
$\underset{\sim}{U}_1(\underset{\sim}{r})$	First order velocity, a function of position only
$\underset{\sim}{U}_{1c}$	Incompressible part of first order velocity
$\underset{\sim}{U}_{1k}$	Irrotational part of first order velocity
U_1	First order velocity in axial direction or parallel to plates
$\underset{\sim}{U}_2$	Second order velocity vector
$\underset{\sim}{U}_2(\underset{\sim}{r})$	Second order velocity vector which is a function of position only
$\overline{\underset{\sim}{U}}_2$	Streaming velocity vector, time-averaged value of U
$\overline{U}_2$	Streaming velocity along axis of cylinder
$\overline{V}_2$	Streaming velocity component perpendicular to flat plates
Z	Coordinate perpendicular to plate
Z_b	Thickness of sound beam propagating between flat plates

f	Frequency
h	Distance between flat plates
j	Complex number, $\sqrt{-1}$
k	Wave number
$\underset{\sim}{r}$	Position vector
r	Radial coordinate
x	Coordinate along axis of cylinder
t	Time
α	Attenuation coefficient
β	Reciprocal of acoustic boundary layer thickness
ϵ	Perturbation parameter
ρ	Density
ρ_0	Zero order density
ρ_1	First order frequency
ρ_2	Second order frequency
ω	Radial frequency

Experimental Gas Absorption Studies

Experimental Apparatus

The apparatus used to measure the amount of gas absorbed into the liquid in the absorption cell is shown in the accompanying diagram (Figure 1). Three vertical manometers, M4, M3, and M1, measure the pressure of tanks 1, 2, and the absorption cell itself, respectively. The pressure regulator and vacuum pump allow operation of the system over a pressure range from a few millimeters of mercury absolute to about 2 atmospheres. The slant manometer uses water as the working fluid and measures the difference in pressure between tanks 1 and 2. The gas used in these initial studies was CO_2, although in later studies it is anticipated that other gases will be used.

Tanks 1 and 2 can be isolated from each other by closing valves VS1 and V10; in addition, if valves V16 and V13 are open, tank 2 is connected directly to the absorption cell, and thus serves as a source of gas for the cell. The number of moles of gas absorbed during a run can then be calculated from the change in height of the slant manometer. Assuming, therefore, that (1) the pressure in tank 1, tank 2, and the absorption cell is initially the same, (2) the pressure in tank 1 is always uniform, (3) the pressure in tank 2 is also uniform, and equal to that in the absorption cell at any time, (4) the system operates isothermally, and (5) the density of the manometer fluid is much greater than that of the gas, the following equation gives a relationship between amount of gas absorbed, n_L, and change in height of the slant manometer in terms of system properties:

$$h = \frac{RT}{\sin\alpha\, P_o\, A_m} \; \frac{n_L}{\frac{1}{2}\left(\frac{V_1}{V_2} + 1\right) + \frac{\rho_m g V_1}{P_o A_m}\left(1 - \frac{A_m h}{2V_1}\right)\left(1 + \frac{A_m h}{2V_2}\right)} \qquad (1)$$

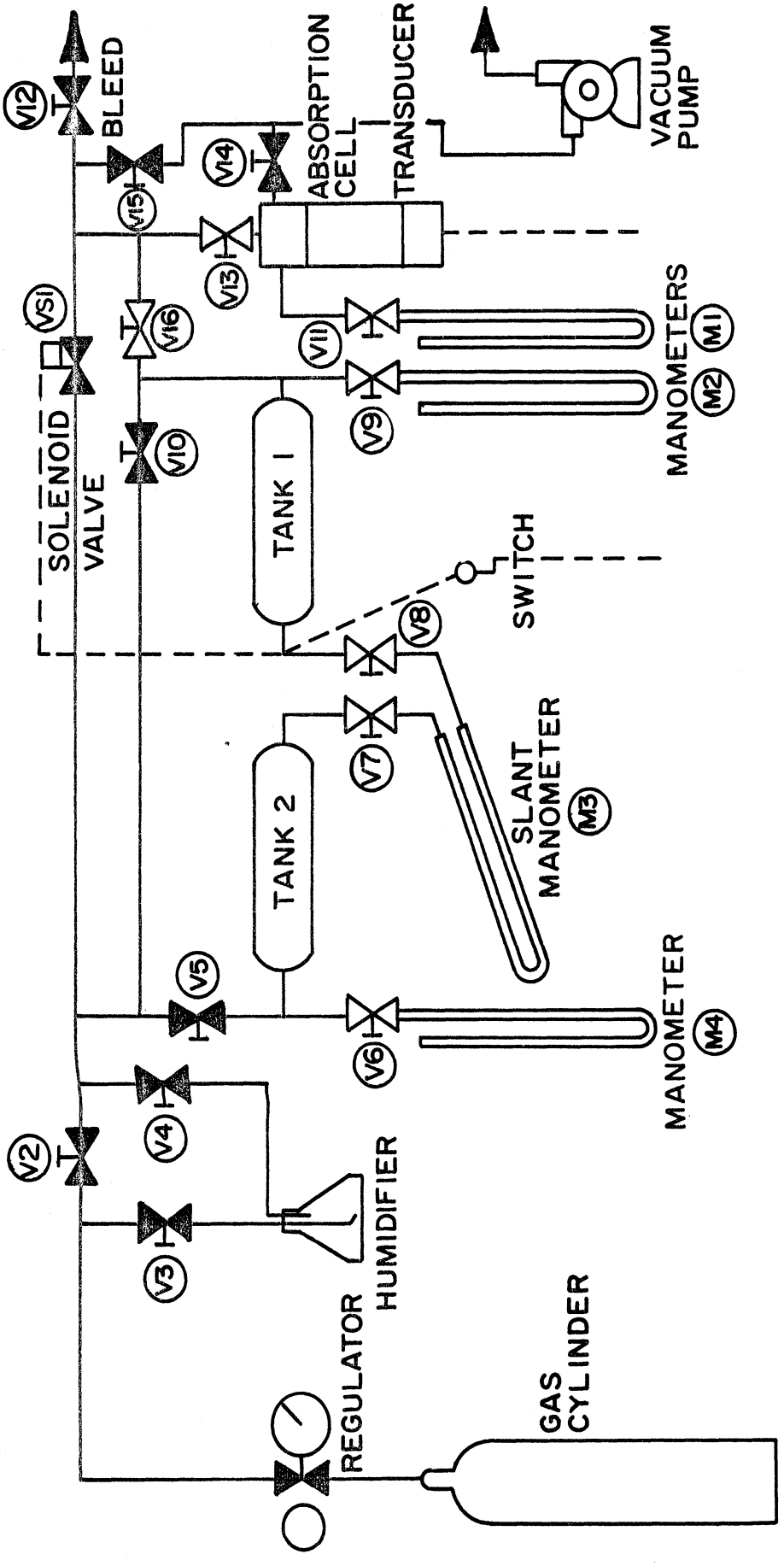

Figure 1. Gas absorption measuring system.

where:

n_L = amount of gas absorbed in cell
h = change in slant manometer height
P_o = initial system pressure
α = angle slant manometer makes with horizontal
A_m = slant manometer cross sectional area
V_1 = volume of tank 1
V_2 = volume of tank 2
ρ_m = density of manometer fluid
g = acceleration of gravity
R = gas constant
T = absolute temperature

For the system shown in the accompanying diagram (Figure 1), $V_1 = 600\ cm^3$, $V_2 = 8{,}200\ cm^3$, $A_m = 0.785 \times 10^{-2}\ cm^2$, $\rho = 1.0\ g/cm^3$, and $\sin\alpha = 0.1$. Because the manometer is designed so that h is always less than 100 cm, V_1/V_2, $A_m h/2V_1$, and $A_m h/2V_2$ are all less than unity. Substituting the above numerical values into Equation (1) and taking P_o = 2 atm. and $T = 298°K$, Equation (1) becomes approximately

$$h \simeq 3.79 \times 10^5\ n_L$$

It is seen that the system is quite sensitive to very small amounts of gas absorbed.

The absorption cell used in this study was cylindrical, 12" long and 1-7/8" inside diameter, and was constructed of 3/8" thick transparent plexiglass. The cell was designed so that a Macrosonics 800 kHz transducer could be bolted to the cell bottom. Thus, ultrasonic energy propagated upward along the axis of the absorption cell; however, the diameter of the radiating diaphragm of the transducer is 1.45", and therefore the ultrasonic beam did not fill the tube entirely. An O-ring seal was placed

between the transducer and bottom of the cell to prevent leaks. Three openings were placed near the top of the cell. One of these openings was connected to manometer M1 to measure the pressure in the cell, another to the gas absorption measuring apparatus, and the third to a line leading to the vacuum pump.

Ultrasonic power to drive the transducer was supplied by a Macrosonics 500-2 Ultrasonic Broad Band generator whose maximum output is 500 watts.

Procedure

At the start of a run, the absorption cell was filled with liquid to approximately the desired height and inserted into the system. (If the fluid was distilled water, it had been boiled for approximately 1 hour before insertion into the system to drive off any dissolved CO_2 vapor.) The cell was then evacuated for 1 hour to draw off any gases that might have dissolved in the fluid as a result of exposing the fluid to air during its transfer into the absorption cell. The height of the liquid above the transducer was then measured with a cathetometer. Once the cell was inserted into the system, gas was fed from the cylinder through the humidifier into tanks 1 and 2. Humidification of the gas was essential when using water as the absorption fluid to minimize evaporation effects. At this time valves V3, V4, V5, V6, V7, V8, V9, VS1, V16, and V10 were open, while valves V12, V13, V14, and V15 were closed. When the system reached desired operating pressure, valves V4 and V3 were closed, and the system was allowed to stand until pressure equilibrium was attained. While this was occurring, the ultrasonic generator was adjusted to give the desired output to the transducer. Measurements of the room temperature

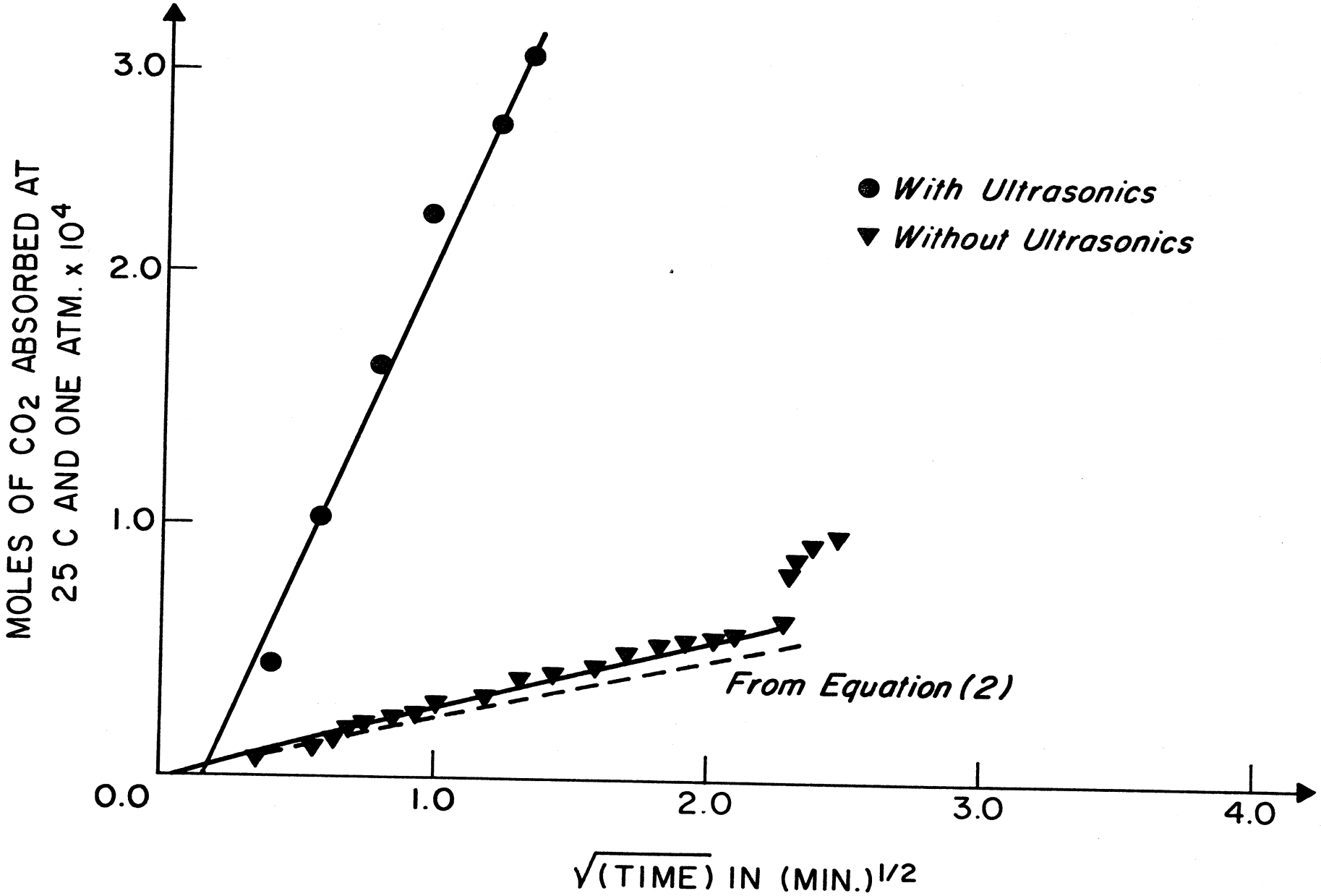

Figure 2. Representative comparison of CO_2 absorption in water with and without ultrasonics.

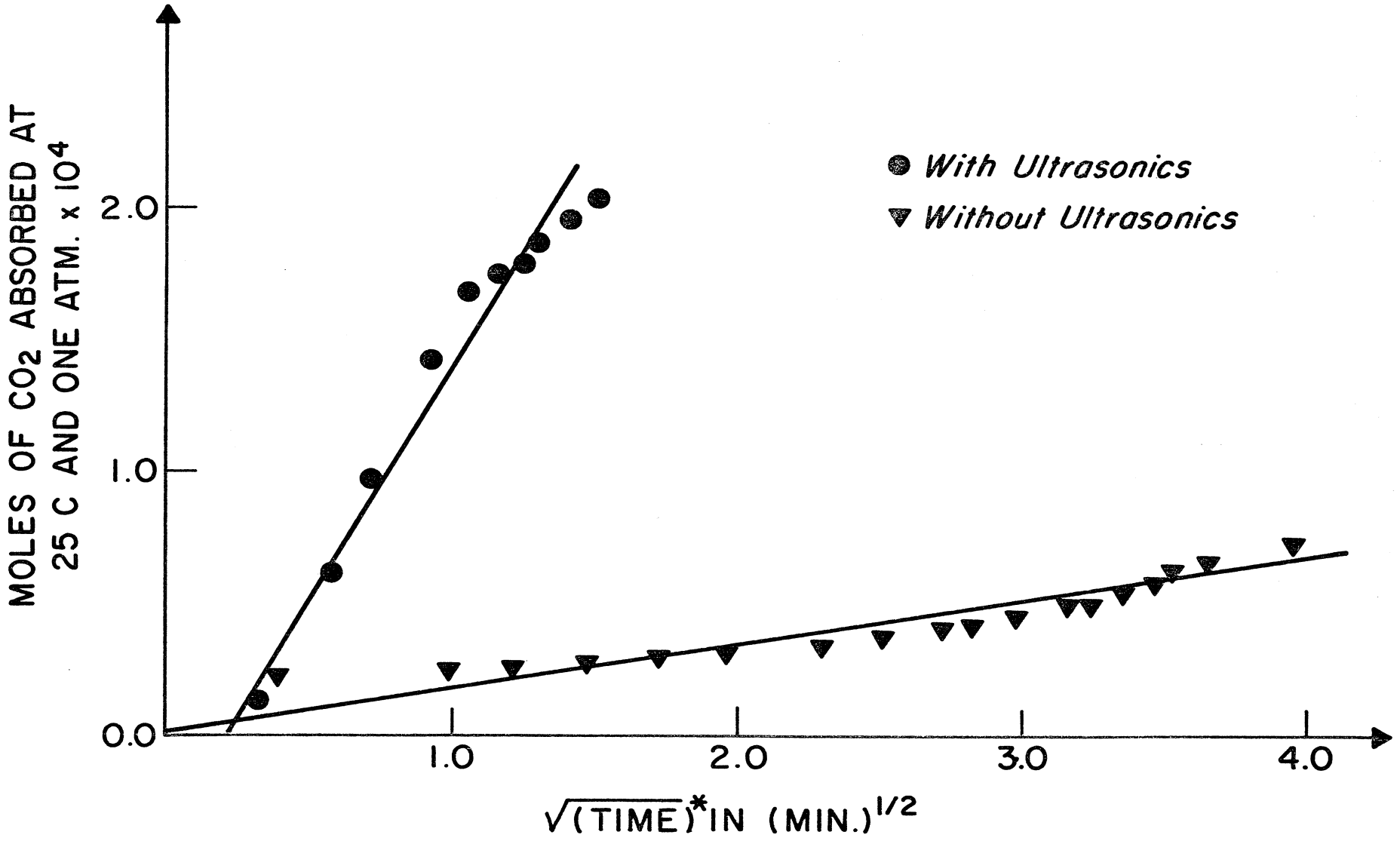

Figure 3. Comparison of CO_2 absorption in glycerol with and without ultrasonics.

and pressure differences in all manometers were taken when equilibrium was attained. The actual absorption run was initiated by opening valve V13 to allow gas to enter the absorption cell. When the pressure in the absorption cell was equal to that in tank 1, valves V10 and then VS1 were were closed, thereby isolating tank 2 from tank 1, which was connected to the absorption cell. The timerwas started when valve VS1 was closed. The change in slant manometer height was recorded as a function of time.

Measured values of h were corrected for system leaks by operating the system without the absorption cell and following the change in manometer height under conditions nearly identical to that in which the actual absorption run was performed.

Preliminary Results

Some results, which might be considered representative of the best data taken thus far, are shown in Figures (2) and (3). Most of the data taken with ultrasonics lie between the two curves depicted in these accompanying figures. Two systems were studied: CO_2 absorption into water and CO_2 absorption into glycerol. The number of moles of gas absorbed was calculated according to the procedure described above and then corrected to 25°C and 1 atmosphere pressure. All data obtained was compared to the amount of gas dissolved if only pure diffusion of gas into the liquid were occurring. The amount of gas absorbed for this latter case (i.e., no ultrasonics) is given by the equation

$$W_a = \frac{AP_a\rho_w}{HM_w}\sqrt{\frac{4D_{AB}t}{\pi}} \qquad (2)$$

where:

W_a = number of moles of gas absorbed at time t

t = time

A = absorption cell cross-sectional area

P_a = partial pressure of absorbing gas above the liquid

H = Henry's law constant

P = density of the liquid

M_w = molecular weight of the liquid

D_{AB} = diffusion coefficient of dissolved gas in the liquid

ρ_w = mass density of the fluid

Thus, results are plotted as the number of moles absorbed versus the square root of time. It must be pointed out that there is as yet no firm theoretical basis for plotting the data labeled "with ultrasonics" in this way. This method, however, does serve as a convenient basis for comparative purposes.

With reference to the data shown in Figure 2 for CO_2 absorption into water, the run labeled "without ultrasonics" was carried out at a pressure of 72.3 cm Hg (CO_2 partial pressure of 69.6 cm Hg) and temperature of 81°F with the cell filled with fluid to a depth of 22.4 cm above the transducer. The run labeled "with ultrasonics" was carried out at a pressure of 75.35 cm Hg (CO_2 partial pressure of 73.6 cm Hg) and temperature of 67°F with the cell filled with water to a height of 9.43 cm. The plate voltage and current of the ultrasonic generator during this run were 0.52 volts and 260 milliamps, respectively.

In the CO_2-glycerol runs shown in Figure 2. the run labeled "without ultrasonics" was carried out at 74.9 cm Hg pressure and 73°F temperature with a liquid height of 9.7 cm, while the run labeled "with ultrasonics" was carried out at 115 cm Hg and 75°F with a liquid height of 9.72 cm. The generator plate voltage and current in this run were .80 volts and 300 milliamps, respectively.

At this time, these results can only be regarded as preliminary. There are inherent experimental difficulties in the operation of any

unsteady state system; this is especially true for gas-liquid systems. As seen in both figures, extrapolation of data "with ultrasonics" to zero moles absorbed indicates that there is a response time lag which is either operational or inherent to the system. Efforts have been made to reduce this lag through slight modifications of the system and through improvements in operating procedure, but as yet no trend can be observed of how this time lag varies with system parameters (in particular, height of the liquid above the transducer and system operating pressure). Nevertheless, this time lag can be estimated by extrapolation of the curve of CO_2 absorption into water "without ultrasonics", and comparison of this curve with Equation (2) using values of diffusion coefficient and Henry's law constant from the literature. On this basis the time scale for this run was adjusted to the left. The dotted line in this figure is that predicted by Equation (2).

At the end of the curve for CO_2 absorption into water without ultrasonics, an abrupt increase in the number of moles of gas absorbed was seen to occur. This increase might be caused by natural convection which has been observed by other investigators in similar gas-liquid systems in which the density of the solution (solute + solvent) is greater than that of the liquid, causing an unstable density gradient to be established in the liquid. The occurrence of natural convection is governed by the Rayleigh number, which in inherently unsteady state systems is time dependent. The runs made in the latter portion of this study used glycerol as the absorbing fluid; because of its high viscosity, natural convection effects should therefore be less important than in the CO_2-water system.

Another difficulty encountered in operation of this system was due to the slant manometer, which is very responsive to only slight upsets

within the system. This manometer had to be refilled frequently or replaced. Although care was taken to fill this manometer with clean, distilled water, after continued use dirt did accumulate at certain points within the capillary tube of the manometer, resulting in erratic manometer response, or manometer fluid separation. Data taken under these conditions were very difficult to interpret.

However, a number of runs were carried out without the above difficulties. An estimate of the increase in the mass transfer rate can be made by comparing the slopes of the curves shown in Figure (1) and (2). On the basis of this comparison, it can be seen that the increase in mass transfer rate with the application of ultrasonics is on the order of 800% for both liquid systems. While no firm conclusions have yet been drawn as to what the cause of this enhancement is, these data were obtained without the effects of cavitation and atomization, and therefore the mechanism causing these increases is most likely convective streaming. It appears, therefore, that surface renewal concepts might be particularly appropriate for modeling this phenomena mathematically.

Preliminary Visual Studies of Streaming

Qualitative visual observations of acoustically induced convection were made at three frequencies, 20, 175, and 800 kHz in various geometrical configurations. Power to the transducers was furnished by a 500-1 Macrosonics Broadband Generator, capable of delivering a 500 w. input over the frequency range of 10 to 1000 kHz. Glycerol was used as the fluid; because of its low vapor pressure (.0025 mm Hg) and its high viscosity (1440 cp) at 25°C, cavitation effects should be small. The fluid movement was followed by the use of tracer particles of either

alumina or cigarette ashes. In some cases, the observed convection patterns were photographed with a motion picture camera.

High Frequency Studies. Two geometrical systems were used with 800 kHz insonation. In the first, a geometry identical to that used in the gas absorption studies was employed. A cylinder 9" long and 1-7/8" in diameter was filled to a depth of about 4-1/2" with glycerol. Insonation was accomplished by fastening an 800 kHz transducer to the bottom of the cylinder such that the vibrating diaphragm of the transducer was in direct contact with the fluid. The diameter of this diaphragm was 1.45", and therefore the sound beam did not fill the tube. When the liquid was insonated, intense streaming currents were observed throughout the liquid. These currents appeared to be circular, symmetrically located about the axis of the cylinder, and ordered - that is, tracer particles within the fluid appeared to move along well-defined paths, which they repeated after a certain period of time. The most intense streaming appeared along the axis of the cylinder; velocities here were estimated to be on the order of 10 cm/sec. The magnitude of these currents increased with an increase in the power supplied to the transducer. There was no evidence that cavitation was present during insonation in this experiment. A sketch of the observed streaming patterns appears below.

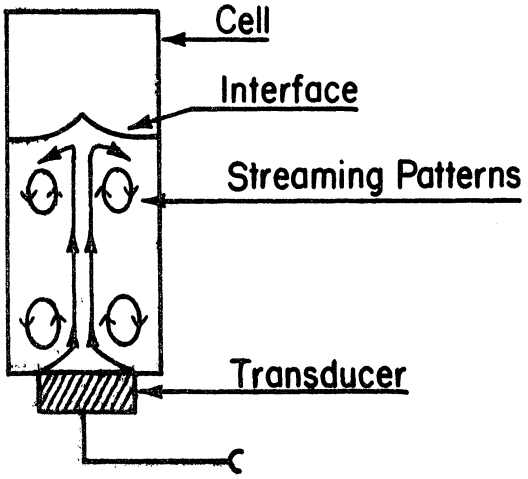

Figure 4. Approximate Fluid Patterns in 800 kHz Cell

In the second study at 800 kHz, a cylinder whose diameter was about 5-1/2" was filled to a depth of about 1" with glycerol. An 800 kHz transducer identical to that used in the study described above was fastened to the bottom of the cell about 2" from the axis of symmetry of the cylinder. Enough power was supplied to the fluid to produce streaming, but not enough to make the interface unstable. The induced fluid motion brought about by insonation was recorded on standard motion picture film at a speed of 18 fps. Streaming speeds near the transducer were estimated to be 2 cm/sec, about 5 times smaller than that observed in the first 800 kHz study. Fluid motion was most prominent near the transducer, and there were pockets of stagnation in areas away from the transducer. Again, no cavitation phenomena were observed. A sketch of the patterns observed appears below.

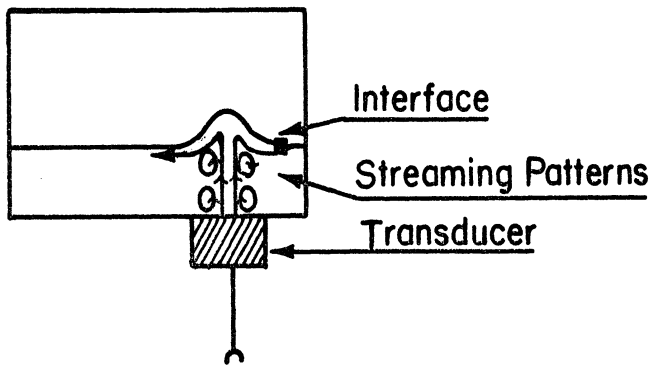

Figure 5. Streaming Patterns in a 5-1/2" Diameter Cell at 800 kHz

Intermediate Frequency Study. A 175 kHz transducer with a radiating diaphragm 59.5 mm in diameter was placed in a rectangular box 5" wide, 8" long, and 5" deep. The box was filled with glycerol until the top of the transducer housing was slightly over an inch below the face of the transducer. The transducer was placed approximately in the center of the box. The streaming patterns formed upon insonation are sketched below; particle speeds were greater than those in the last 800 kHz study, and were on the order of 5 cm/sec at a point about 1 cm below the gas liquid interface. This motion, however, was confined to that area directly above and slightly to the sides of the transducer. Streams of cavitation bubbles were emitted at points of rapid fluid motion; there was also evidence of the existence of resonating bubbles existing on the transducer surface which also might have contributed to the fluid motion.

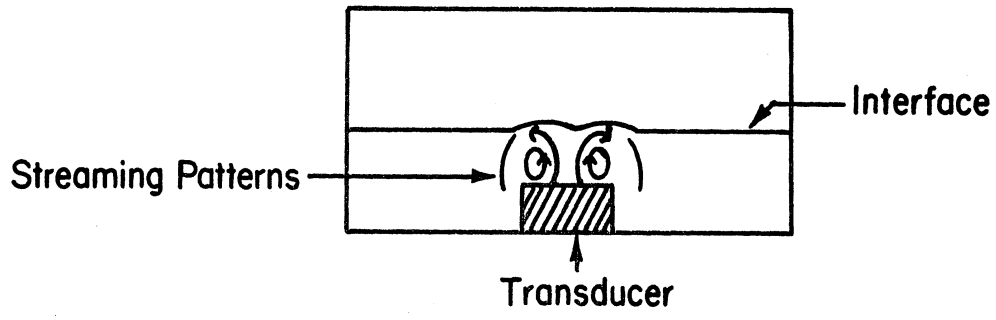

Figure 6. Streaming at 175 kHz in a Rectangular Box

Moving pictures of this motion did not come out as well as expected because of mechanical difficulties encountered in operating the camera, and because of very rapid particle dispersion upon insonation.

Low Frequency Study. Observations at 20 kHz were performed in three different geometries. In the first about 50 ml of glycerol were added to a 150 ml beaker, and the tip of a sonic gun transducer was immersed about 1/2 cm from the fluid air interface. Insonation was applied and the streaming pattern from the side appeared as if two vortex rings had formed between the bottom of the beaker and the tip of the transducer. Photographs were taken of the streaming patterns from the side, but because of extensive dispersion of the particles, an estimate of the streaming velocity could not be obtained.

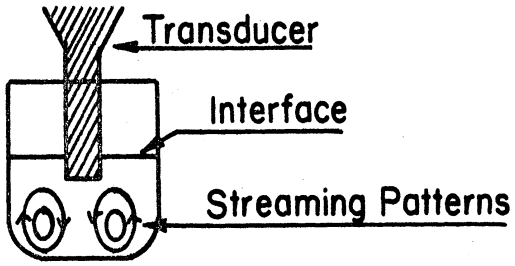

Figure 7. Streaming Patterns at 20 kHz in a Beaker

In the second low frequency experiment, the box used for the 175 kHz study was filled to a depth of 3/4" and insonated indirectly by placing the tip of the transducer gun perpendicular to the bottom of the stainless steel bottom of the box. Moving pictures of the ultrasonically induced fluid motion were taken from both the side and the top view of the box. A sketch of the streaming motion is shown in the following figure.

Surface velocities, measured by following tracer particles at a distance of about 1" from the axis defined by the center of the tip of

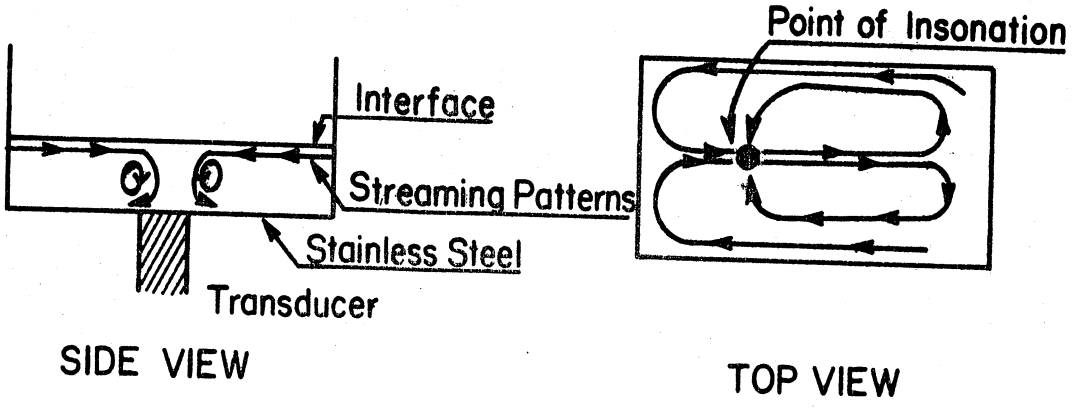

Figure 8. Streaming Patterns in a Box at 20 kHz

the transducer, were on the order of 3 to 6 cm/sec and increased rapidly as these particles approached the point of insonation. Also, small rapid vortices, on the order of 3/16" in diameter, existed around this point. There was, however, activity around the point of insonation indicating that cavitation was present.

In the last set of observations carried out at 20 kHz, a cylindrical tube,1 11/16"in diameter, fitted with a stainless steel bottom, was filled to a depth of 1-3/8" with glycerol and again insonated indirectly by placing the tip of the transducer on the stainless steel bottom. Streaming patterns were symmetrical about the point of insonation, as shown in the sketch below and in the photographs taken. The velocity along the axis of symmetry was estimated to be about 1.0 cm/sec, although this figure may be low due to the extensive amount of dispersion of tracer particles. The presence of cavitation could not be discerned from the photographs.

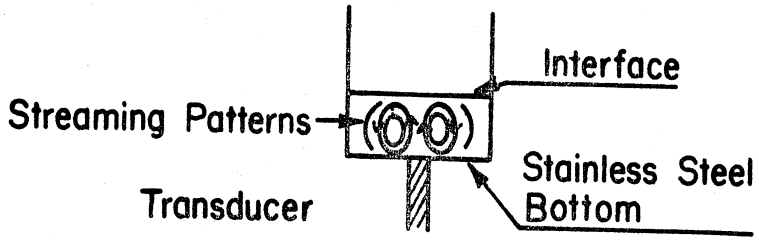

Figure 9. Streaming Patterns in a Cylinder at 20 kHz - Moderate Liquid Depth

The liquid height in the cell was then reduced to 1/2". Exceptionally rapid mixing was observed when the fluid was insonated and streaming was especially rapid a few millimeters from the point of insonation. A sketch of the streaming patterns appears below.

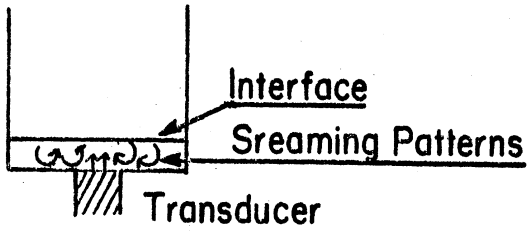

Figure 10. Rapid Streaming Patterns at 20 kHz in a Cylinder - Small Liquid Depth

An attempt was made to take moving pictures of the ensuing motion, but because of the difficulty of simultaneously operating the camera and turning on the sonic power, and as a result of very rapid particle dispersion, it was not possible to obtain a good film strip suitable for giving and estimate of the magnitude of the streaming velocity. The pictures that were taken, however, indicate the presence of cavitation.

When the transducer was moved off center and forced upon the stainless steel bottom of the cell, very rapid streaming velocities were encountered, in the pattern similar to Figure .

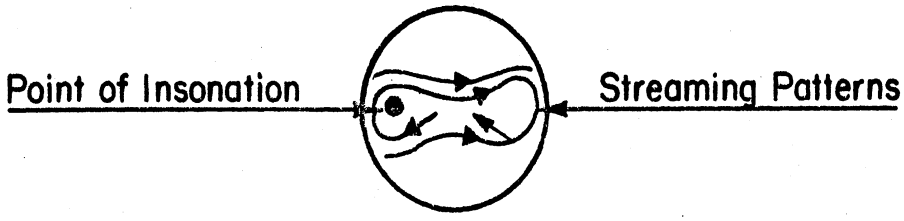

Figure 11. Top View of Rapid Streaming at 20 kHz in a Cylinder - Small Liquid Depth

This pattern may be due, however, to the "fountain" effect encountered in ultrasonics at high intensities, i.e., interfacial instabilities.

Discussion of Observed Patterns

These preliminary studies indicate that with the equipment available in the Sonochemical Laboratory, low frequency insonation induces larger convective velocities than high frequency insonation. This observation is especially true for the case of streaming occurring in liquids whose distance between the transducer and the gas-liquid interface is much less than the wavelength of sound. Because of the wavelength (λ) associated with 800 kHz insonation is only .19 cm. this observation is difficult if not impossible to verify for high frequencies. While the studies described here can at best be termed exploratory, some comparison and comment on the modes of induced convection normally attributed to ultrasonic insonation can be made.

Order of magnitude estimates of the streaming velocity can be made from elementary streaming theory reviewed previously. For a traveling wave, an order of magnitude estimate of streaming velocity is (Piercy and Lamb, 1954)

$$u_2 \simeq \frac{u_1^2 w^2}{2c^3} \left(\frac{4}{3} + \frac{K}{u} + \frac{R\rho_o}{u} \right) R_b^2$$

And for a standing wave, the maximum streaming speed should be (Rayleigh, 1945)

$$u_2 \simeq \frac{3u_1^2}{16c}$$

The first order velocity u_1 is equal to the product of particle displacement amplitude (S) and the frequency. If the value for s is taken as 10 microns at 20 kHz, and 0.12 microns at 400 kHz, and if it is assumed that $K/u \ll 1$ and $R\rho_0/u \ll 1$, for the system used in this study Piercy's

and Lamb's (1954) analysis gives a streaming speed of 0.6 cm/sec at 20 kHz, and 1085 cm/sec at 800 kHz; using Rayleigh's expression, u_2 is .002 cm/sec for both high and low frequency. These theoretical estimates are at least one to three orders of magnitude lower than that observed at low frequency, and, for the case of a traveling wave, two or three orders of magnitude higher. The experimental observations do not agree at all with the theoretical prediction for the traveling wave case that an increase in frequency results in an increase in streaming velocity.

Several investigators (Eckart, 1949, and Westervert, 1960) have advanced the explanation that at sufficiently high ultrasonic energy level inputs, a transition occurs from laminar to turbulent streaming. In turbulent streaming, particle velocities and vortex sizes far exceed that predicted by the classical equation governing acoustic streaming.

One study (Westervelt, 1960) in infinitely long cylinders subjected to oscillation perpendicular to the axis of the cylinder indicates that the transition from laminar to turbulent streaming occurs at a "streaming Reynolds number," s^2w/v, equal to unity, as long as the wave displacement amplitude (s), to cylinder radius, R, is sufficiently small. For the same system, others (Andres and Ingard, 1953) have shown theoretically that the classical solution offered by Schlichting (1932) applies for higher streaming Reynolds numbers.

An estimate of the streaming Reynolds number as defined by Westervelt can be made since it is independent of system geometry. Glycerol, the fluid used in this study, has a viscosity of 1440 cp and density of 1.2 g/cm^3 at 25°C. With a particle displacement amplitude of 20 microns at 20 kHz, the streaming Reynolds number is about .001; at 800 kHz, with

a particle displacement amplitude of 0.12 microns, the streaming Reynolds number is about 10^{-4}.

According to Westervelt, then, both low and high frequency regimes studies here should be described by the "classical" equations of acoustic streaming. While this appears to be the case for high frequency studies, it does not appear so for the low frequency cases. This analysis assumes that the particle displacement amplitude, s, is small compared with some (as yet undefined) length of the system. However, the cylinder radii, liquid heights, and wave lengths (7.5 cm at 20 kHz, .1875 cm at 800 kHz) are all greater than s, and hence his criteria appear to be satisfied.

These observations were performed at sonic power inputs of about 300 - 500 watts. Assuming that the energy efficiency is about 25%, the average sonic energy intensity with respect to the cross-sectional area is 16-26 watts/cm^2. Since the threshold cavitation intensity for castor oil, whose viscosity is about 630 cp at 25°C, or about 1/2 that of glycerol, is 5.3 watts/cm^2 at 20 kHz, it is conceivable that cavitation was present in the observations made at low frequency. This might be especially true near the point of insonation where the sonic intensity would be a maximum, possibly two or three times as great as the above estimated values. On the other hand, because the viscosity of glycerol is several times that of water, whose cavitation threshold is 250 watts/cm^2 at 800 kHz, no cavitation should be present in high frequency insonation. This is in substantial agreement with what was observed. What role cavitation plays in the observed convection process has not been ascertained at this time.

Although agreement with simplified theory is poor, it appears that

at high frequency a form of acoustic streaming similar to that observed by others predominates as the convective mechanism; however, the very high speeds and rapid vortices observed at low frequency, do not appear to be explainable right now in terms of elementary streaming theory.

Recent Discoveries on Rapid Streaming in Small Liquid Depths

As mentioned previously, intense streaming vortices were observed when the liquid level, h, was reduced such that $h/\lambda << 1$. These rapid streaming vortices cannot be explained in terms of previously derived streaming solutions which, in most cases, neglect the depth of the liquid above the transducer. In this regime, it appears that steep velocity gradients are induced because of the low liquid level. Because of the short distance between the transducer and the gas-liquid interface, these gradients induce exceptionally rapid streaming vortices which extend from the point of insonation up to the interface; thus, this type of streaming appears to be particularly applicable to gas-liquid mass transfer, especially when analyzed from a surface renewal viewpoint. To our knowledge, this type of streaming has not been uncovered before, either experimentally or theoretically. Since the efficiency of most mass transfer equipment, and especially apparatus like the artificial lung and kidney machines, is increased considerably as the surface area to volume ratio is decreased, the form of streaming described here will be studied in greater depth. Experimental work will be pursued to define and specify the conditions under which this unique streaming occurs. Photographic studies will be conducted to establish the optimum streaming pattern with respect to mass transfer. Our preliminary photographs indicate that the important parameters in this high-speed streaming are the ratio of liquid height/sonic

wavelength, type of fluid, ultrasonic intensity, point of insonation, and cavitation intensity. It is also believed that these patterns can be adequately explained mathematically if the appropriate approximations are made to the streaming equations.

Literature Citations

Andres, J. M., and Ingard, U., J. Acoust. Soc. Am., 25, 928, (1953).

Eckart, C., Phys. Rev., 73, 68, (1948).

Markham, J. J., Phys. Rev., 86, 497, (1952).

Nyborg, W. L., "Acoustic Streaming," Ch. 11 in Physical Acoustics, Vol. II-B, Muson, W. (ed), Academic Press, New York, N.Y., (1964).

Piercy, J. E., and Lamb, J., Proc. Roy. Soc., A226, 43, (1954).

Rayleigh, Lord., Theory of Sound, Vol. II, Dover Press, New York, N.Y., (1945).

Schlichting, H., Physic Z., 33, 327, (1932).

ULTRASONIC GAS ABSORPTION AND ACOUSTIC STREAMING OBSERVATIONS

M. L. Cadwell and H. S. Fogler
Division of Chemical Engineering
University of Michigan
Ann Arbor, Michigan 48104

INTRODUCTION

The transport of mass across an interface has been traditionally explained in some manifestation of the film, penetration, or surface renewal theory. In the film theory steady state mass transport is assumed to occur across a thin film of stagnant fluid which resides at the interface; in the penetration theory, unsteady state diffusion is assumed to occur in a region of fluid which is located at the interface, and whose depth is much greater than the depth of penetration of the solute species. The surface renewal theory, originally developed by Dankwerts (1951), is an extension of this latter theory. It also envisions that unsteady state mass transport of the absorbing species takes place in an element of fluid exposed to the interface. However, after residing at the interface for some time, the element of fluid is then swept back into the bulk of the liquid and replaced by another (solute-free) fluid element. These concepts have been combined, or modified and expanded through the inclusion of fluid-mechanical effects. One of these modifications is a "roll cell" model developed by Fortescue and Pearson (1967), who hypothesized that circular vortices exist at an interface and extend from the interface into the bulk of the liquid. Both diffusive and convective effects are included explicitly in their model. Thus, the magnitude of these eddies, and the size of the roll cells determine the rate of mass transport.

It has been observed in many instances that the application of sonic and ultrasonic waves can increase the rates of mass transfer over and above that which could be obtained by other means. Several of these studies

(Jameson, 1964, Arkangelskii and Statinkov, 1969, and Burdakov and Nuborykov, 1963), have attributed increases in mass transport rates observed at solid fluid boundaries to the effects of acoustic streaming. Indeed, the vorticular acoustic streaming patterns developed for simple geometries in mathematical analyses by Rayleigh (1883) and others and reviewed by Nyborg (1964) lend thought to the idea that the enhancement in rate processes might be achieved and/or explained in terms of some form of acoustic streaming surface renewal pattern.

In this paper, we are reporting some visual observations in which the essential roll cell structure described above is induced in a fluid by perturbing it ultrasonically. However, because of the intensity of the vortices, the observations here are not believed to be simple manifestations of elementary acoustic streaming theory as described and reviewed by Nyborg (1964), and indeed the estimated speed of the eddies induced in this study are an order of magnitude greater than any reported directly in the literature so far. It is expected that the type of convective patterns shown here are specifically applicable in those processes in which mechanical agitation of the fluid cannot be achieved or is undesirable.

In addition, preliminary results of an experimental study involving measurement of the amount of gas absorbed into a fluid which is being perturbed ultrasonically are presented.

EXPERIMENTAL SYSTEMS FOR VISUAL STUDIES

Acoustically induced convective patterns are shown in this paper for three different geometries. The first set of patterns were obtained in the

container labeled "A" shown in Figure 1. A 31.6 mm ID glass tube was inserted into the cell base, which was constructed of Plexiglas. This base was grooved to accept a rubber o-ring which thus served as a seal at the juncture of the glass tube and cell base. An 800 kHz Macrosonics type HFS-804 submersible transducer, whose radiating diaphragm diameter was also 31.6 mm, was fastened to the base of the cell; thus the sound wave was propagated through the liquid along the axis of the glass tube. The upper liquid surface in the first set of convective patterns was exposed to the atmosphere.

For the second set of patterns, the upper interface of the fluid was fixed by insertion of a metal rod into the 31.6 mm diameter glass tube. Insonation was again accomplished by fastening an 800 kHz transducer to the bottom of the container such that the radiating diaphragm of the transducer was in direct contact with the liquid. This system is labeled "B" in Figure 1.

The final set of convective patterns was obtained in the cylindrical container labeled "C" in Figure 1. This cell was 27.6 mm in diameter and filled with liquid to a depth of 0.6 to 0.8 cm. This tube was fitted with a .009 in. thick stainless steel plate bottom. Insonation was accomplished by physically forcing the tip of a Dukane Model 41A-10 transducer, whose resonant frequency is 20 kHz, to bottom of the tube as shown in Figure 1.

In the 800 kHz studies fluid motion was ascertained by observing the paths of polyvinylchloride spheres suspended in glycerol; this suspension was made by using 0.5 g of spheres with 1000 g of fluid. In the 20 kHz study,

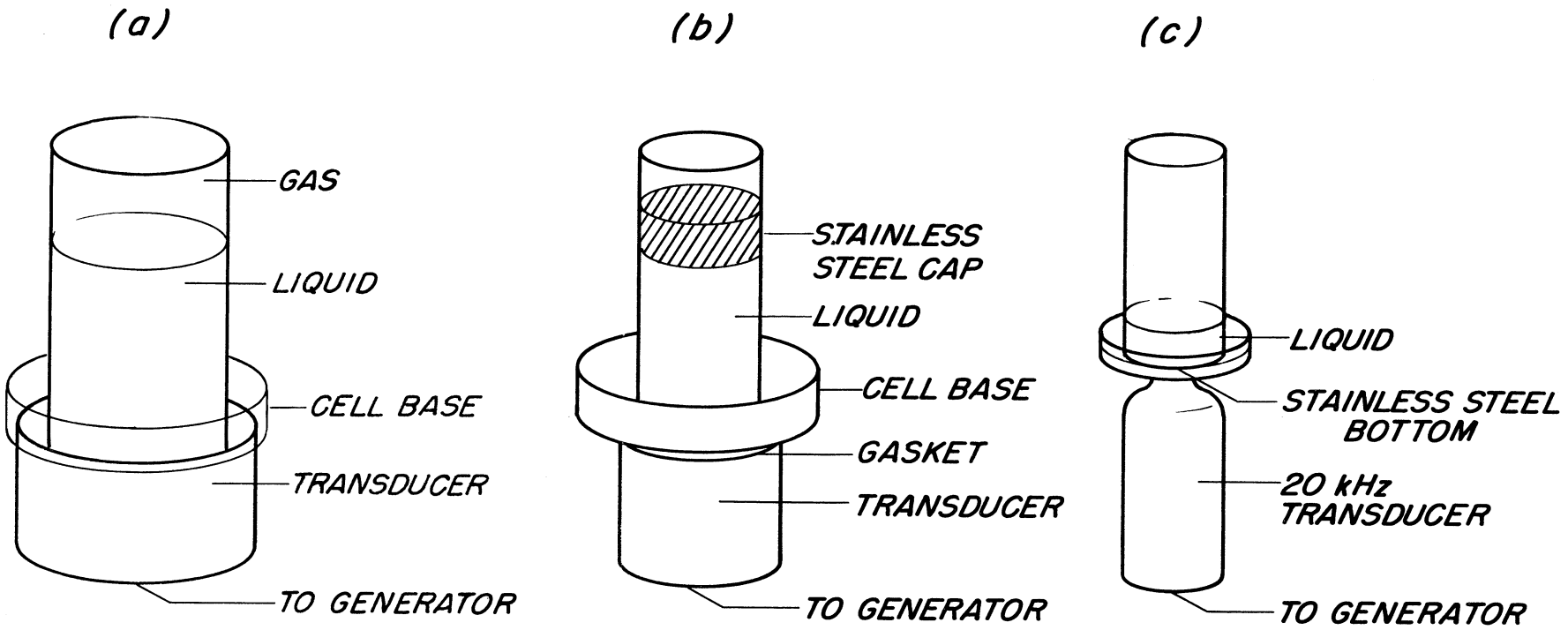

Figure 1. Streaming cells.

fluid motion was observed by followed Number 53 Venus G.C.P. extra brilliant aluminum particles which were suspended in the liquid at an approximate concentration of .05 to 0.2 g per 1000 g of fluid. Power to the transducers was furnished by a Macrosonics type 500-1 Multisons Broad Band Generator, or by a Macrosonics Type 180 VF Multisons High Frequency Generator.

PRELIMINARY RESULTS OF THE GAS ABSORPTION STUDY

Experiments were performed in which the amount of CO_2 absorbed into a fluid subjected to ultrasonic perturbations was measured as a function of time. These studies were carried out in a container identical to that labeled "A" in Figure 1 except that the top of the container was sealed and modified to fit into the apparatus shown in Figure 2. Glycerol was used as the absorbing fluid, and the frequency of insonation was 800 kHz.

The apparatus shown in Figure 2 served as a source of absorbing gas and was also used to measure the amount of gas absorbed by the liquid. The three vertical manometers, M4, M3, and M2 measure the pressure (relative to the atmosphere) of tank 1, tank 2, and the absorption cell, respectively. The slant manometer M4, which uses water as its working fluid, measures the difference in pressure between tanks 1 and 2.

Tanks 1 and 2 can be isolated from each other by closing valves VS1, and V10; in addition, if valves V16 and V13 are open, tank 2 is connected directly to the absorption cell and thus serves as a source of gas for the cell. The number of moles of gas absorbed during a run can then be calculated from the change in height of the slant manometer. For this system operating at a pressure of 2 atm and temperature of 25°C, this change in height is approximately

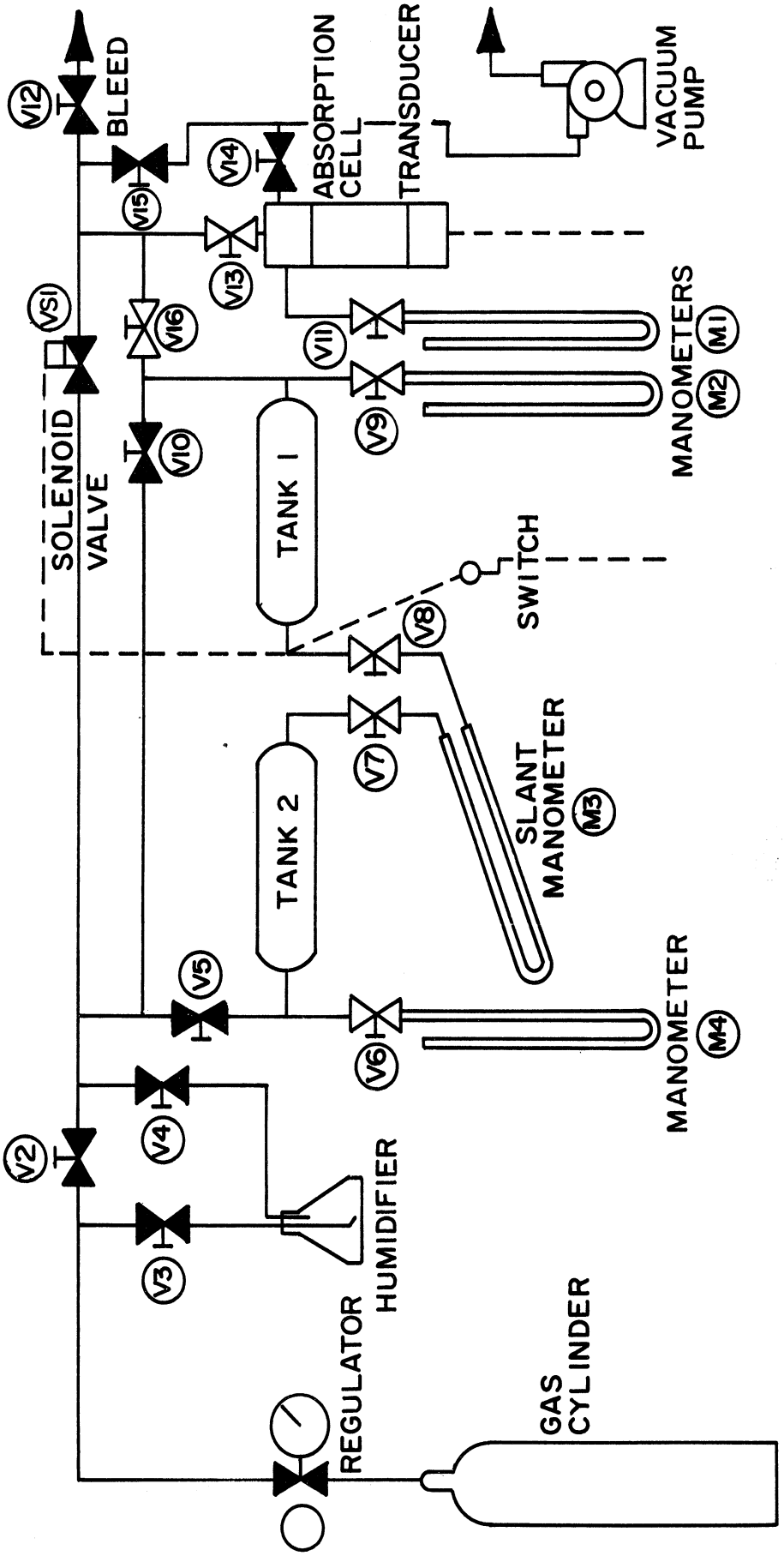

Figure 2. Gas absorption measuring system.

related to the number of moles of gas absorbed in the fluid by the following equation,

$$h = 3.79 \cdot 10^{3} n_L$$

Some results representative of the best data taken so far are shown in Figure 3 and compared to data taken in the absence of ultrasonic perturbations. In both cases the measured amount of gas absorbed was corrected to 25°C and 1 atm pressure. No theoretical interpretation is implied in the manner of plotting the data (i.e., in terms of the square root of time) labeled "with ultrasonics" as depicted in Figure 6. However, one expects that the amount of CO_2 absorbed into a quiescent liquid initially of uniform solute concentration should be proportional to the square root of time. An estimate of the increase in mass transfer rate brought on by ultrasonics can be made by comparing the slopes of the lines in this figure; on this basis, the increase in transport rate accompanying the use of ultrasonics is on the order of 800%.

800 kHz FREE SURFACE VISUAL OBSERVATIONS

In Figure 4, observations of acoustically induced convective patterns are shown in a liquid whose upper surface is exposed to a gas. The ratio of transducer diaphragm diameter to tube diameter in this figure is about 1.0. Although this ratio was 2/3 for the gas absorption run described previously, the convective patterns shown here are qualitatively similar to those induced in the gas absorption run. It has been observed experimentally that when the ratio of transducer diameter to tube diameter is decreased, the ensuing surface renewal patterns decrease in intensity, despite a slight increase in sonic

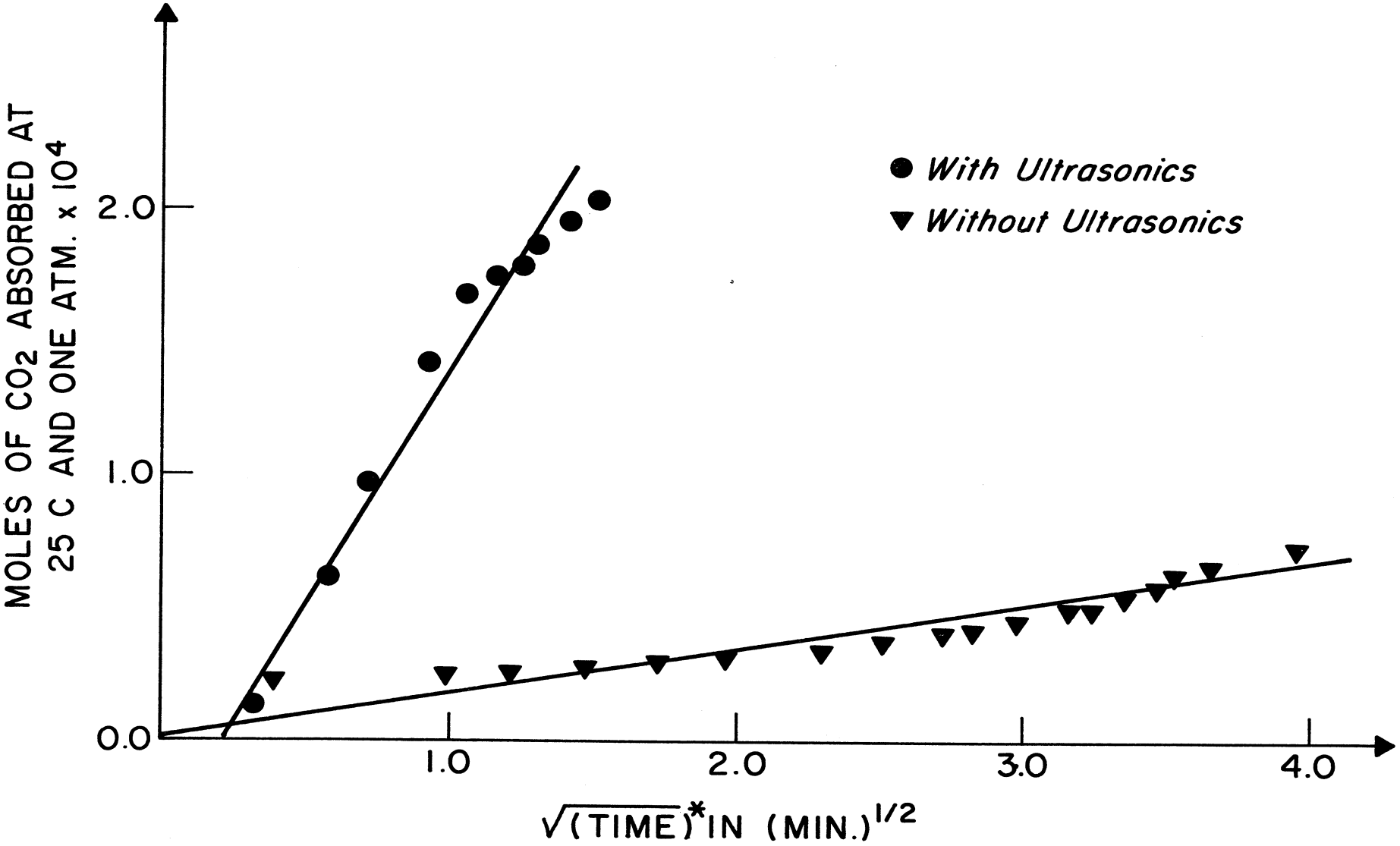

Figure 3. Comparison of CO_2 absorption in glycerol with and without ultrasonics.

power input per limit total cross sectional area.

800 kHz FIXED SURFACE OBSERVATIONS

The convective patterns obtained with the use of container "B" sketched in Figure 4 are shown in Figure 5. Considerably more intense convective patterns were obtained at approximately the same power input to the 800 kHz transducer when the upper surface was "fixed" than when it was free. A rough estimate of the fluid velocity can be obtained by noting the length of a streak made by a particle on the film and the exposure time; along the axis of the tube, this speed appears to be about 30 to 50 cm/sec. It should be noted that the wavelength at 800 kHz is only .19 cm, and therefore the distance between the radiating diaphragm of the transducer and the upper surface of the liquid is much greater than the wavelength. Thus, the essential "roll cell" type streaming pattern, in which fluid moving along the centerline of the tube impinges upon the upper surface and returns via the side of the container shown here, is retained even though the distance between the transducer and upper liquid surface is decreased. It might be argued that at points within the fluid unaffected by "end effects"—i.e., those points located at distances of the order of several ultrasonic wavelengths from either the upper liquid surface or the transducer surface, the velocity profile is similar to that observed by Leiberman (1952) and described mathematically by Eckart (1949). However, the velocities of the patterns reported here are at least an order of magnitude greater than those experimentally observed or predicted by others.

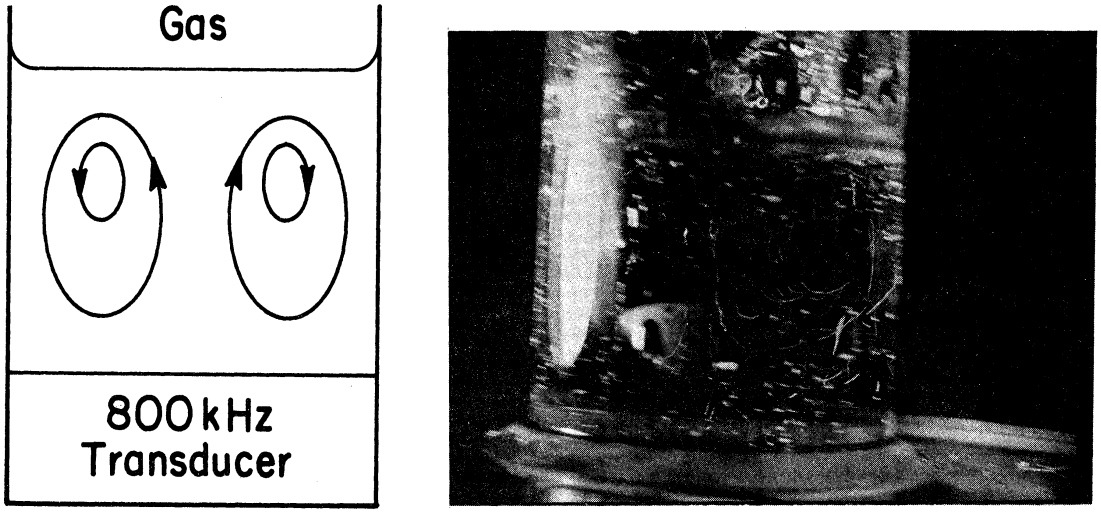

Figure 4. Acoustic streaming at 800 kHz at a gas-liquid interface.

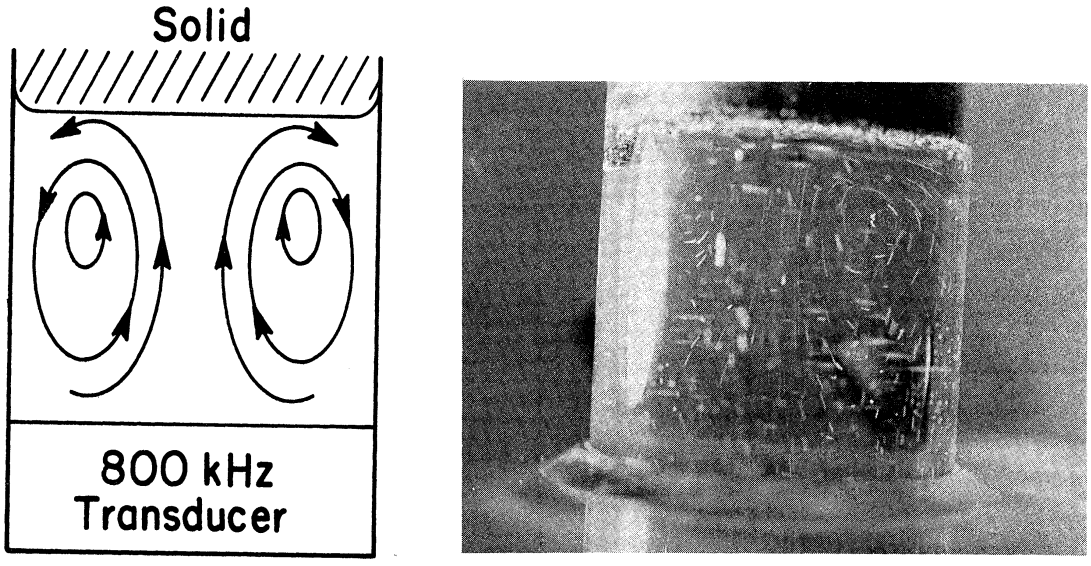

Figure 5. Acoustic streaming at 800 kHz at a solid-liquid interface.

20 kHz FREE SURFACE STREAMING

Figures 6 and 7 are photographs of 20 kHz acoustically induced free surface convection taken in container "C" sketched in Figure 1. At low sonic inputs relatively slow vortices exist which appear similar to those shown in Figure 4; these regular vortices exist above the cavitation threshold. As the power input to the transducer is further increased, however, the gas liquid interface becomes noticeably distorted, and the induced vortices more intense. At a still greater power input, the interface becomes violently distorted, and in some instances uses four or five times its quiescent height. This phenomena is shown in Figure 6. This streaming is fundamentally different than that shown in Figures 4 and 5 with 800 kHz sound; for in addition to the presence of cavitation, the liquid height here is about 0.6 cm, which is much less than the wavelength, 7.7 cm at 20 kHz.

Figure 7 reveals that intense, circular type vortices are indeed formed at the gas-liquid interface at the side of the tube, the nature of which could be of particular importance in mass transfer applications. The speed of these "surface renewal"-type vortices is estimated to be on the order of 70-100 cm/sec. To our knowledge these intense, unsteady state, free surface acoustically induced vortices have not been reported before in the literature.

SUMMARY

We have observed ultrasonically induced convective streaming patterns at both a fixed and a free liquid surface which, if analyzed from a roll cell or surface renewal point of view, will find particular application to mass transfer processes in which conventional fluid agitation is difficult to achieve or

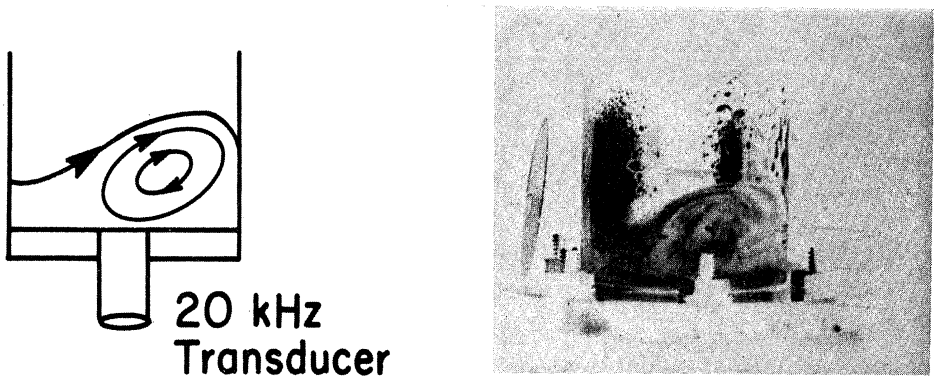

Figure 6. High intensity streaming at 20 kHz at a gas-liquid interface.

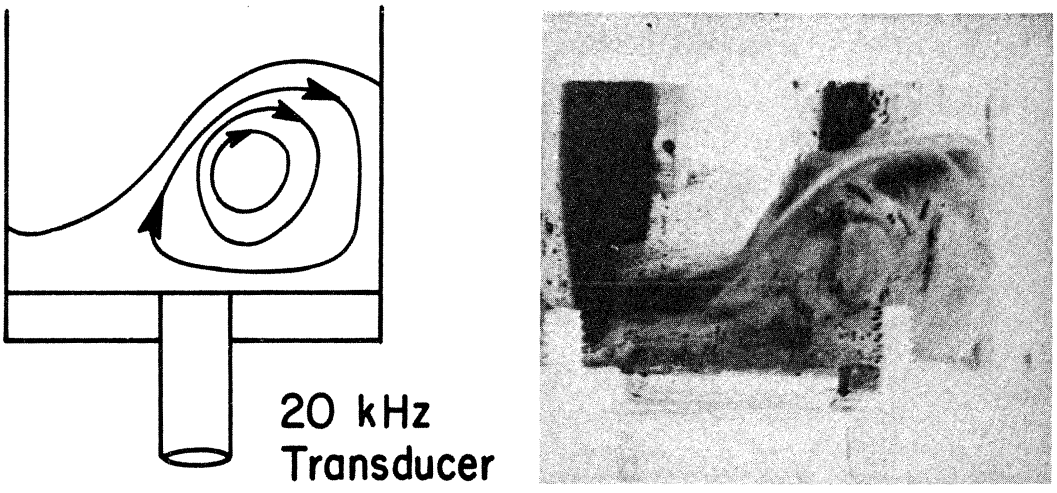

Figure 7. Close-up view of high intensity streaming at 20 kHz at a gas-liquid interface.

undesired. For the convective patterns shown in this paper the estimated velocities are an order of magnitude greater than what has been observed for acoustic streaming in a liquid, or predicted through the use of elementary acoustic streaming theory. Also, we have observed very rapid streaming to occur when the height of the liquid is much less than the sonic wavelength.

LITERATURE CITED

Arkangelskii, M. E., and Statinkov, Y. G., Sov.-Phys. Acoustics 14, 432 (1969).

Burdakov, A. P., and Nukoryakov, V. Y., Zh. Prikl. Mekh Teck. 2, 62 (1965).

Dankwertz, P. V., I. and E. C. 43, 1460 (1951).

Eckart, C., Phys. Rev. 73, 1415 (194).

Fortescue, G. E., and Pearson, J.R.A., Chem. Eng. Sci. 22, 1163 (1967).

Jameson, G. J., Chem. Eng. Sci. 19, 793 (1964).

Leiberman, L. N., Phys. Rev. 73, 68 (1949).

Nyborg, W. L., "Acoustic Streaming," Ch. 11 in Physical Acoustics, Vol. II-B, ed. by Mason, W. P., Academic Press, 1964.

SECTION III

Effect of Ultrasonic Waves on Membrane Transport

(To be submitted for publication)

EFFECT OF ULTRASONIC WAVES ON MEMBRANE TRANSPORT

H. S. Fogler, W. Franklin, V. K. Verma, M. L. Cadwell, and J. Crittenden
Division of Chemical Engineering
University of Michigan
Ann Arbor, Michigan 48104

I. Introduction

The resistance to the transfer of a solute species across a membrane is due to the concentration boundary layers which exist on either side of the membrane, and to the membrane itself. Membrane transport is the principal mode of mass transfer in nearly all vital organs of the body, but because of the extremely high ratio of surface area for mass transfer to volume of most of these organs, artificial duplication of these organs has been very expensive, both in terms of operation and investment. Artificial machines designed so far have been of limited utility due to their large size.

Efforts have been made to reduce the size and inherent complexities of operation. The size of these machines can be reduced by reducing the resistance to membrane transfer. In steady flow systems, the boundary layer resistances on either side of the membranes can be significantly reduced by increasing the through-put of material, and in batch operated systems, these resistances can be reduced by agitation. However, the induced fluid-mechanical shear rates brought on by these increases almost always result in permanent damage to cells transported in vital fluids. In addition, if the principal resistance to mass transfer is in the membrane, increasing throughput in steady flow systems and increasing agitation in unsteady systems are only marginally effective in increasing the efficiency of the artificial machine.

Under proper conditions, the application of ultrasonics can significantly reduce all three resistances to mass transfer. Ultrasonic microstreaming has been observed at solid-fluid interfaces; this microstreaming

should significantly reduce the resistances to mass transfer outside the membrane. Also, since the ultrasonic wave can be propagated into the micropores of the membrane, this mechanism should also enhance mass transport within the membrane itself. At sufficiently low intensity levels, both of these reductions can be achieved with a minimum of cellular or membrane damage. In summary, the application of ultrasonic waves to membranes has shown significant increases in the mass transport rate. In addition to enhancing transport rates in artificial membrane devices, ultrasonics could also enhance internal cellular mass transport in the body fluids and cells.

II. Experiments Utilizing a Non-flow System

A. Apparatus

Two pyrex glass half cells, each of 300 ml capacity, were separated by a membrane and clamped together with slip-on flanges. An O-ring seal was inserted to prevent leakage. The solutions in both cells were stirred by the propeller type variable speed stirrers introduced into position as shown in Figure (A). Samples were drawn at suitable intervals (1/2 or 1 minute) through sample holes, and the samples were returned after conc. measurement to maintain a constant volume of solution in the cells for

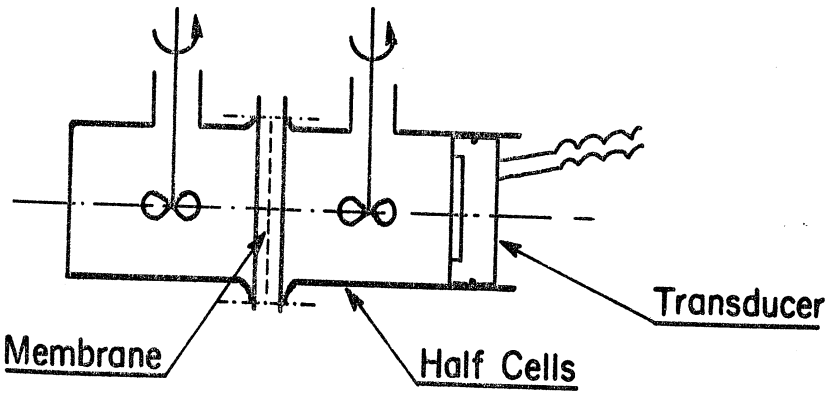

Figure A

each run. Since sodium chloride solutions were used, the concentration of the solution was monitored by a Beckman conductivity bridge in conjunction with standard conductivity cells. Ultrasonics was applied directly to the solution, in a direction perpendicular to the membrane, by a transducer operated at its natural frequency of 800 kHz, and the intensity of the ultrasonic waves was controlled indirectly by monitoring the power output from a Macrosonic 500-1 generator.

B. Mathematical Analysis

Pseudo-steady state mass balance for the solute in the two half cells gives

$$-V_1 \frac{dC_1}{dt} = V_2 \frac{dC_2}{dt} = KA(C_1 - C_2) \qquad (1)$$

where:

V_1, V_2 = solution volumes, constant

C_1, C_2 = solute concentrations

A = area for transfer

K = overall mass transfer coefficient

Integrating Equation (1) with initial conditions of:

at $t = 0$, $C_1 = C_{1_o}$ and $C_2 = C_{2_o}$, we have:

$$V_1C_1 + V_2C_2 = V_1C_{1_o} + V_2C_{2_o} = \alpha \text{ (a constant)} \qquad (2)$$

Eliminating C_1 from Equations (1) and (2), we have:

$$V_2 \frac{dC_2}{dt} = KA\left(\frac{\alpha - V_2C_2}{V_1} - C_2\right) \qquad (3)$$

Equation (3) can be integrated between concentration C* at some reference time t*, and concentration C at time t to give:

$$\ln (\beta - C) = \ln (\beta - C^*) - \nu K(\Delta t) \qquad (4)$$

where:

$$\beta = \frac{\alpha}{V_1 + V_2} = \frac{V_1 C_{1_0} + V_2 C_{2_0}}{V_1 + V_2} \text{ , constant}$$

$$\nu = \frac{V_1 + V_2}{V_1 V_2} \text{ , constant}$$

$$\Delta t = (t - t^*)$$

Equation (4) shows that the plot of ln (β - C) vs. time will be a straight line with a slope of νK, giving the value of K, since ν is known from initial conditions.

C. Results Obtained in the Non-flow System

The purpose of these experiments was to determine the difference in mass transfer coefficient with ultrasonics and without ultrasonics at the same constant stirrer speed. This was necessary in order to determine the magnitude of the effect of ultrasonics on the boundary layer and membrane resistances. At low stirrer speeds, the boundary layer resistance is expected to be predominant, whereas at high stirrer speeds the membrane resistance to mass transfer would be controlling. We may note that the membrane resistance will essentially be unaffected by the stirrer speed which can only be effective in reducing the boundary layer thickness.

The results (in spite of difficulties as mentioned in Section D) had the following trends: (1) there was an increase of 15-200% in the overall transfer coefficient; (2) this increase was high at low stirrer speeds and low at high stirrer speeds; so much so that at a stirrer speed of over 1300 rpm the increase was less than 15%; (3) these results indicate that ultrasonics is more effective in reducing the boundary resistance than the membrane resistance.

From conclusion (3) above, it is obvious that in systems using low velocities near the membrane, resulting in a larger boundary layer resistance, the application of ultrasonics can be very effective in increasing the mass transfer rate.

D. It must be noted that the use of the stirrers, and the occurrence of entrained bubbles in the system, interfered somewhat with the ultrasonic field, thereby reducing its effectiveness. Also, although efforts were made to control the temperature during each run, isothermal operation was difficult to achieve and maintain. Thus, the data at very high stirring speeds or high intensity ultrasonics was difficult to reproduce. Nevertheless, the trends outlined above are clearly discernable. It was felt that many of these difficulties could be circumvented in switching to a steady flow membrane transport system.

III. Experiments Utilizing a Continuous Flow System

A. Apparatus

The apparatus depicted in Figure 1 was used to study steady-state mass transport across a membrane. The diffusion cell designed to handle either co-current or counter-current flow is shown in Figure 2. The cell was constructed in a sandwich manner of transparent plexiglass plates, 6" high, 7/8" thick, and 24" long, which are separated in the middle by two 1/16" thick metal sheets.

A rectangular channel, 1" high, 1/16" wide, and 18" long, was milled in the interior portion of each plexiglass plate. At both ends the channels were beveled to eliminate entrance effects, and holes were drilled to accommodate both feed and discharge of material. Thus, the

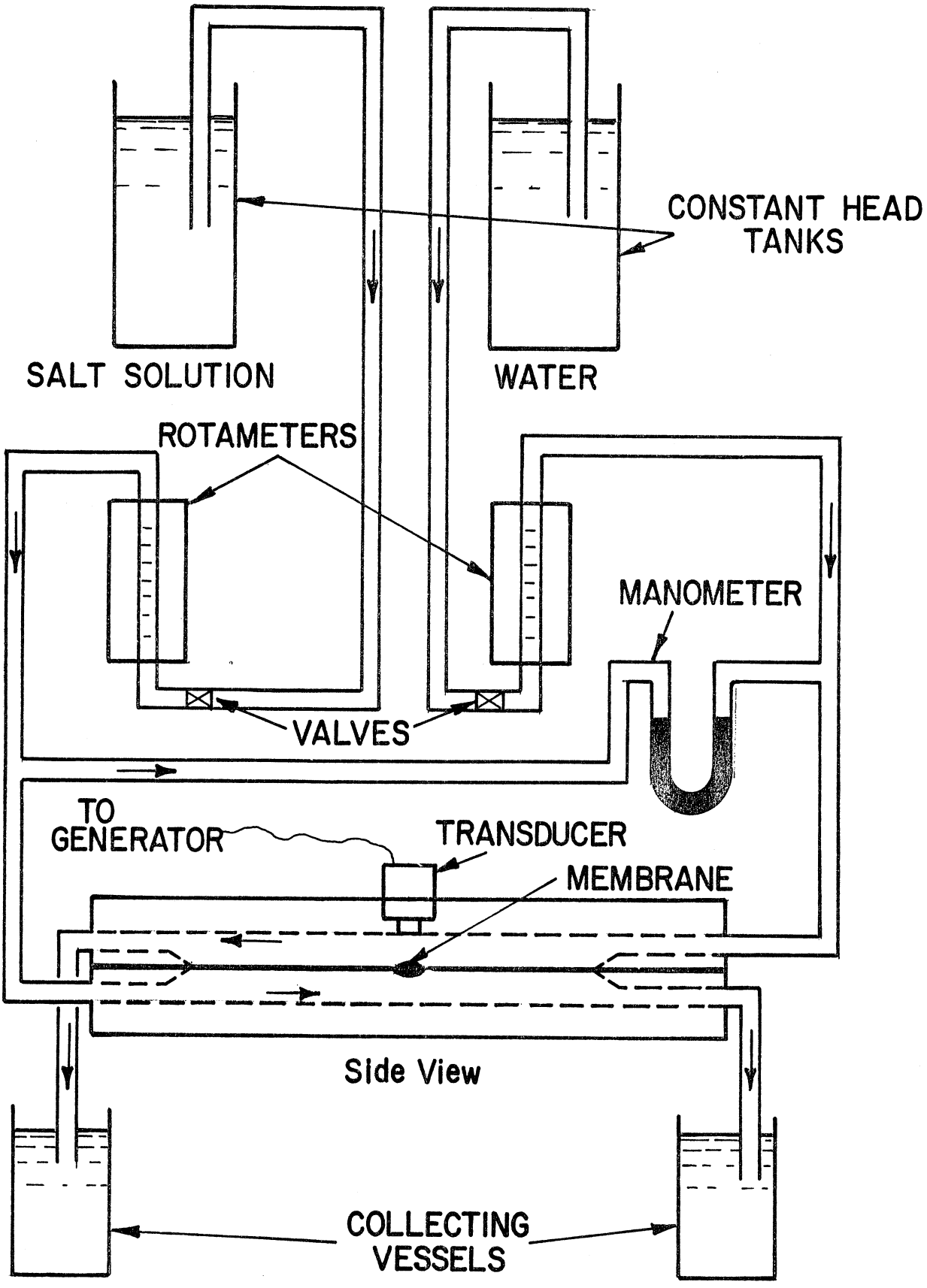

Figure 1. Apparatus for study of steady-state mass transport across a membrane.

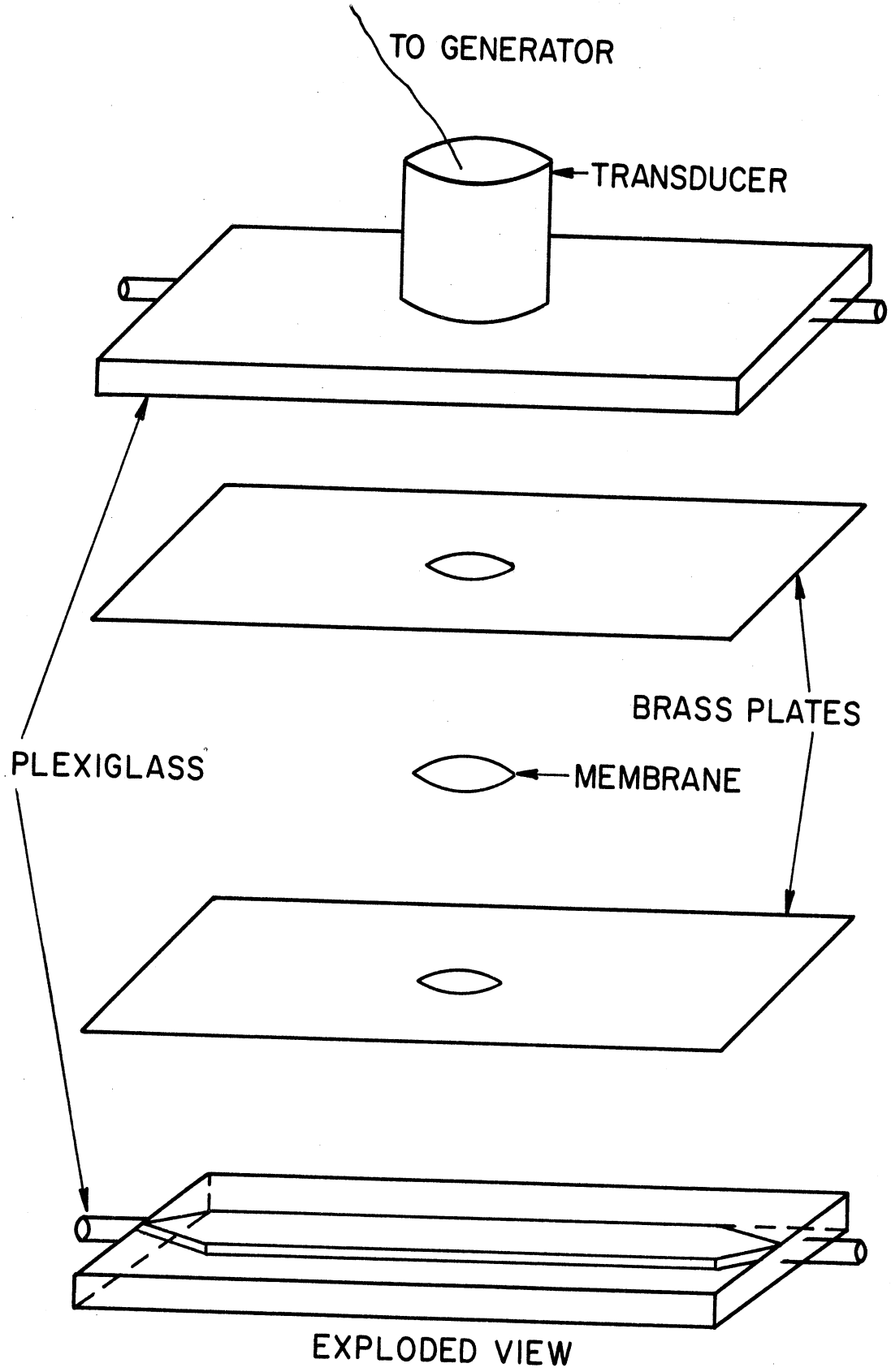

Figure 2. Membrane diffusion cell.

metal sheets which were placed between the two plexiglass plates separated the high and low concentration streams.

In the middle of each metal plate, a 1" diameter hole was bored to allow diffusion. Amicon Corp. Diaflow ultrafiltration membranes (type XM-100 , PM-30) were fitted and held between each plate by bolting together the entire cell.

The bottom plexiglass plate was designed to accommodate a Macrosonics 800 kHz stainless steel transducer. The radiating diaphragm was placed in a direct line with the membrane. Therefore, ultrasonic waves were propagated perpendicular to the cross-sectional area of the membrane, and perpendicular to the direction of channel flow.

The total experimental apparatus and its arrangement are shown in Figure 1. Two five gallon tanks located 2.5 feet above the cell were used to provide an approximately constant rate of flow for both the high and low concentration streams. Each stream was fed from the storage tanks through a rotameter and into the cell.

A tap was inserted in each stream between the rotameters and the cell and connected to a mercury manometer to measure the pressure difference between the high and low concentration streams. Both streams exited into collection tanks and could be tapped for sample analysis. A Beckman type electrical conductivity cell was used to determine the concentrations of each stream.

The transducer was driven by a power supply from a Macrosonics 500-1 ultrasonic generator capable of delivering 0-500 watts of power. The power delivered to the transducer was measured by a Tectronix oscilloscope. Voltage

and current probes were attached to the line between the generator and the transducer and fed into the oscilloscope. Thus the oscilloscope displayed the voltage and current amplitudes and the phase angle between the voltage and current.

B. Procedure

Before a series of runs, a 23% weight salt solution was prepared from Merck reagent grade salt and distilled water, and inserted into the constant head tank. The low concentration constant head storage tank was filled to the same liquid level with distilled water.

Flow was initiated by opening the valves on the rotameters. Steady state was assumed to have been reached when constant flow was observed. Samples were taken from the discharge of the diffusion cell and their concentrations determined with the conductivity bridge. The volumetric flow rates were noted and the temperature was taken from the solutions in the collection tanks.

Runs with the ultrasonics on both the high concentration side and the low concentration side were performed. During these runs, the voltage and current amplitudes, the wave length, and the phase angle were read off the oscilloscope display.

C. Mathematical Analysis

For the well developed steady state flow of two streams exchanging solute across a permeable membrane of constant width, the diffusional flux can be defined as

$$dJ = k \cdot dA \cdot \Delta C \quad , \qquad (1)$$

where:

dJ = diffusional flux across an element of area dA of the membrane

ΔC = difference in bulk concentrations, $(C_1 - C_2)$

k = overall mass transfer coefficient as defined by Eqn.1 .

The mass balance for the solute transferred gives

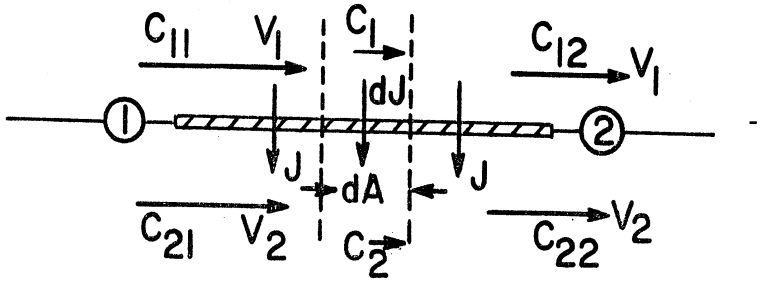

$$dJ = V_1 dC_1 = \pm V_2 dC_2 \qquad (2)$$

where:

V_1, V_2 = flow rates on sides 1 and 2 ,

dC_1, dC_2 = differential change in bulk concentration during the flow over the area dA, and

the sign is plus for counter current and negative for co-current.

Integration of Eqn. 2 shows that for constant V_1 and V_2, the plots of J vs. C and J vs. ΔC are straight lines;

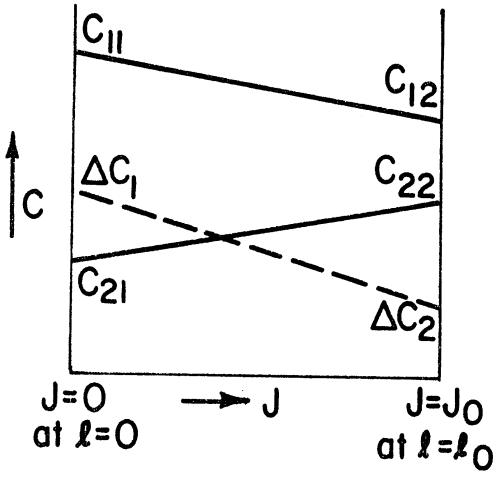

thus,

$$\frac{d(\Delta C)}{dJ} = \frac{\Delta C_2 - \Delta C_1}{J_0} \qquad (3)$$

Eliminating dJ from Eqns. 1 and 3 and integrating over the total area (hence length) for constant k, we get

J_0 = mass transferred/time

$$= k \; A_T \bar{\Delta} C_{ln} \qquad (4)$$

where

$\bar{\Delta} C_{ln}$ = log mean concentration difference

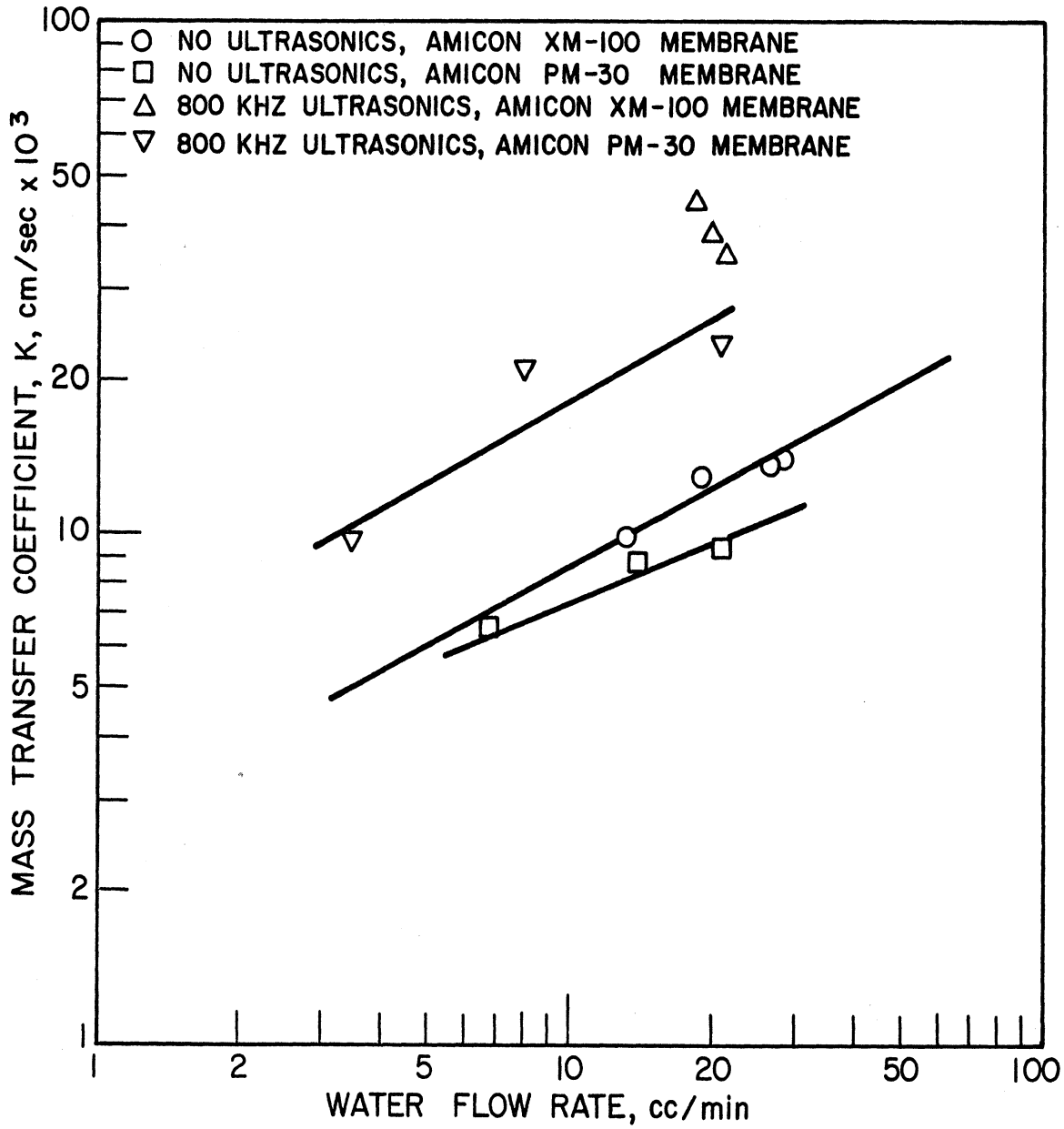

Figure 3. Mass transfer coefficient vs. water flow rates with and without the application of ultrasonics.

$$= \frac{\Delta C_2 - \Delta C_1}{\ln(\Delta C_2/\Delta C_1)}$$

Thus, knowing J_0 and $\bar{\Delta}C_{ln}$, which can be computed by noting the solute balance on either of the two streams, and knowing A_T, the value of the mass transfer coefficient can be determined.

D. Results Obtained in the Continuous Flow Systems

A typical set of data taken with the constant flow membrane cell is shown in Figure 3. In these runs, the flow rate of the stream whose concentration was high in salt content("salt side" of the cell) was held constant and the flow rate of the distilled water stream ("water side" of the cell) was varied from 4 - 30 cc/min. Under these conditions, flow on both sides of the membrane was laminar. However, the salt side concentration and flow rate was arranged such that the principal resistances to mass transfer occurred in the membrane and on the water side. If under these conditions, the membrane resistance is also much smaller than the water side resistance, a log-log plot of the mass transfer coefficient vs. flow rate should be linear with a slope of 1/3. The fact that the mass transfer coefficient for the runs taken with the PM-30 membrane is always lower than that for the XM-100 membrane at the same conditions indicate that there was membrane resistance to mass transfer, and therefore the lines drawn through the data points in Figure 3 are first approximations.For the data shown, the water side of the cell was subjected to ultrasonics. During the runs carried out with ultrasonic irradiation, the power input to the transducer was held constant, with the exception of the data taken using the PM-30 membrane, for which the power level varied due to some fluctuations in the power output of the generator.

It is seen from the data using the XM-100 membrane that the application of ultrasonics increases the mass transfer coefficient between 100-300% for all conditions in this study; for the PM-30 membrane, this increase is of the order of 350%. The fact that the increase differed with the type of membrane used suggests that ultrasonics not only favorably affects transport of solute from a solid surface to the bulk, but also perhaps transport through the membrane itself. This latter result is of special significance since there is no mechanical means of enhancing mass transport through a membrane. It should also be noted that,at the power levels used thus far in this study, no membrane destruction has been observed when ultrasonics is employed.

Further work is anticipated with the constant flow membrane cell. Efforts will be made to delineate further the effects ultrasonics has on the three principal resistances to mass transfer. The recently initiated study of the effects of ultrasonic power level applied under constant flow conditions will be continued with some emphasis given to examination of the properties of the membrane before and after insonation. Ultrasonic irradiation will be applied to the side of the cell in which the least resistance to mass transfer is encountered to ascertain whether the ultrasonic waves propagate through the membrane. Experiments with and without ultrasonics will be carried out at flow rates in which the primary resistance to mass transport is in the membrane itself.

The effect of ultrasonic on ultrafiltration was examined. The apparatus used is the same one that was used to study steady-state diffusion shown in Figures 1 and 2. The only difference is that one establishes a small pressure drop across the membrane which results in a small flow in the direction of the pressure drop. For a fixed pressure drop, water flow rate, and salt flow rate, the effect of ultrasonic intensity on the mass transport rate of a solute was examined. A 17-fold increase in mass transport rate was obtained and this occurred without the destruction of the membrane.

The procedure followed in this study are similar to those followed in steady-state diffusion. The solute used was sodium chloride and the solution used was about 23% by weight salt. The diffusion cell that was used is shown in Figure 2. Countercurrent flow with distilled water was used as shown in Figure 1. A pressure drop from the salt side to the water side was obtained by the manipulation of the constant load tanks. The transducer is on the water side since this is the side which offers the greatest resistance to the mass transfer. A Beckman conductivity bridge was used to determine the concentration of salt in the water side collecting vessel. Using a quasi-steady-state analysis one could determine the maximum time one needs to wait to establish a steady-state condition. This turned out to be from 5-30 min depending on flow rates and on that basis the system was allowed to reach steady-state before collecting samples. The intensity of the signal to the transducer was monitored using an oscilloscope. In the future we plan more precisely to measure the ultrasonic field intensity throughout the membrane system. After each run with ultrasonics an identical run was made without ultrasonics to determine if the

membrane had undergone any decay as a result of ultrasonic irradiation. But after every run the mass transport rate shows that the membrane was unharmed. The rest of the detailed procedure is the same as that which was used for steady-state diffusion.

All the data in Figure 4 represent an increase in mass transport rate with ultrafiltration using ultrasonics. In those runs the salt flow rate, the water flow rate, and the pressure drop all were kept the same. And the only system variable that was changed was the ultrasonic intensity. And after each ultrasonic run, a run without ultrasonics was made to determine if the membrane had experienced any decay. Each time the membrane was not harmed. The most astounding result found was the 17-fold increase in mass transport rate as a result of ultrasonic irradiation.

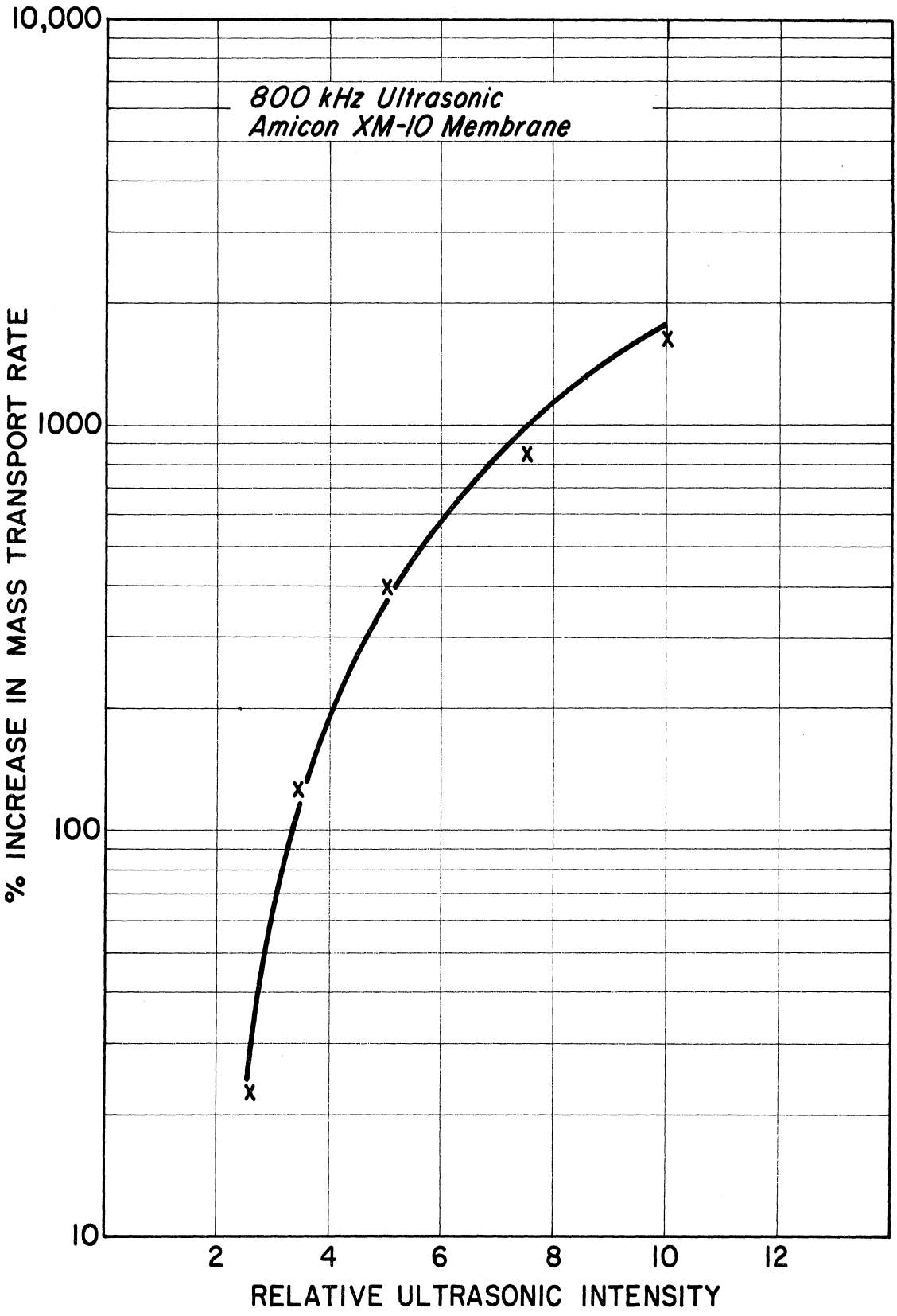

Figure 4. Effect of ultrasonic waves on ultrafiltration-type membrane transport.

SECTION IV

Acoustically Induced Facilitated Diffusional Transport in Membrane Ducts

This paper has been presented at the 79th meeting of the Acoustical Society of America. The abstract of this paper has been published in J Acoust Soc Am 48, 104 (1970). Since the meeting, the entire text has been submitted for publication.

ACOUSTICALLY INDUCED FACILITATED DIFFUSIONAL TRANSPORT IN MEMBRANE DUCTS

Scott Fogler and Kasper Lund
Division of Chemical Engineering
The University of Michigan
Ann Arbor, Michigan 48104

ABSTRACT

The present work considers enhancement of mass transport in membrane ducts by superimposing a convective transport induced by ultrasonics on a diffusional transport. As a result of the non-linearities in the Navier-Stokes equation, a time independent secondary flow, called acoustic streaming, can be produced when an acoustic wave is passed through a medium. Between adjacent vortices or cells, molecular diffusion is the only means of transport; however, within each cell, mass transport is primarily by convection. Increases in the rate of mass transfer of the order of 150% above the normal diffusional flux were found. Ultrasonics may be applied to increase mass transfer through membrane systems (e.g., dialysis) and to increase the efficiency of very active catalytic systems.

I. INTRODUCTION

Traditionally, there are two great challenges in industrial activity: increasing the quality of products, and increasing the efficiency of the processing operation. In many such operations, efficiency can be greatly increased through the application of acoustic waves. The enhancement of the rates of transport resulting from the application of ultrasonic waves through membranes is termed ultrasonically facilitated transport.

In this study, we are interested in the enhancement in mass transfer through membrane type ducts. The use of ultrasonic waves as a means to achieve this goal has been receiving ever increasing attention in recent years. Sonic and ultrasonic waves have been found to increase heat and mass transfer rates by several orders of magnitude in a number of situations.[1-4] Recent studies on water desalinization have shown enhancement in transport rates through semi-permeable membranes.[5] The advantageous effects of acoustic waves on various transport phenomena and chemical reactions has been discussed in some detail by Fogler.[6-7]

In the present work attention will be focused on the enhancement of mass transport in gas and liquid diffusion resulting from acoustic streaming. Various studies have been conducted on the effect of acoustically induced vortices and microstreaming on heat transfer. The majority of these studies have emphasized streaming on the exterior of vibrating objects such as streaming around a cylinder or sphere. In certain limited situations heat transfer studies have been conducted on streaming inside ducts and tubes. However, of these studies

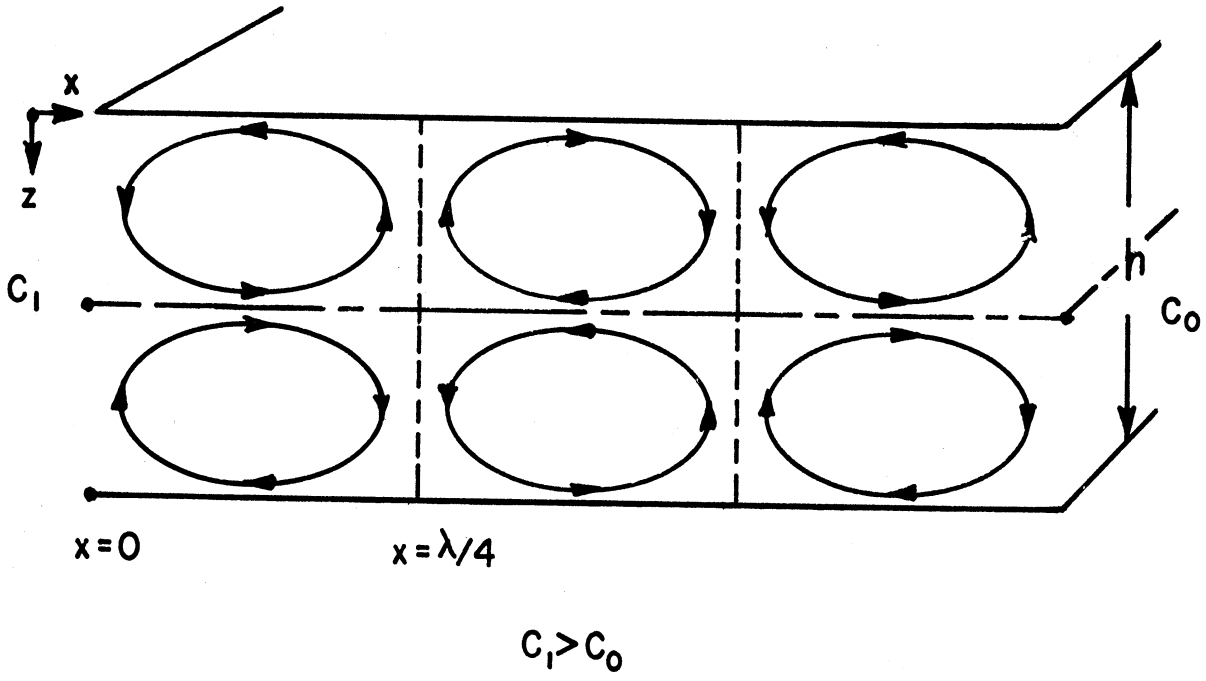

Figure 1. Schematic diagram of streaming cells and concentration difference.

which have been conducted in ducts and tubes, energy transfer was in the direction normal to the wall. In order for enhancement to occur in diffusional transport in membrane pores, there must be an increase in mass transfer parallel to the duct walls. Complete reviews of acoustic streaming have been given by Nyborg[3] and by Richardson.[8]

In this study we shall consider the case in which the convective streaming transport is superimposed on the diffusive transport in diffusion in ducts in membrane pores. The streaming cells induced by acoustic waves should greatly enhance the rate mass transport through the system.

II. THEORY

Acoustic streaming is a secondary flow which produces time independent vortices when an acoustic wave is passed through the medium. The formation of these vortices or cells inside ducts, tubes, and pores can increase the rate of mass transfer through these enclosures. In this study, diffusional transport is in the direction of wave propagation. Figure 1 shows a schematic diagram of these cells in a wide membrane duct. Between adjacent cells molecular diffusion is the only means of mass transport; however, within each cell, transport is primarily by convection.

Before engaging in discussion of the coupled transport processes, it would be beneficial to give a brief development of the streaming equations, since previous solutions to these equations do not hold in certain regions which predict large increases in diffusional transport. Consequently, new solutions had to be obtained for these regions. Starting from the continuity and Navier-Stokes equation, we shall closely follow the development of Nyborg.

$$\frac{\partial \rho}{\partial t} + \nabla \cdot (\rho \vec{V}) = 0 \qquad (1)$$

$$\frac{\partial (\rho \vec{V})}{\partial t} + \rho(\vec{V} \cdot \nabla)\vec{V} + \vec{V}\nabla \cdot (\rho \vec{V}) = \nabla p + [\mu' + \frac{4}{3}\mu]\nabla\nabla\cdot\vec{V} - \mu\nabla x\Delta x\vec{V} \qquad (2)$$

Since there is no external force other than the sound field, the solution to these equations will take the form

$$u = \varepsilon\vec{V}_1 + \varepsilon^2\vec{V}_2$$

$$P-P_o = \varepsilon P_1 + \varepsilon^2 P_2 \qquad (3)$$

$$\rho-\rho_o = \varepsilon\rho_1 + \varepsilon^2\rho_2^2$$

$\vec{V}$ has x and z componenets u and w respectively. The first order components u_1 and w_1 are time dependent velocities which directly arise from the sinusoidal movement of the transducer surface. The non-linear coupling of these first order velocities gives rise to the second order flow patterns. The streaming velocity components u_2 and w_2 consist of a time independent and a time dependent term. In this investigation we are only interested in the time independent part of the streaming velocities.

Upon substitution of Equation (3) into equation (1) the first order approximation of velocity becomes

$$\rho_o \frac{\partial \vec{V}_1}{\partial t} = c^2\nabla\rho_1 - R\nabla\rho_1 + (\mu' + \frac{4}{3}\mu)\nabla\nabla\cdot\vec{V}_1 - \mu\nabla x\nabla x\vec{V}_2 \qquad (4)$$

and the time average of the second order velocity $\vec{V}_2$ is

$$\rho_o \langle(\vec{V}_1 \cdot \nabla)\, \vec{V}_1 + \vec{V}_1 \nabla \cdot \vec{V}_1 \rangle = -\nabla P_2 - \mu \nabla x \nabla x \vec{V}_2 \qquad (5)$$

It is precisely the second order velocity $\vec{V}_2$ which gives rise to the circular streaming cells.

A. Solutions to Streaming Equations for Transport in Membrane Ducts

The solution to Equation (4) in terms of first order velocity components u_1 and w_1 was given by Rayleigh (1895, 1945) to be

$$u_1 = A \cos kx \, [\cos wt - e^{-\beta z} \cos (wt - \beta z)] \qquad (6)$$

$$w_1 = \frac{-Ak}{\beta\sqrt{2}} \sin (kx) \left(\cos \left(wt - \frac{\pi}{4}\right) - e^{-\beta z} \cos \left(wt - \beta z - \frac{\pi}{4}\right)\right) \qquad (7)$$

Upon taking the curl of both sides of Equation (5), one obtains

$$\mu \nabla x \, (\nabla^2 V_2) = -\nabla x \vec{F} \qquad (8)$$

where

$$-\vec{F} = \rho_o \langle(\vec{V}_1 \cdot \nabla)\, \vec{V}_1 + \vec{V}_1 (\nabla \cdot \vec{V}_1)\rangle \qquad (9)$$

With $\nabla \cdot \vec{V}_2$ approximately zero, one can substitute for V_2 in terms of the stream function.

$$\nabla^2 (\nabla^2 \psi_2) = \nabla x F \qquad (10)$$

Upon substituting Equations 6, 7 and 9 into Equation 10, one obtains

$$\nabla^4 \psi_2 = -\frac{1}{2\mu} [\beta \rho_o k A^2 \sin 2kx] [2C + S - e^{-2n}] \tag{11}$$

where

$$C = e^{-\beta z} \cos \beta z$$

$$S = e^{-\beta z} \sin \beta z$$

By approximating this fourth order spatial derivative by

$$\nabla^4 \psi_2 \simeq \frac{d^4 \psi_2}{dz^4} \tag{12}$$

we obtain the solution to this equation in terms of the x and z components of the streaming velocity given by Nyborg.[3]

$$U_2 = -\frac{3A^2}{8c} \sin 2kx [e^{-2\beta z} + 2S - 1 + 6n_1 (1 - n_1)] \tag{13}$$

$$W_2 = -\frac{3kA^2}{8\beta c} \cos 2kx [e^{-2\beta z} + 2(S + C) - 3 + 2\beta h n_1 (1 - n_1) (1 - 2n_1)] \tag{14}$$

When these velocity components were coupled to the diffusion transport equations, we observed that we only obtained significant increases in mass transfer when the product kh was large (the order of one or greater). However the approximation made in Equation (12) is not valid for large values of (kh). Consequently, Equation (11) was resolved to yield

$$\psi_2 = A^2 \sin 2kx \,(A_1 \cosh khn + B_1 \sinh khn +$$

$$C_1\, n \cosh khn + D_1\, n \sinh khn +$$

$$e^{-\beta z}\,(4 \cos \beta z + 2 \sin \beta z) + \frac{1}{2} e^{-2\beta z}) \qquad (15)$$

where

$$A_1 = -9/2$$

$$B_1 = \frac{3}{2} \frac{(h\beta - 3)}{kh - \sinh kh \cdot \cosh kh}$$

$$C_1 = \frac{3}{2}(h\beta - 3)$$

$$D_1 = \frac{3}{2}(h\beta - 3) \cosh hk$$

$$n = z/(h/2)$$

The second order velocity components u_2 and w_2 are obtained by differentiating Equation (15) with respect to x and z respectively, i.e.,

$$W_2 = -\frac{\partial \psi_2}{\partial x} \qquad (16)$$

$$U_2 = -\frac{\partial \psi_2}{\partial z} \qquad (17)$$

One can readily show that Equation (15) reduces to the Equation given Nyborg for small values of kh. Now that we have the flow field defined for large values of kh, we determine the effect of acoustic streaming on diffusional mass transport.

B. Coupling of the Streaming and Diffusional Transport Equations

If the fluid in the duct consists of a mixture of species and their concentrations are different at the two ends of the duct, mass will be transferred through the duct partly by diffusion and partly by convection. For dilute solutions, the mass transfer equation can be coupled with the acoustically induced velocity field. The unsteady mass balance is

$$\frac{\partial C}{\partial t} + \bar{V} \cdot \nabla C = D\nabla^2 C \tag{18}$$

with boundary conditions

$$C = C_0 \text{ at } X = 0$$

Let $\phi = \dfrac{C - C_1}{C_0 - C_1}$ be a dimensionless concentration.

$$C = C_1 \text{ at } X = L$$

$$\frac{\partial C}{\partial Z} = 0 \text{ at } Z = 0 \text{ and } Z = h/2$$

The velocity, $\bar{V}$, can be taken as the mass average velocity and D as the binary diffusion coefficient for a dilute solution. Further, the length of the duct L is taken as an integer multiple of $\pi/2k$. We now substitute for $\bar{V}$ to obtain

$$\frac{\partial C}{\partial t} + (U_1 + U_2)\frac{\partial C}{\partial X} + (W_1 + W_2)\frac{\partial C}{\partial Z} = D\left(\frac{\partial^2 C}{\partial X^2} + \frac{\partial^2 C}{\partial Z^2}\right) \tag{19}$$

We now time average Equation (19) over several cycles and assume first order interactions between velocity in concentration gradient be neglected.

$$U_2 \frac{\partial \bar{C}}{\partial X} + W_z \frac{\partial \bar{C}}{\partial Z} = D \frac{\partial^2 \bar{C}}{\partial X^2} + \frac{\partial^2 \bar{C}}{\partial Z^2} \qquad (20)$$

where

$$< C > \equiv \bar{C}$$

It can be shown by a perturbation analysis this assumption is exactly valid when there is a phase lag of $\pi/2$ between the first order concentration and the first order velocity. This approximation has been useful in correlating previous results and is consistent with current studies in similar systems.[9-11]

III. DISCUSSION

The dimensionless concentration field is plotted in Figure 2 for the case of a frequency, f, of 20 kcps, a maximum displacement of the transducer surface, s, of 7×10^{-3} cm and a duct height, h, of 2 cm. The increase in mass transfer for this case is 96% and the plot clearly shows that the acoustic streaming pattern strongly modifies the concentration field which would be present when only diffusional mass transfer was occurring. Near the two ends of the duct, large concentration gradients are present and diffusional mass transport will be the most important means of transport at these points. In the middle of the duct, concentration gradients are smaller and convection will be the primary means of transport.

In this analysis there are a large number of parameters one could vary to determine their effect on the rate mass transfer. This somewhat tedious task is most always avoided by the formation of dimensionless groups. When the transport system involves both diffusive and convective transport, one of the

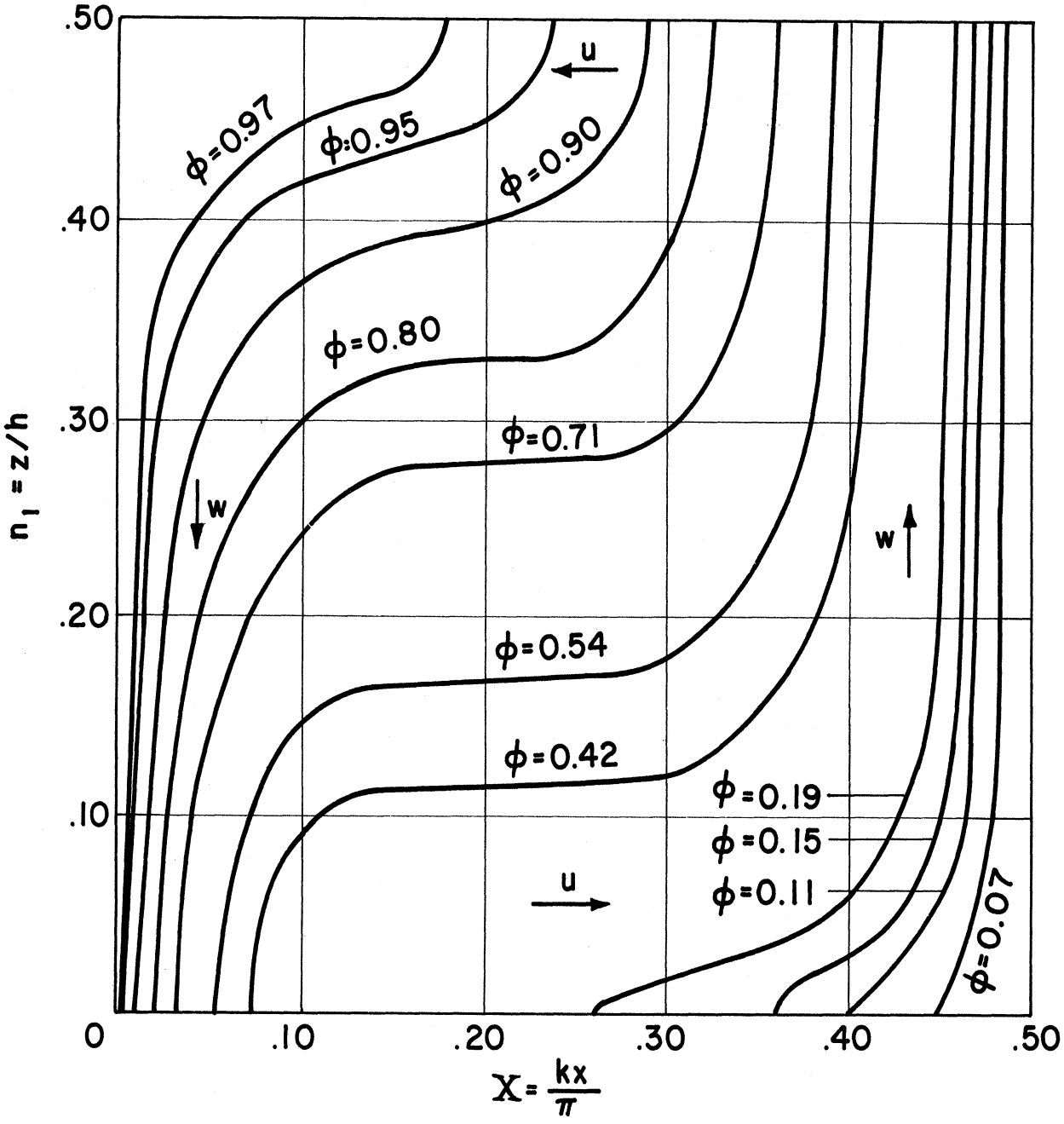

Figure 2. Dimensionless concentration profile under acoustic streaming conditions.

$$\phi = \frac{C - C_1}{C_0 - C_1}$$

primary dimensionless groups used in the correlation and presentation of results is the Peclet number. In Figure 3 the increase in mass transfer is plotted versus the Peclet number, Pe, for diffusion in gases. Figure 4 shows a similar plot for diffusion in liquids

$$Pe = \frac{\text{transport by convection}}{\text{transport by diffusion}}, \quad Pe = \frac{3kh^2A^2}{8D\,c},$$

where c is the speed of sound, k the wave number, A the first order velocity amplitude, and D the diffusion coefficient.

It is seen that at each value of the product kh, the Peclet number has to reach a certain magnitude before any significant increase in mass transfer can be expected. The plot also indicates that much higher increases in mass transfer can be expected, but this could not be investigated because of stability problems with the numerical scheme. The present numerical technique is being modified so as to extend our results into other regions.

The results show that by the application of ultrasonics to mass transport processes, substantial increases in the rate of mass transfer can be expected. Application of ultrasonics will be very beneficial for mass transfer through membranes when a substantial resistance to mass transfer lies in fluid boundary layers and for solid-fluid reactions (catalytic or non-catalytic) where the rate of mass transfer is limiting.

Our initial investigation using the presented ultrasonic streaming equations shows increases of up to 145% in mass transfer can be expected when ultrasonic convective transport is superimposed on a diffusional transport.

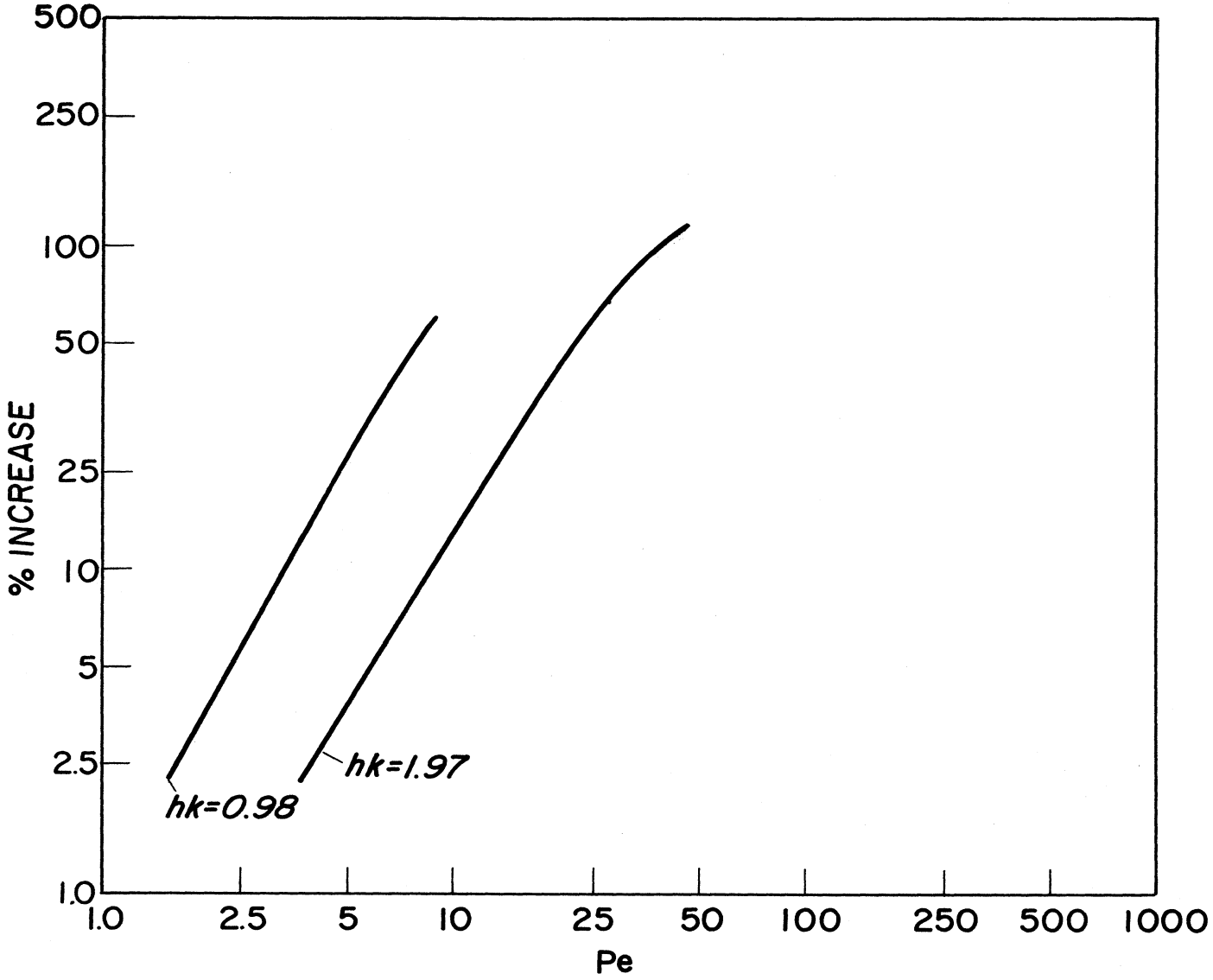

Figure 3. Percent increase in mass transfer in gas systems as a function of the Peclet number.

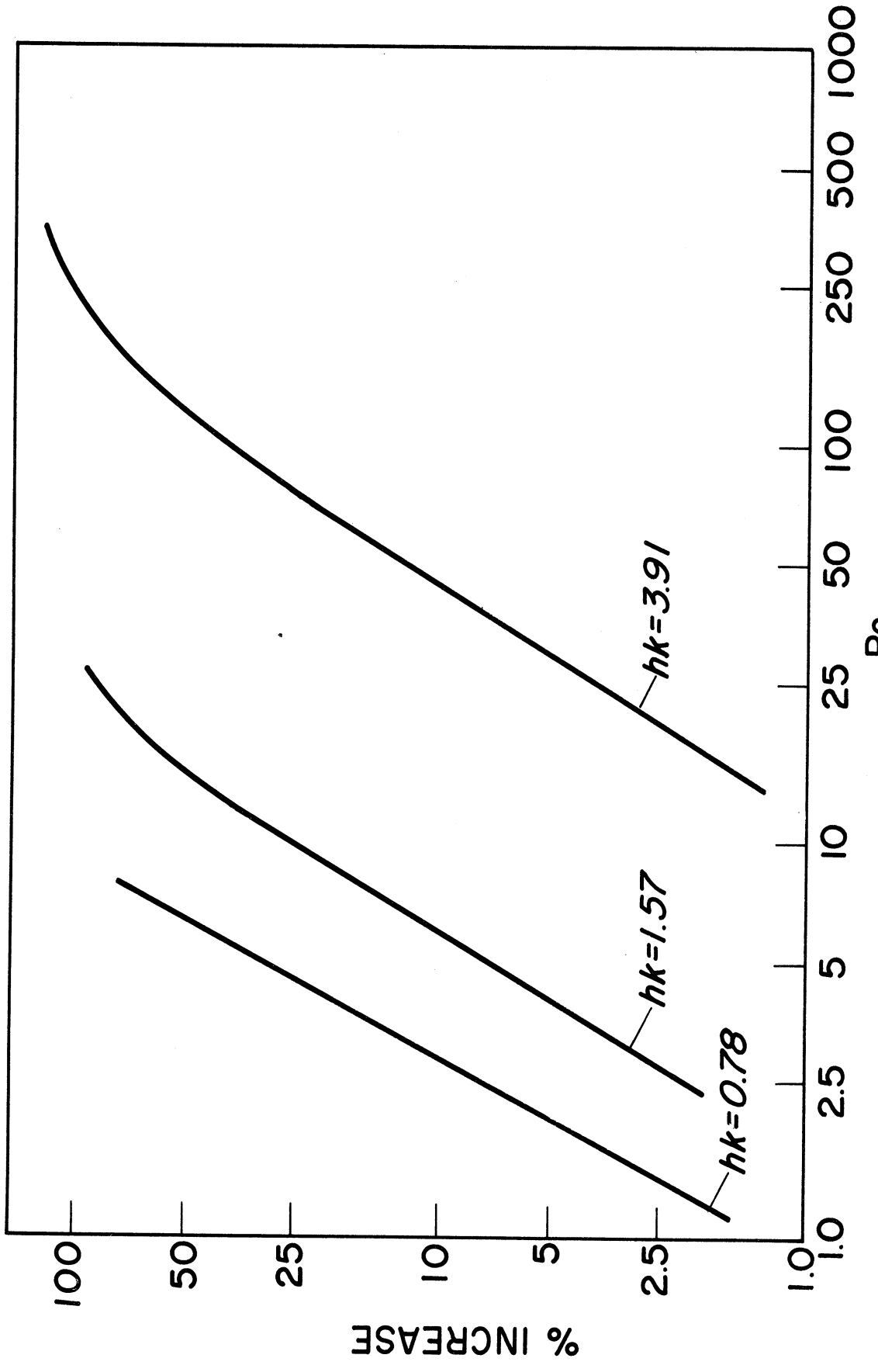

Figure 4. Percent increase in mass transfer in liquid systems as a function of the Peclet number.

IV. SUMMARY

Upon the passage of an acoustic wave through a duct, one can observe the formation of time independent vortices. This phenomena, which is commonly called acoustic streaming, can enhance mass transport by superimposing a convective transport on a diffusive transport. The differential mass transport equation was coupled with the second order time independent streaming equations in a rectangular membrane duct and solved by finite different techniques. A frequency range of 5-800 kcps in liquids and gases was investigated for different acoustic and physical variables. The acoustic streaming strongly modifies the concentration field which would be present when only diffusional mass transfer takes place. Regions with large concentration gradients are formed near the two ends of the duct, and only small concentration gradients are present in the middle of the duct. At each frequency the Peclet number, and thereby the first order velocity amplitude, has to reach a certain magnitude before any significant increase in mass transfer can be expected. At high Peclet numbers the increase in mass transfer is proportional to the logarithm of the Peclet number. Preliminary results show that with the application of ultrasonics increases are up to 150% above the normal diffusive transport.

APPENDIX

METHOD OF SOLUTION

The partial derivatives can be approximated by the following finite difference formulas:

$$\frac{\partial^2 C}{\partial X^2} = \frac{\bar{C}_{i,j-1} - 2\bar{C}_{i,j} + \bar{C}_{i,j+1}}{(\Delta X)^2} \qquad \frac{\partial^2 C}{\partial Z^2} = \frac{\bar{C}_{i-1,j} - 2\bar{C}_{i,j} + \bar{C}_{i+1,j}}{(\Delta Z)^2}$$

$$\frac{\partial C}{\partial X} = \frac{\bar{C}_{i,j+1} - \bar{C}_{i,j-1}}{2\Delta X} \qquad \frac{\partial C}{\partial Z} = \frac{\bar{C}_{i+1,j} - \bar{C}_{i-1,j}}{2\Delta Z}$$

Let $\Delta X = \Delta Z$

Boundary conditions:

$$C_{i,1} = C_o \text{ at } X = 0 \text{ and } C_{i,m+1} = C_1 \text{ at } X = L$$

$$C_{2,j} = C_{1,j} \text{ at } Z = 0 \text{ and } C_{n+1,j} = C_{n,j} \text{ at } Z = h/2$$

$$i = 1, 2, 3, \ldots, m+1, \text{ and } j = 1, 2, 3, \ldots, n+1$$

Substituting into the differential equation and rearranging yields

$$C_{i,j} = C_{i,j} + Q/4[(1+U_{i,j} \cdot \Delta X/2)\, C_{i,j+1} + (1-U_{i,j} \cdot \Delta X/2)\, C_{i,j-1}$$

$$+ (1+W_{i,j} \cdot \Delta X/2)\, C_{i+1,j} + (1-W_{i,j} \cdot \Delta X/2 C_{i-1,j} - 4C_{i,j}]$$

where Q is an accelerating factor $1 < Q < 2$. The system of linear equations is solved by a Gauss-Seidel interation scheme (Carnahan, et al., 1969).[12]

REFERENCES

1. Fogler, H. S. and Timmerhaus, K. D., AIChE 12, 90 (1966).

2. Richardson, P. D., J. Fluid Mechanics 30, 337 (1967).

3. Nyborg, W. L. in Physical Acoustic Vol. II B, pp. 265-331. W. P. Mason, ed., Academic Press, New York (1965).

4. Boucher, R.M.G., Chem. Engr. 66 (Sept. 1959).

5. Harvey, R. F., Chemistry 40, No. 4, 28 (1967).

6. Fogler, H. S., Sound and Vibration 1, No. 8, 18 (1967).

7. Fogler, H. S., CEP Symposium Series (in press).

8. Richardson, P. D., Appl. Mech. Rev. 20, No. 3, 201 (1967).

9. Kapustina, O. A., and Y. G. Statnikov, Sov. Phys.-Acoust. 13, No. 3, 327 (1968).

10. Arkhangel'skii, M. E. and Y. G. Statnikov, Sov. Phys.-Acoust. 14, No. 4, 432 (1969).

11. Rowe, W. E. and W. L. Nyborg, J. Acoust. Soc. Am. 39, 965 (1966).

12. Carnahan, B., Luther, H. A., and Wilkes, J. O., "Applied Numerical Methods," Wiley, New York (1969).

SECTION V

Acoustic Cavitation in Viscoelastic Fluids

The first paper in this section by Prof. H. S. Fogler and Prof. J. D. Goddard was presented at the 62nd National A.I.Ch.E. meeting in Washington D. C., and has been published in the Physics of Fluids 13, 1135, 1970. The second paper has been submitted for publication in J. Appl. Phys.

ACOUSTIC CAVITATION IN VISCOELASTIC FLUIDS

As previously mentioned the overall objective of this research is to utilize ultrasonic waves to accelerate kinetic and mass transport phenomena in biological type systems. Preliminary results, both theoretical and experimental, have shown that substantial increases in mass transfer can be brought about by ultrasonics. With the application of acoustic waves to biological systems, one must be sure that the wave conditions are properly adjusted so as not to induce any harmful side effects to the tissue and body fluids. In some cases, acoustic cavitation could degrade these materials if it is induced beyond a certain level. It is known that various biological fluids behave as viscoelastic liquids [Trans. of the Soc. Rheology 9, Part 1, p. 448 (1965)]. Consequently, a brief and preliminary investigation was undertaken on cavitation in viscoelastic fluids to determine whether the degrading effects of cavitation could be accelerated or retarded in this fluid type. As a result of the complexity of the problem, only a few limiting cases were studied. These cases were chosen such that if they showed the cavitation process was unaffected by the elastic effects in the liquid, then the other situations would in all probability show the same results. The paper which follows was presented at the 62nd Annual A.I.Ch.E. meeting and has also been accepted for publication in the Physics of Fluids and concerns the collapse of a spherical void in a viscoelastic fluid. These preliminary results show that the elasticity can significantly retard the collapse process and certain situations produce damped oscillatory motion of the cavity rather than the usual catastrophic collapse observed in purely viscous liquids. Since first results show viscoelasticity could

quite significantly retard material and fluid degradation, we have outlined a program for further study in this area in our recent proposal to NIH for continued support on this project.

ON THE STABILITY AND COLLAPSE OF SPHERICAL CAVITIES IN VISCOELASTIC FLUIDS

H.S. Fogler and J.D. Goddard
University of Michigan, Ann Arbor, Michigan

Preprint 63A

Presented at the Session on
Fundamental Research in Fluid
Mechanics - Part II

SIXTY-SECOND ANNUAL MEETING

Washington, D. C.

November 16-20, 1969

AMERICAN INSTITUTE OF CHEMICAL ENGINEERS
345 East 47 Street, New York, New York 10017

75 cents

ABSTRACT

An analysis is given of the collapse of a spherical cavity in a large body of an incompressible viscoelastic liquid. Proceeding from a linear rheological model for the liquid, one obtains a non-linear integro-differential equation for the motion of the cavity. Analytical solutions are derived for certain limiting values of the parameters governing collapse, and some numerical solutions are presented for various other values.

As one of the more interesting results of this work, it is found that elasticity in the liquid can significantly retard the collapse of a void and produce prolonged, oscillatory motion whenever the relaxation time of the fluid is moderately large in comparison to the Rayleigh collapse time. This is in sharp contrast to the catastrophic collapse which will always occur for voids in purely viscous liquids. Both numerical and approximate analytical solutions are presented to demonstrate the damping effect of liquid viscosity on the cavity motion.

1. INTRODUCTION

The term cavitation usually refers to the phenomenon of growth and collapse of flow-induced voids or vapor bubbles in liquids. The effects resulting from cavitation are known to produce metal erosion, luminescence, and increases in various chemical reaction rates.

In the previous works on this subject, attention has been restricted mainly to classical liquids. The earliest theoretical treatment is apparently that of Lord Rayleigh (1), who considered the collapse of a spherical void in an inviscid liquid. In later theoretical works, attempts have been made to account for viscous effects in both the bubble phase and in the surrounding liquid, and most of the analyses have dealt with Newtonian (Flynn, 2 ; Plesset, 3 ; Fogler, 4) or purely viscous fluids (Yang, 5). An interesting question arises as to the effects that elasticity might have on cavitation in viscoelastic liquids. In other contexts, it has been observed that the presence of elasticity, such as that produced by addition of small amounts of high polymers, can drastically change the flow behavior of liquids. Hence, one might well inquire as to the possible and, perhaps, beneficial effects of viscoelasticity on bubble collapse, such as suppression or reduction in the intensity of cavitation.

An analysis of bubble growth in viscoelastic fluids has already been given by Street (6), but, because of the applications contemplated in his analysis, inertial effects were neglected. It is precisely these effects,

however, that tend to predominate in the collapse phenomena usually associated with cavitation. This provides part of the motivation for the present work, in which we shall focus our attention primarily on the collapse of spherical voids, (i.e., regions containing no gas) in an idealized viscoelastic fluid.

We recall that previous studies have shown that collapsing cavities which contain permanent gases will generally always rebound short of actual collapse, such that the cavity radius never actually decreases to zero. On the other hand, a void will generally always collapse to zero radius, at least in purely viscous fluids. It is therefore interesting to reconsider this question of rebound versus complete collapse for the case of a void in a viscoelastic fluid.

2. EQUATIONS OF MOTION

We wish to treat here the motion of a spherical bubble contained in a large body of an incompressible liquid. Initially at time $t = 0$ the system is at rest, with a bubble radius R_o and a uniform pressure P_o. It has been previously (Flynn, [2] ; Plesset, [3]) shown that the equation for the spherically symmetric motion for a bubble, in which there is no condensation or evaporation of fluid, can be reduced to

$$R \cdot \ddot{R} + (3/2)\dot{R}^2 = \frac{P_\ell - P_o}{\rho} - \frac{1}{\rho}\int_R^\infty (\nabla \cdot \tau)_r \, dr \qquad (1)$$

where $(\nabla \cdot \tau)_r$ denotes the radial component of $\nabla \cdot \tau$, the

divergence of the deviatoric or "extra" stress for the liquid phase, and r = R(t) is the radial position of the bubble-liquid interface, with P_ℓ and P_o denoting the pressure in the liquid at r = R(t) and r = ∞, respectively. The dots denote derivatives with respect to t, and ρ is the liquid density.

Irrespective of the fluid rheology, the radial velocity at any radial position r in the liquid is required by continuity , incompressibility, and the assumed symmetry to be

$$u = \frac{\dot{R}R^2}{r^2} \tag{2}$$

By the usual force balance at the bubble-liquid interface in the cavity, the term P_ℓ in (1) can be expressed in terms of surface tension and the radial stresses as

$$\tau_{rr,g} + P_g = P_\ell + \tau_{rr,\ell} + \frac{2\sigma}{R} \tag{3}$$

where g refers to any gas which may be present in the cavity and ℓ refers to the liquid phase.* Since neither surface elasticity nor viscosity are considered in this analysis, the surface tension force is given by the static surface tension σ.

---

* As in Fogler (4) we adopt here the sign convention of Bird, Stewart, and Lightfoot for the stress tensor: The symbol $\underset{\sim}{\tau}$ (or τ_{ij}) denotes the deviatoric stress tensor reckoned as a compressive stress (7).

For bubbles containing an ideal gas in a uniform state the gas-phase stress at the bubble surface is equal to the pressure alone; hence $\tau_{rr,g} = 0$ (Fogler, 4), and the liquid-phase interfacial pressure is given by

$$P_\ell = P_g - \frac{2\sigma}{R} - \tau_{rr,}\Big|_{r = R} \tag{4}$$

Furthermore, the term $(\underset{\sim}{\nabla} \cdot \underset{\sim}{\tau})_r$ which occurs in (1) can be written in terms of three normal stresses as

$$(\underset{\sim}{\nabla} \cdot \underset{\sim}{\tau})_r = \frac{\partial \tau_{rr}}{\partial r} + \frac{2\tau_{rr}}{r} - \frac{(\tau_{\phi\phi} + \tau_{\theta\theta})}{r} \quad , \tag{5}$$

and, since the sum of these deviatoric stresses is by definition zero, one can express the ϕ and θ stresses in terms of the radial stress as

$$\tau_{\theta\theta} + \tau_{\phi\phi} = - \tau_{rr} \quad , \tag{6}$$

which with (5) yields

$$(\underset{\sim}{\nabla} \cdot \underset{\sim}{\tau})_r = \frac{\partial \tau_{rr}}{\partial r} + 3 \frac{\tau_{rr}}{r} \, . \tag{7}$$

Then, upon substituting (4) and (7) into (1), one obtains the equation

$$R \cdot \ddot{R} + \frac{3}{2} \dot{R}^2 = \frac{P_g - P_o}{\rho} - \frac{2\sigma}{\rho R} - \frac{3}{\rho} \int_R^\infty \frac{\tau_{rr} dr}{r} \tag{8}$$

for the bubble radius R(t). In order to complete the description of motion, we must now relate the liquid-phase radial stress τ_{rr} to the bubble motion.

In the case of a general viscoelastic fluid exhibiting long-range memory effects, the stresses will depend on the past history of strain or rate of strain. For the simple, radially symmetric flow field considered in Eqn. (2), the strain consists merely of an unsteady simple extension. Hence, we expect that for an isotropic material the instantaneous radial stress $\tau_{rr}(t)$ can be expressed as a functional on the past history of the radial strain rate $e_{rr}(t')$, $0 \leqq t' \leqq t$. Here, as in the following analysis, $t = 0$ corresponds to the beginning of the collapse process, where we assume the liquid to be in a completely "relaxed" state of purely hydrostatic stress.

As with other analyses involving viscoelastic fluids, we must now postulate a relation between the strain and the kinematic history of the motion to be considered, and, for this purpose, we adopt the usual material coordinates. Thus, we let r' denote the position at past time t', $0 \leqq t' \leqq t$, of a particle which is at position r at the present time t, so that, with the velocity field given by Eqn. (2), we have

$$(r')^3 = r^3 + R^3(t') - R^3(t) . \tag{9}$$

Now, at any position (r,t) the radial deformation rate is given by

$$e_{rr}(r,t) = \frac{\partial u}{\partial r} = - \frac{2R\dot{R}^2}{r^3} , \tag{10}$$

and, therefore by (9) and (10), the history of the deformation rate is determined by

$$e_{rr}(t',r') = - \frac{2\dot{R}(t')\, R^2(t')}{r^3 + R^3(t') - R^3(t)} \quad . \tag{11}$$

For the present work, we shall employ a rather simple, linear viscoelastic fluid model, in which the normal radial stress is related to the corresponding strain rate by

$$\tau_{rr}(t) = - 2 \int_0^t N(t-t')\, e_{rr}(t')dt' \tag{12}$$

where N(t) is a "memory" function or relaxation modulus. On combining (11) and (12) we have

$$\tau_{rr} = 4 \int_0^t \frac{N(t-t')\, \dot{R}(t')\, R^2(t')\, dt'}{r^3 + R^3(t') - R^3(t)} \, , \tag{13}$$

and the integral in equation (8) becomes

$$\int_R^\infty \frac{\tau_{rr}}{r} dr = 4 \int_o^t \int_R^\infty \frac{N(t-t')\, \dot{R}(t')\, R^2(t')dt'dr}{r(r^3 + R^3(t') - R^3(t))}$$

$$= - 4 \int_o^t \frac{N(t-t')\, \dot{R}(t')\, R^2(t')\ln(R(t')/R(t))dt'}{R^3(t') - R^3(t)} \tag{14}$$

Under these restrictions the complete equation governing the collapse of a cavity is the non-linear integro-differential equation:

$$R \cdot \ddot{R} + \frac{3}{2} \dot{R}^2 = \frac{P_g - P_o}{\rho} - \frac{2\sigma}{R\rho}$$

$$- \frac{12}{\rho} \int_o^t \frac{N(t-t')\, \dot{R}(t')\, R^2(t')\ln(R(t')/R(t))dt'}{R^3(t') - R^3(t)} \tag{15}$$

For the purpose of the analysis to follow we shall adopt an elementary form of the relaxation modulus N, consisting of linearly viscous or "Newtonian" contribution and "Maxwellian" contribution, as follows:

$$N(t) = \mu\, \delta\,(t) + G_o e^{-t/\lambda}\ , \tag{16}$$

where δ denotes the delta function, μ a constant viscosity, λ a relaxation time, and G_o an elastic modulus.

In terms of dimensionless variables, (15) becomes

$$\psi \cdot \ddot{\psi} + \frac{3}{2}\dot{\psi}^2 = \frac{P_g - P_o}{P_o} - \frac{2}{N_{We}\psi} - \frac{4\dot{\psi}}{N_{Re}\psi}$$

$$- \frac{12N_{EL}}{N_{Re}} \int_0^{t^*} \left[\exp\left(-\frac{(t^*-t_1)}{N_{De}}\right)\right] \frac{\dot{\psi}_1 \psi_1^2 \ln(\psi_1/\psi)}{\psi_1^3 - \psi^3}\, dt_1 \tag{17}$$

with $\psi(0) = 1$ and $\dot{\psi}(0) = 0$, where

$$N_{De} = \frac{\lambda}{tc} \text{ (A Deborah number *)},$$

$$N_{EL} = \frac{G_o t_c}{\mu} \text{ (An elastic number)},$$

$$N_{Re} = \frac{\rho R_o^2}{\mu t_c} \text{ (A Reynolds number)},$$

$$N_{We} = \frac{\rho R_o^3}{t_c^{\,2}\sigma} \text{ (A Weber number)},$$

and $\psi = R/R_o$, $t^* = t/t_c$, $\psi_1 = \psi(t_1)$.
Also, $t_c = R_o\sqrt{\frac{\rho}{P_o}}$ is a characteristic ("Rayleigh") collapse time, with P_o being the initial pressure. In this manner one can readily identify the relevant physical parameters characterizing the collapse process.

In view of the number of parameters, even in this relatively simple model, one is practically forced to consider some special limiting cases where certain effects may be assumed

* Reiner (8), Metzner et al. (9)

to predominate. Thus, we focus our attention first and foremost on fluids with long relaxation times, corresponding to $N_{De} \to \infty$. Here, as in the remainder of the analysis, we shall consider only voids, such that $P_g = 0$ in (17).

3. COLLAPSE CRITERIA AT LARGE DEBORAH NUMBERS

3.1 Large Reynolds Number

To begin with, we treat the case where both the Deborah and Reynolds numbers are large. In this limit, $N_{De} \to \infty$, $N_{Re} \to \infty$, the fluid behaves essentially as a purely elastic material, and one obtains in effect a "conservative" dynamical process characterized by an energy integral. Considering first the case where surface tension is negligible, $N_{We} \to \infty$, and reverting to dimensional variables, one has for the equation of motion,

$$R \cdot \ddot{R} + \frac{3}{2} \dot{R}^2 = - \frac{P_o}{\rho} - \frac{G}{\rho} \tag{18}$$

where

$$G = 12\, G_o \int_{R_o}^{R} \frac{R_1^{\,2} \ln (R_1/R)\, dR_1}{R_1^{\,3} - R^3} = \frac{4}{3} G_o \int_{\left(\frac{R_o}{R}\right)^3}^{1} \frac{\ln s}{s - 1}\, ds \,.$$

On multiplying equation (18) by $2R^2 \rho\, dR$ and integrating, we obtain

$$\rho \dot{R}^2 R^3 = \frac{2}{3} P_o (R_o^{\,3} - R^3) - 2 \int_{R_o}^{R} G R^2\, dR \,. \tag{19}$$

One will immediately recognize that this equation is an energy integral, with the left-hand side representing

the total kinetic energy of the liquid, which is expressed as the difference between the stored elastic energy and the work done by the ambient pressure. Rebound short of collapse is therefore possible and will occur at a "rebound" radius R, which is the root of the equation

$$\frac{2}{3} P_o(R_o^3 - R^3) - 2 \int_{R_o}^{R} GR^2 \, dR = 0, \tag{20}$$

corresponding to zero kinetic energy in (19). With the substitution into (18)

$$y = 1/s, \quad z = (R/R_o)^3 ,$$

the integral in (20) can be written as

$$H = 2 \int_{R_o}^{R} GR^2 \, dR = - \frac{8R_o^3 G_o}{9} \int_1^z \int_1^x \frac{\ln y}{(1-y)y} \, dy \, dx, \tag{21}$$

which, after changing the order of integration, can be expressed as the infinite series

$$H = \frac{8R_o^3 G_o}{9\rho} \left((1-z) \sum_{n=1}^{\infty} \frac{(1-z)^n}{n^2} - \frac{z}{2} (\ln 1/z)^2 \right). \tag{22}$$

Thus (20) becomes

$$\frac{P_o}{G_o} = \frac{4}{3} \left| \sum_{n=1}^{\infty} \frac{(1-z)^n}{n^2} - z \, \frac{(\ln (1/z))^2}{2 (1-z)} \right|, \tag{23}$$

which provides the criterion for rebound, giving the rebound radius $R = R^* \equiv R_o z^{1/3}$ as a function of P_o/G_o.

In the "marginal" case, that is, rebound at R = 0, we have

$$\frac{P_o}{G_o} = \frac{4}{3} \sum_{n=1}^{\infty} \frac{1}{n^2} = \frac{2\pi^2}{9} = 2.1932 \ldots \tag{24}$$

from (23), and therefore the condition for collapse without rebound is

$$\frac{P_o}{G_o} > \frac{2\pi^2}{9} , \tag{25}$$

whereas, for rebound short of collapse, $R^* > 0$, we must have

$$\frac{P_o}{G_o} < \frac{2\pi^2}{9} \tag{26}$$

In the latter case, equation (23) provides us with a plot of rebound radius R^*/R_o versus the ratio of initial pressure to elastic modulus, P_o/G_o, which is displayed as the lower curve in Figure 1.

If we consider the case of a finite Weber number, where surface tension is included in the equation of motion, the criterion for collapse is no longer independent of the initial bubble radius. By an analysis similar to that above, one can show that the condition now becomes

$$\frac{P_o + \frac{2\sigma}{R_o}}{G_o} > \frac{2\pi^2}{9} , \tag{27}$$

instead of (25). From this relation one sees that surface tension effects will tend to be important only in small bubbles.

We should like next to determine the importance of viscous retardation on the collapse process, corresponding to a finite Reynolds number in (17). Whenever N_{Re} and N_{De} are finite, the system is no longer conservative and, hence, does not in general admit an energy integral like (19). We are thus forced to treat (17) with numerical techniques, as will be discussed below. First, however, it is worthwhile to note that for infinite Deborah numbers a cavity is characterized by a certain "equilibrium" radius R_{eq}, as determined by the static balance between pressure, surface tension, and elastic forces. One can easily derive an expression for this radius, and, considering the case of negligible surface tension $N_{We} = \infty$, one finds from (20) that the condition of static equilibrium is

$$\frac{P_o}{G_o} = \frac{4}{3} \sum_{n=1}^{\infty} \frac{(1-z)^n}{n^2} + \frac{2}{3} (\ln z)^2 \quad , \tag{28}$$

with $R_{eq} = R_o z^{1/3}$. The upper curve in Figure 1 gives the corresponding plot of R_{eq}/R_o versus P_o/G_o. This curve is of course independent of the Reynolds number, since it refers to a static situation.

For the purposes of obtaining the numerical solutions, a finite-difference technique was employed to treat eqn. (17). In particular, a modified Milne "four-point predictor" formula was used, and the numerical solutions thus obtained were compared for accuracy with existing numerical solutions for bubble collapse in ordinary liquids(Flynn, [2], Fogler [4]). In all cases, the solutions were the same.

3.2 Finite Reynolds Number - Viscous Damping

Figure 2 gives a plot of cavity radius versus time for infinite N_{De} and N_{We}. The cavity is seen to oscillate about an equilibrium radius subject to viscous damping which increases with N_{Re}^{-1}. Under these circumstances, one would expect to observe "critical" damping below some threshold value, N_{Re_c}, say, which we shall refer to here as the "critical" number.

To obtain an estimate of this number, we shall make use of the techniques of linear stability theory. Thus, letting ψ_e represent the dimensionless equilibrium radius and ψ' a small perturbation about this radius, we have

$$\psi = \psi_e + \psi', \quad \psi \ll \psi_e \tag{29}$$

Then substituting Equation (29) into the equation of motion (17) and neglecting terms of the second order in ψ', we obtain the corresponding linearized equation for a collapsing void, which in the case of infinite Weber numbers becomes

$$\psi_e\ddot{\psi}' - 1 + \frac{4\dot{\psi}'}{N_{Re}\psi_e} + 12\left[G(\psi_e) + \left.\frac{\partial G}{\partial \psi}\right|_e \psi'\right] = 0 \tag{30}$$

Since $12\,G(\psi_e) = 1$ by Equation (18), the preceding equation becomes

$$\ddot{\psi}' + \frac{4\dot{\psi}'}{N_{Re}(\psi_e)^2} - \frac{4G_o}{P_o}\left[\frac{\ln(\psi_e)^3}{(\psi_e)^2(1-\psi_e^3)}\right]\psi' = 0, \tag{31}$$

or, simply,

$$\ddot{\psi}' + b\dot{\psi}' + c\psi' = 0, \tag{32}$$

where b and c are constants. In the usual way, it can be seen that the oscillation of the cavity will be critically damped whenever $b^2 = 4c$. With the appropriate values of these constants from Equation (31), this criterion becomes

$$N_{Re}^2 = N_{Re_c}^2 = \frac{P_o}{G_o} \frac{1 - \psi_e^3}{\psi_e^2 \ln(1/\psi_e^3)}, \tag{33}$$

which on rearrangement and making use of the definition in (17) becomes

$$N_{Re_c} N_{EL} = \frac{1 - \psi_e^3}{\psi_e^2 \ln(1/\psi_e^3)} \tag{34}$$

Since the equilibrium radius corresponding to ψ_e is determined by P_o/G_o, we may express the critical Reynolds number as given by Equation (34) in terms of P_o/G_o or, alternatively, in terms of ψ_e. In the latter case one obtains a plot of the critical Reynolds number as a function of the equilibrium radius as shown in Figure 3.

A physical interpretation can be given to the shape of the curve in the following way. Near $\psi_e = 1$ where the elastic force is, relatively speaking, not very large, a greater viscous force is required to damp oscillations as the cavity approaches its equilibrium radius. However, when ψ_e is only slightly less than unity (e.g., $\psi_e = .7$ as in Figure 2), the elastic force, which increases rapidly in a non-linear way, exerts a greater degree of retardation on the motion, and consequently a smaller viscous force is necessary for critical damping.

Owing to the method of derivation, the present expression for the critical Reynolds number, at which cavities move from their initial radius to their equilibrium radius on a critically damped path, can be regarded as strictly valid only for cavities in which ψ_e is close to unity. For cavities with equilibrium radii close to zero, the departure from equilibrium ψ' at the initial state $\psi = 1$ is effectively much greater than the equilibrium ratio ψ_e, and hence the above linearization technique cannot provide an adequate description of the cavity motion from $\psi = 1$ to $\psi = \psi_e$. One notes, however, that for an equilibrium radius ratio of .74, the critical Reynolds number obtained from Figure 3 is 1.25, and from Figure 2 it is observed that for this value of the Reynolds number the cavity does indeed approach equilibrium in a critically damped way. Thus, the linearization is evidently valid in this range.

In general, one might also use Figure 3 to determine the Reynolds number at which critical damping occurs when the equilibrium radius is shifted from some value ψ_e to a second value, $\hat{\psi}_e$, say, by a change in the total pressure. In this case, one would use $\hat{\psi}_e$ in Figure 3 to find N_{Re_c}. This prediction of the damped shift would be valid irrespective of the magnitude of $\hat{\psi}_e$, provided only that $|\psi_e - \hat{\psi}_e| \ll \psi_e$.

For large but finite Deborah numbers, Figure 4 shows the numerically computed motion of the cavity. One observes complete collapse for $P_o/G_o = 100$, with a collapse time very nearly equal to the Rayleigh collapse time for an inviscid, non-elastic liquid. Furthermore, it is evident that for the

case N_{De} = 1000 shown there, the motion on the first few cycles is effectively the same as for $N_{De} = \infty$. Also, it can be observed that the Reynolds number has a significant effect on the initial motion only when it is numerically on the order of magnitude of ten or less. Because of the greater energy dissipation at the lower Reynolds numbers, it appears that the rebound radius decreases with the increasing Reynolds numbers.

4. COLLAPSE AT SMALL DEBORAH NUMBERS

While it is evident that for any finite Deborah number a void must eventually collapse to zero radius, it is nonetheless of interest to investigate how collapse is delayed by the elasticity of the fluid. In particular, we may consider the first cycle of motion, as in Figure 5. For a given P_o/G_o, the rebound radius on the first cycle decreases with decreasing Deborah number as shown there. If the fluid is "inviscid" ($N_{Re} = \infty$) the "critical" Deborah number at which the cavity collapses completely on the first cycle is .51 for a P_o/G_o ratio of 1.43, whereas for a finite Reynolds number the cavity no longer collapses on the first cycle at N_{De} = .51, but instead rebounds as shown in the figure.

For various cases, the numerical solutions were carried out for several cycles of the motion, and some of the results are shown in Figure 6. One observes in this figure that for a Deborah number of 2/3, the cavity collapses in approximately three major cycles. One also notes that the maximum radius reached after each rebound decreases in an almost linear fashion for the first few oscillations when N_{De} = 1. The "modulation" within the later cycles

and the exact radius values in final stages of collapse are uncertain at this time, since numerical integration difficulties were encountered at long times. (The longest time shown represents some thirty to forty minutes of IBM 360 computation time for a single run).

5. CONCLUSIONS

The results of the preceeding analysis indicate that elastic effects may well have a strong influence on cavitation in viscoelastic liquids. We should certainly expect such effects to occur at high Deborah numbers λ/t_c, where the relaxation time λ of the fluid is long compared to the classical Rayleigh collapse time t_c.

In particular, for the Maxwellian liquid considered here, the present analysis shows that in the limit of large Deborah numbers, $\lambda/t_c \to \infty$, a spherical void may either collapse or undergo oscillations about an equilibrium radius, depending on whether the ratio of ambient pressure to the elastic modulus of the fluid exceeds a definite, critical value. The presence of viscosity in the fluid tends to damp the oscillations, and a critical-damping phenomenon occurs for Reynolds numbers below a certain value.

Even for finite and moderate Deborah numbers, $\lambda/t_c = 0(1)$, the ultimate collapse of a void is delayed for several cycles of expansion and contraction.

Although we have not considered in detail the possible effects of gases or vapours in the collapsing cavity, we should not expect such effects to greatly alter the rôle

of liquid elasticity in the collapse process. In fact, one might reasonably anticipate that the combined effects of volume elasticity in the gas and shape elasticity in the liquid would reinforce one another in such a way as to retard or completely suppress the collapse of bubbles. From the results of previous studies of gas-filled bubbles in Newtonian fluids, we might also expect that, in many instances, the effects of liquid elasticity would be important at a much earlier stage in the collapse process. In such cases, the build-up of the liquid-phase momentum, which gives rise to catastrophic collapse, would be greatly suppressed.

In addition to any experimental work which may be suggested by the present study, it would also be of some interest to investigate theoretically the hydrodynamic stability of the spherically-symmetric motion of cavities collapsing in viscoelastic liquids. While one might be tempted to employ a somewhat more refined rheological model for the liquid, this would probably lead to rather difficult analytical and computational problems, without necessarily providing much additional insight on the physics of the collapse phenomenon.

ACKNOWLEDGEMENT

A portion of this work was supported by NIH Grant HE-10549.

e_{rr} radial strain rate, Sec^{-1}

G_0 an elastic modulus, $dyne/cm^2$

G defined by Eqn. 18

H defined by Eqn. 21

N_{De} a Deborah Number

N_{EL} an Elastic Number

N_{Re} a Reynolds Number

N_{We} a Weber Number

N(t) memory function, $gm/cm/sec^2$

n integer

P pressure, $dyne/cm^2$

R radius of the cavity wall, cm.

R_1 cavity radius at some previous time, cm.

R_0 initial cavity radius, cm.

r radial coordinate, cm.

u velocity, cm/sec.

t time, sec.

t_c modified collapse time, sec.

x dummy variable

z $(R/R_0)^3$

Subscripts

c critical

g gas

L liquid

e equilibrium radius

1 refers to a previous time

Greek Symbols

ψ dimemsionless cavity radius R/R_0

τ_{ii} normal stress, $dyne/cm^2$

σ surface tension, dyne/cm

ρ	liquid density, gm/cc
λ	relaxation time, sec.
μ	viscosity, gm/cm/sec.
$\delta(\tau)$	delta function

REFERENCES

1. Rayleigh, Lord, 1917, Phil. Mag. 34, 94.

2. Flynn, H. G., 1964, Physical Acoustics W. P. Mason Ed., Academic Press, New York.

3. Solomon, L. P. and M. S. Plesset, 1967, Report No. 85-38, Division of Engineering and Applied Science, California Institute of Technology.

4. Fogler, H. S., 1969, Chem. Engrg. Sci. 24, 1043 (1969)

5. Yang, W. J. and H. C. Yeh, 1966, AIChE J. 12, 927.

6. Street, J. R., 1968, Trans. Soc. Rheol. 12, 103.

7. Bird, R. B., W. E. Stewart and E. N. Lightfoot, 1960, "Transport Phenomena", John Wiley, New York.

8. Reiner, M., 1964, Physics Today 17, 62.

9. Metzner, A. B., J. L. White and M. M. Denn, 1966, AIChE J. 12, 863.

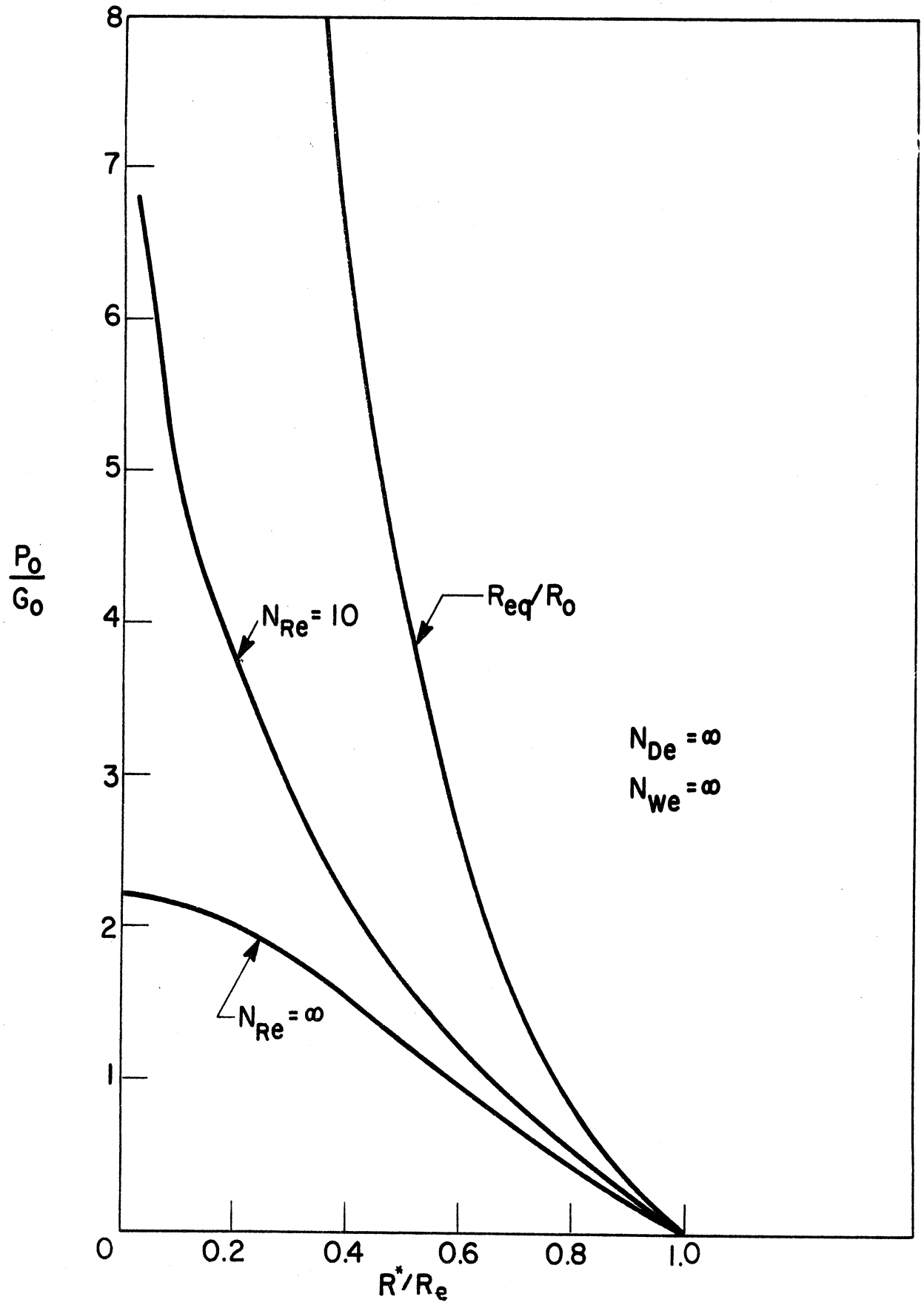

Figure 1. The initial rebound radius and equilibrium radius as a function of P_o/G_o. The middle curve was computed from Eq. (17).

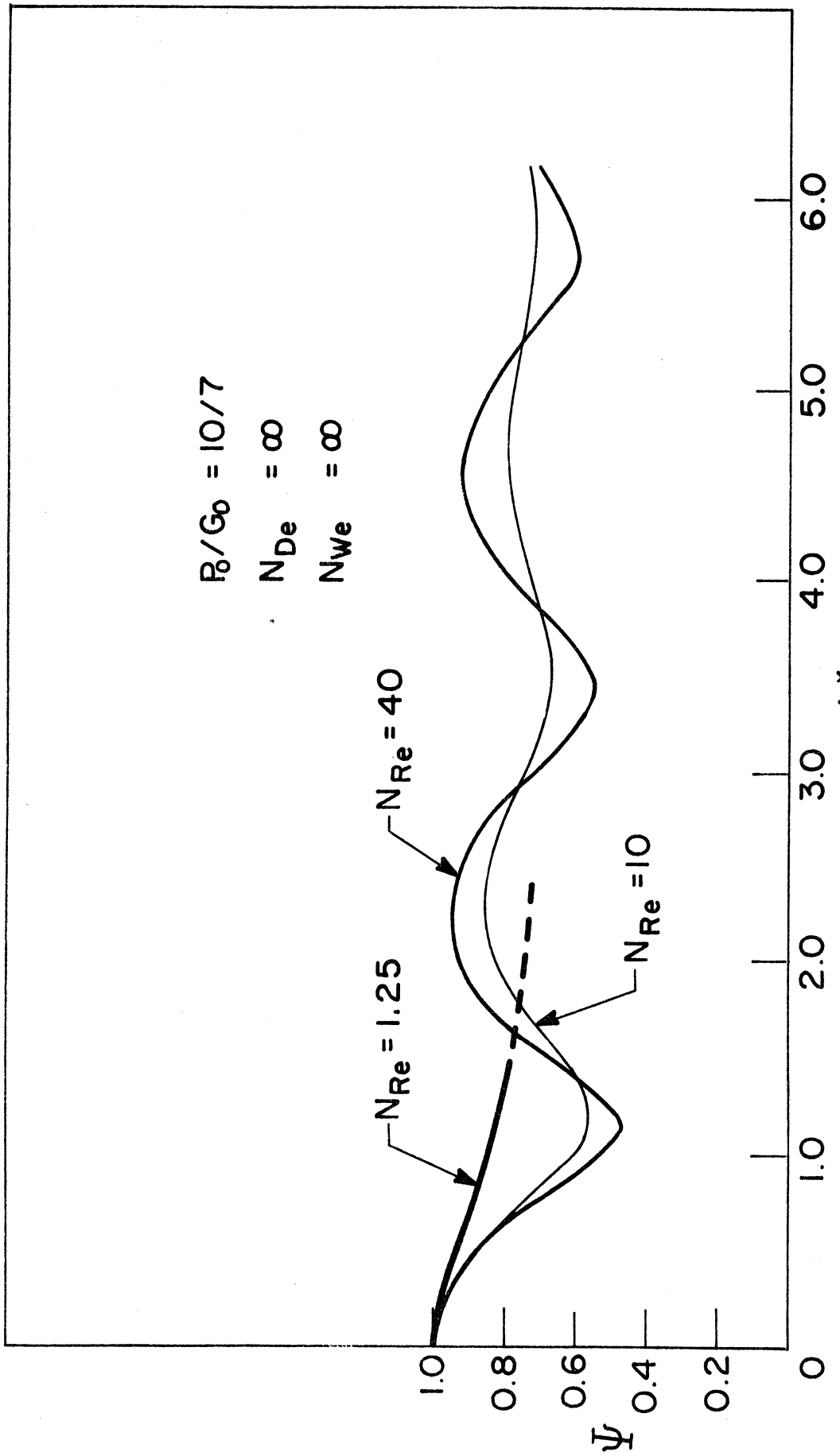

Figure 2. The influence of the Reynolds number on the damping of stably oscillating cavities.

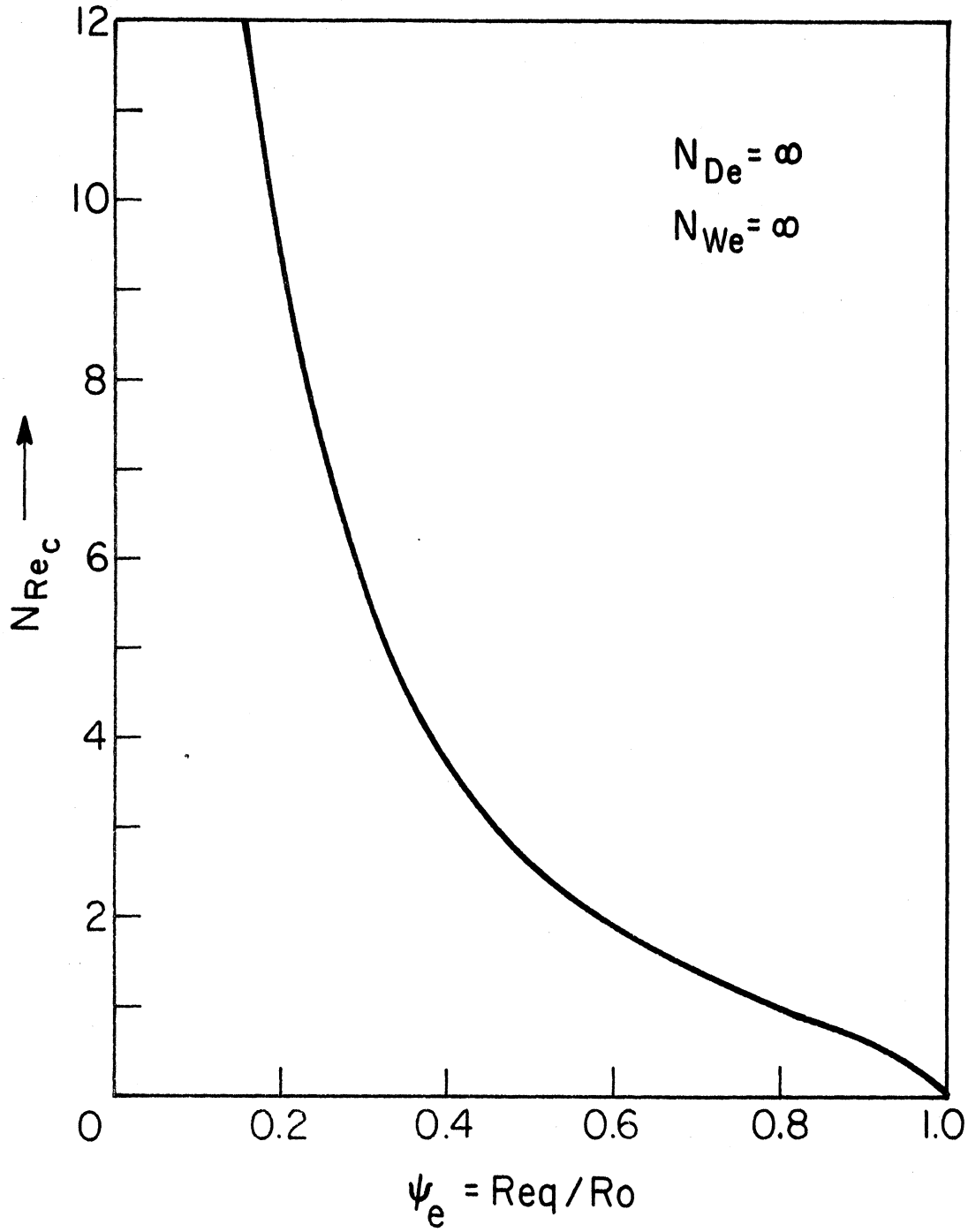

Figure 3. The "critical" Reynolds number as a function of the equilibrium radius.

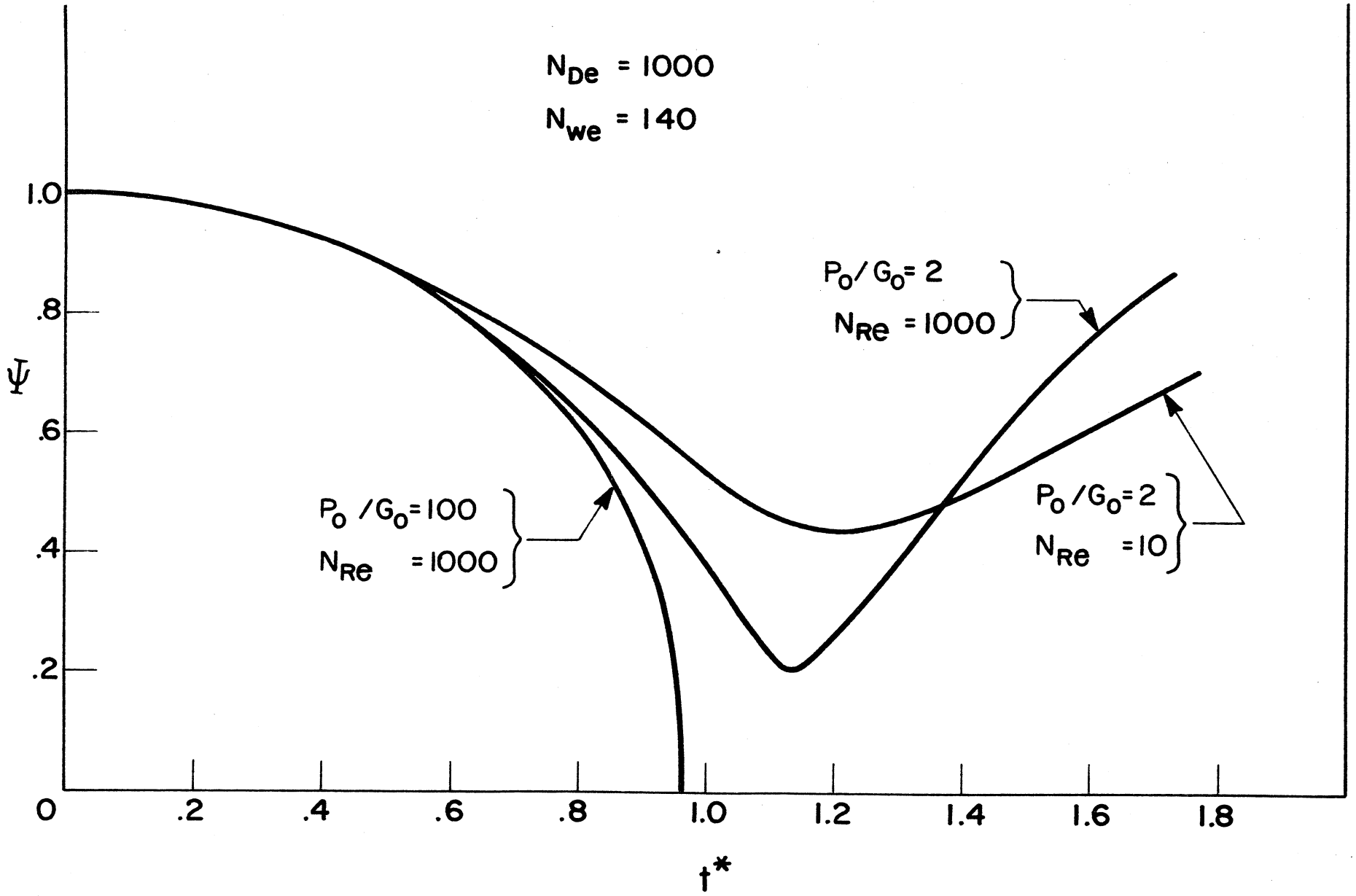

Figure 4. The effect of the Reynolds number and the P_o/G_o ratio on the collapse of a cavity.

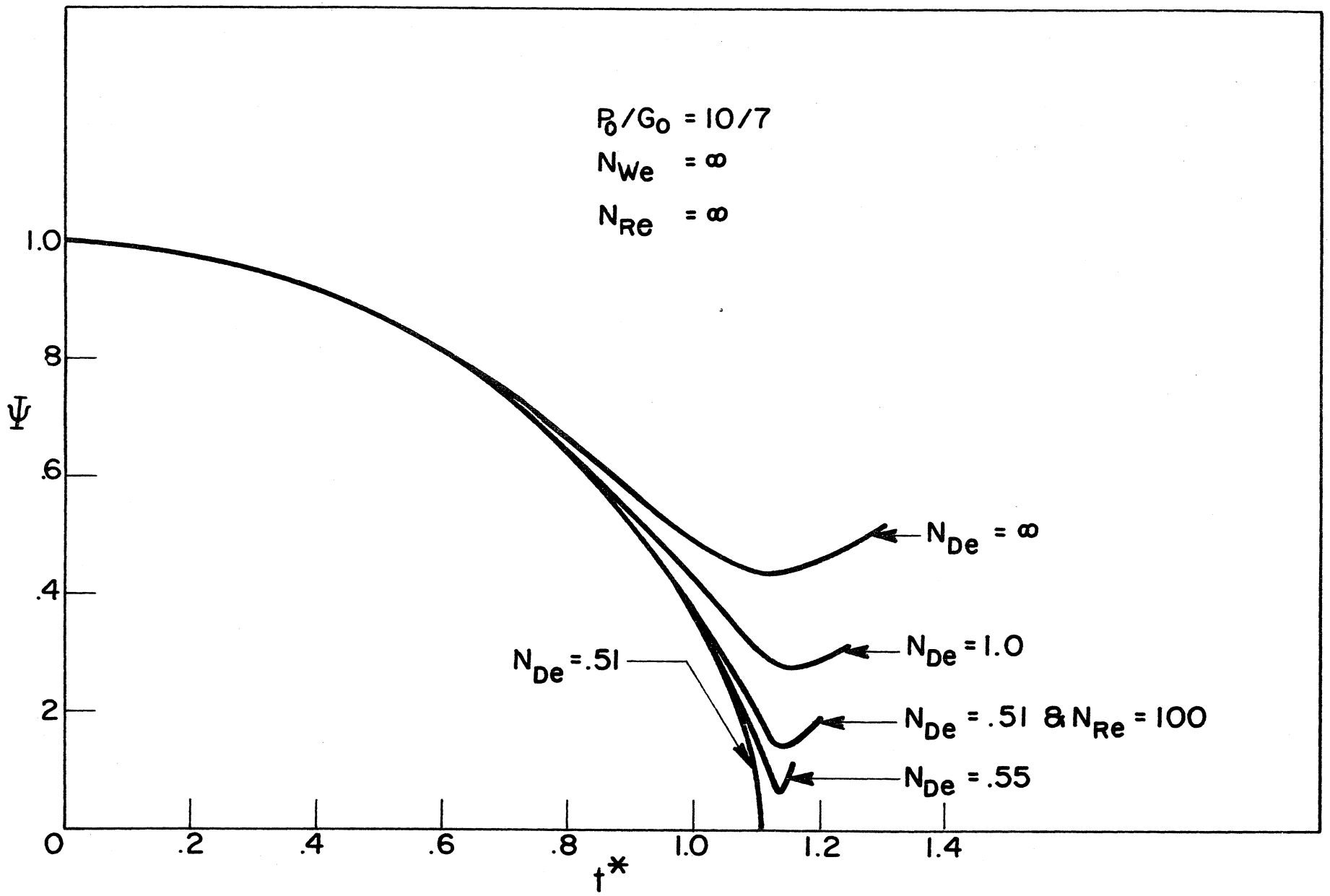

Figure 5. The effect of the Deborah number on the initial motion of a cavity.

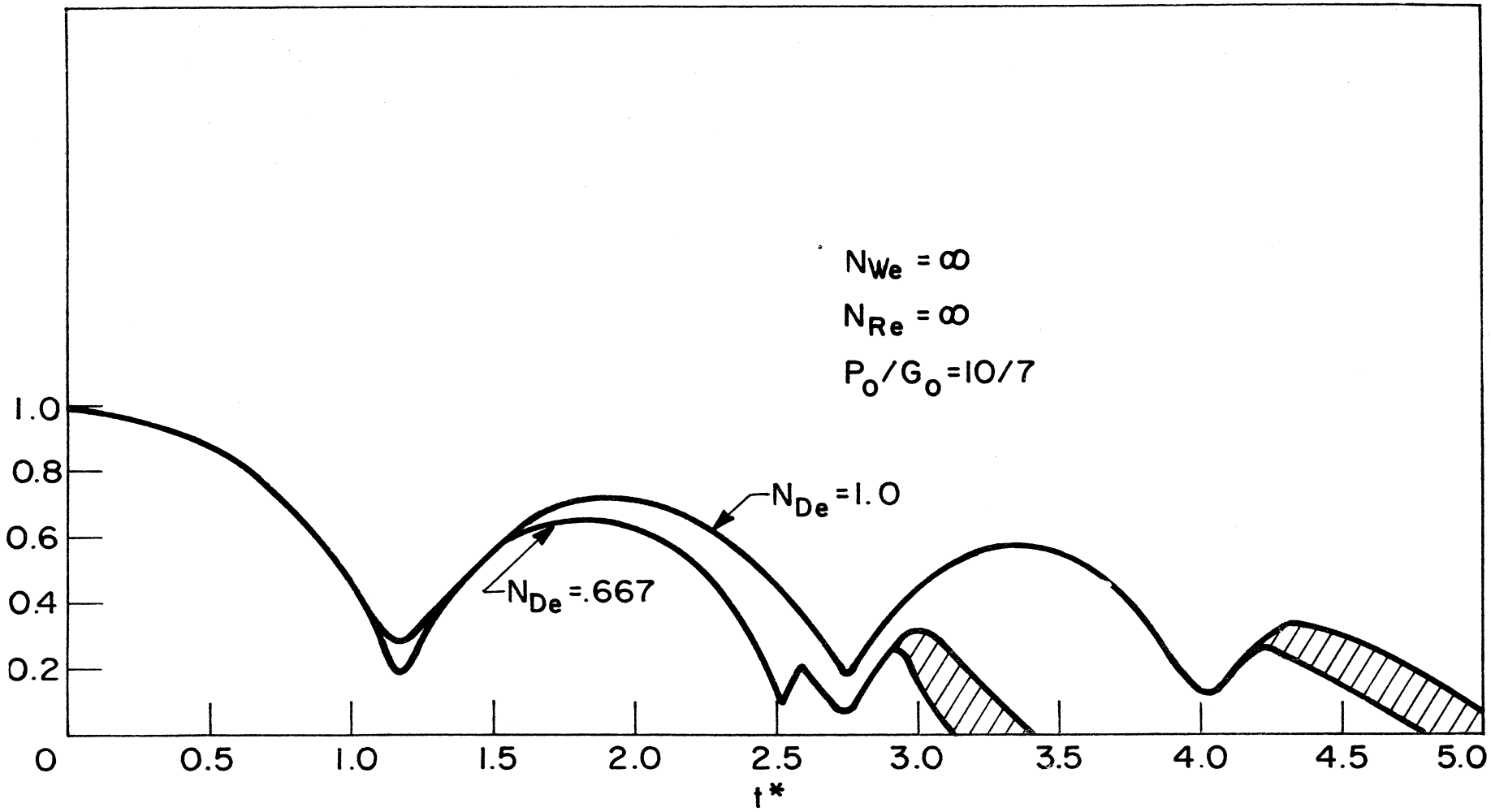

Figure 6. The effect of the Deborah number on the cavity motion.

OSCILLATIONS OF A GAS BUBBLE IN VISCOELASTIC LIQUIDS SUBJECT TO ACOUSTIC AND IMPULSIVE PRESSURE VARIATIONS

H. S. Fogler and J. D. Goddard
Division of Chemical Engineering
The University of Michigan
Ann Arbor, Michigan 48104

ABSTRACT

Oscillations of a Gas Bubble in Viscoelastic Liquids Subject to Acoustic and Impulsive Pressure Variations

H. S. Fogler and J. D. Goddard
Division of Chemical Engineering
The University of Michigan
Ann Arbor, Michigan 48104

An analysis is presented of the forced oscillations of a gas-filled bubble at rest in a large body of a linear viscoelastic fluid. Two types of forcing are considered. In the first, oscillations are induced by a pressure surge on the system. For the three-parameter fluid model employed, numerical computations show that, for a given ratio of the fluid's elastic modulus to the pressure surge, the damping of the bubble motion exhibits a maximum as a function of the fluid relaxation time, at a value of this parameter equal approximately to one-fifth the natural period of oscillation. At very high or very low relaxation times, the damping becomes insignificant. As the second type of forced oscillation, we consider the motion induced by the application of ultrasonic waves to the system. Here, damping is found to depend strongly on the product of impressed frequency and fluid relaxation time.

I. INTRODUCTION

Previous studies on bubble oscillation and collapse in liquids have primarily dealt with bubble motion in Newtonian fluids[1-3]. Although there have been studies carried out on bubble oscillation in "non-Newtonian" liquids[4,5] these analyses have been limited to fluids belonging to the Stokesian- i.e., viscous, group in the rheological classification of materials[6]. It is of both practical and theoretical interest to consider the possible reduction or suppression of acoustical or flow induced cavitation by the presence of viscoelasticity in the ambient liquid.

The motion of bubbles in fluids for which the stress-strain functionality involves memory effects or dependence on the history of the fluid motion has only been treated in a few limiting cases. Fogler and Goddard[7] have presented an analysis of the collapse of spherical voids in viscoelastic fluids under the action of a "step-function" pressure surge. For the case of a particular linear viscoelastic fluid model, it was shown, among other things, that the presence of shear elasticity could significantly retard the collapse of voids in liquids having relaxation times comparable to the classical Rayleigh collapse time. Also, some speculations were made concerning the effects that liquid-phase elasticity might have on the motion of gas-filled bubbles and, in a later work, Tanasawa and Yang[8] have addressed themselves to this problem. However, their analysis[8] relating to bubble collapse induced by a sudden pressure surge,

fails to reveal some important aspects of the collapse phenomenon, which appears to result from the inappropriate mechanical analogue they propose.

Apart from a somewhat more careful analysis of this type of oscillation, the present work will treat another type as well. In this latter type, we shall again consider a gas bubble initially at rest in a large body of viscoelastic liquid; however, the bubble motion will now be induced by the application of acoustic pressure variations to the system.

II. PROBLEM FORMULATION

Consider a spherical gas-filled bubble in a large body of an incompressible liquid which initially, for all time $t<0$, is at rest with a radius R_o, a uniform pressure on the liquid system, $P_\infty = P_{oe}$, and with a gas pressure inside the bubble P_{go}; the latter is determined from the relation

$$P_{go} = P_{oe} + \frac{2\sigma}{R_o} \tag{1}$$

where σ represents the surface tension. We wish to analyze motions which have been induced by two different methods: In the first, the motion is induced by a sudden surge of pressure on the system, i.e.

$$\begin{aligned} &\text{at} \quad t<0, \; P_\infty = P_{oe} \\ &\qquad\quad t>0, \; P_\infty = P_o \end{aligned} \tag{2}$$

Whereas in the second, it results from the application of

acoustic waves to the system. In this case, the pressure at a large distance from the bubble, for any time $t > 0$, will be given by

$$P_\infty = P_{oe} - P_a \sin \omega t, \tag{3}$$

where P_a is the "acoustic pressure" and ω is the angular frequency of oscillation.

In either case, the general equation describing the spherically symmetric motion of a bubble containing a uniform gas phase, in which there is no condensation or evaporation of fluid, has been shown[7] to reduce to

$$R \cdot \ddot{R} + \frac{3}{2}\dot{R}^2 = \frac{P_g - P_\infty}{\rho} - \frac{2\sigma}{\rho R} - \frac{3}{\rho} \int_R^\infty \frac{\tau_{rr} dr}{r} \tag{4}$$

where τ_{rr} is the radial component of deviatoric compressive stress in the liquid phase. As a rheological constitutive equation, relating stress $\tau_{rr}(t)$, at a fluid particle to the past history of the deformation rate $e_{rr}(t')$, $0 \leq t' \leq t$, we adopt the linear viscoelastic model used in our previous work:

$$\tau_{rr}(t) = -2 \int_o^t N(t-t') \, e_{rr}(t') \, dt', \tag{5}$$

with

$$N(t) = \mu \delta(t) + G_o \, e^{-t/\lambda}, \tag{6}$$

where, as constant parameters, μ is a viscosity, G_o an elastic modulus and λ a relaxation time for the fluid, and where $\delta(t)$

denotes the delta function.

We note, incidentally, that this fluid model is identical* with the "linear Oldroyd model"

$$\tau_{rr} + \lambda_1 \frac{D\tau_{rr}}{Dt} = -2\eta_o \left(e_{rr} + \lambda_2 \frac{De_{rr}}{Dt} \right) \qquad (7)$$

of the form employed by Tanawasa and Yang (which follows directly by an elementary integration of (7) together with the transformation of the three parameters:

$$\lambda_1 = \lambda, \quad \eta_o = \mu + \lambda G_o, \quad \lambda_2 = \frac{\lambda\mu}{\eta_o} \quad)$$

From a consideration of the liquid - phase velocity field for spherically symmetric motion, it can be shown[7] that Equations (4), (5), and (6) combine to give the complete dynamical equation for the bubble motion:

$$\psi\cdot\ddot{\psi} + \frac{3}{2}\dot{\psi}^2 = \frac{P_g}{P_o} - \frac{4\dot{\psi}}{Re\psi} - \frac{12EL}{Re} \int_o^{t^*} \left[\exp\left(- \frac{(t^*-t_1)}{De} \right) \right] \frac{\dot{\psi}_1 \psi_1^2 \ln(\psi_1/\psi)}{\psi_1^3 - \psi^3} \, dt_1$$

$$- \frac{2}{We\psi} - \frac{P_\infty}{P_o} \qquad (8)$$

with

$$\psi(0) = 1 \text{ and } \dot{\psi}(0) = 0,$$

---

* In view of this, it is difficult to appreciate the statement in reference 8 that our previous work[7] employed a "two-parameter" model as well as the implication that Equation (7) is more general than Equation (5).

where

$$De = \frac{\lambda}{t_c} \quad \text{(A Deborah number)}, \qquad Re = \frac{\rho R_o^2}{\mu t_c} \quad \text{(A Reynolds number)}$$

$$EL = \frac{G_o t_c}{\mu} \quad \text{(An elastic number)}, \qquad We = \frac{\rho R_o^3}{t_c \sigma} \quad \text{(A Weber number)}, \tag{10}$$

and $\psi = R/R_o$, $t^* = t/t_c$, $\psi_1 = \psi(t_1)$.

Also, $t_c = R_o\sqrt{\frac{\rho}{P_o}}$ is a characteristic ("Rayleigh") collapse time, with P_o being the initial pressure.

To provide an intuitive appreciation of the system, a mechanical analogue representing the effect of the first three terms on the right-hand side of Equation (8) is shown in Figure 1. These terms, representing the effects of gas compressibility, liquid viscosity, and liquid viscoelasticity correspond to the elements, A, B, and C, respectively, in a spring-dashpot assemblage. One can also note that the conceptual model in Figure 1 differs from that proposed in Reference 8, in that the element representing the effect of gas pressure has been placed in parallel here with the other elements rather than in series. The latter arrangement would suggest that the bubble could collapse to zero radius as the fluid viscosity and relaxation time both approach zero, which of course is not possible as long as there is a non-condensable gas inside the bubble.

As discussed in our previous work, the rather large number of parameters, even in this relatively simple fluid model,

requires one practically to consider some special limiting cases. In all the calculations made in the present work, we have adopted fixed values, μ = 1 cp, ρ = 1 gm/cm^3, σ = 72 dynes/cm (corresponding to the equivalent values for water). These values correspond generally to large values of the Reynolds and Weber numbers, defined above, and imply that the "purely viscous" and surface tension effects, as represented by the second and fourth terms on the right hand side of (8), are small. This is not a severe restriction since it turns out that the parameters μ and σ could easily be changed by a factor of ten to a hundred without rendering these effects important.

III. OSCILLATION INDUCED BY A SUDDEN PRESSURE SURGE

With the initial conditions expressed mathematically in Equation (9) and the pressure surge given by Equation (2), Equation (8) was solved numerically for $\psi(t^*)$ by a slightly improved version of our previous integration technique.[7] Figure 2 portrays the resulting oscillations, for various values of the ratio of the elastic modulus to incremental pressure surge, $\Delta P = (P_o - P_{oe})$. The radius-time curves in this figure correspond to fluids in which the relaxation time is much greater than either the "natural" period of oscillation or the Rayleigh collapse time for an ideal fluid. For this condition, i.e. large "Deborah numbers", the amplitude of oscillation decreases with increasing elastic modulus, G_o. In addition, it is noted that as time proceeds, a phase shift develops between the viscoelastic

oscillation, $G_o > 0$, and the "purely viscous" oscillation, for which $G_o = 0$.

The bubble motion is shown in Figure 3 for various Deborah numbers and for the fixed value 0.46 of $G_o/\Delta P$. One observes in this figure that the amplitude of oscillations for a Deborah number of 0.4 is less than that for a Deborah number of either 0.01 or 2.0. In other words, for a given $G_o/\Delta P$, there appears to be a minimum amplitude of oscillation as the Deborah number is increased from zero.

One possible parameter for characterizing the degree of damping for this type of oscillation is the maximum radius reached after initial rebound of the bubble, R_{1max}. There are of course other, more standard, methods of specifying the damping in oscillating systems; however, they usually involve several cycles of bubble collapse and rebound. For the system discussed here, the calculation of numerous cycles would require excessive computational time with perhaps little, if any, additional information gained. Hence, we shall use the first maximum rebound radius as a measure of damping, and this quantity is shown as a function of the Deborah number in Figure 4. On this basis, one concludes, by a rough extrapolation, that damping of the bubble motion at high Reynolds numbers would be small at Deborah numbers greater than 3 or less than .01.

In terms of the conceptual analogue above, one sees that a high Deborah number corresponds effectively to an immobile dashpot in element C, while a very low Deborah number corresponds to a "frictionless" dashpot in C. In the former case, we are

left with two springs in parallel with a "weak" dashpot B (for high Re), while the latter case results in one spring in parallel with the same dashpot, B. In this manner, it is easy to understand the occurrence of a minimum in damping as we vary fluid relaxation time. As a final remark on these calculations we note that, for all the curves in Figure 4, the minimum value of R_{1max} occurs at a value of the Deborah number corresponding roughly to a relaxation time equal to one-fifth the natural period of oscillation. One also observes from this plot that the minimum value of R_{1max} decreases with increasing elastic modulus.

While the elementary fluid model used here would probably not provide an exact description of real viscoelastic liquids, it may not be too implausible to expect that they might exhibit a qualitative relation between damping and relaxation effects, of the type presented here.

IV. OSCILLATIONS INDUCED BY ACOUSTIC WAVES

The application of ultrasonic waves to liquids has been observed experimentally to produce a number of unusual and interesting phenomena: (1) sonoluminescence, (2) erosion, (3) rectified diffusion, and (4) increased chemical reaction rates.[1] These phenomena are usually attributed to acoustically induced cavitation. Hence, it is of interest to consider the effect which fluid viscoelasticity might have on these phenomena, through its specific effect on bubble motion. In the present

model for oscillation, induced by this method, the ambient pressure is given by Equation(3). Again, a numerical solution to the integro-differential equation of (3) is required. As in the previous case, an extended calculation of bubble motion would require prodigious amounts of computation time. Consequently, we have limited our calculation to the first few cycles of oscillation.

A number of radius-time curves for bubble motion in Newtonian fluids have already been presented by Flynn[1]. For purposes of comparison, one of Flynn's curves ($G_o = 0$) was recalculated by our numerical procedure and is presented in Figure 5, along with the radius-time curves of the present work. For large Deborah numbers one observes from this figure that the damping of bubble motion increases systematically with increasing elastic modulus. In Figure 6, the radius-time curves show that the damping of the motion also increases with increasing Deborah number. One can note that elasticity in a fluid may or may not have significant effects on the motion. Indeed, it appears that, for the relatively large amplitude acoustic waves considered here ($P_a/P_o > 1/3$), the bubble oscillation can be significantly damped by "elastic" response at the higher frequencies, where $\lambda\omega$ is order unity or greater. However, the same fluid subjected to ultrasonic waves of much lower frequency, ($\lambda\omega << 1$) may show insignificant elastic damping.

V. SUMMARY

We have considered briefly here the oscillations of gas-filled bubbles in idealized viscoelastic liquids induced by two different

methods: (1) Single Pressure Surge, and (2) Acoustic Pressure Waves. In the first case, it is observed that for a given ratio of the elastic modulus to the amplitude of the pressure surge, the damping effect on the bubble motion exhibits a maximum, as a function of the Deborah number. In the second case, it is observed that the extent of damping depends strongly on the product of applied frequency and relaxation time for the fluid.

In conclusion, we have attempted to show in our calculations the importance of the parametric regime to the occurrence of significant elastic effects. It can be reasonably expected that similar care would have to be exercised in any further calculations, based on other viscoelastic fluid models, or in any experimental explorations of such effects in real fluids.

ACKNOWLEDGMENT

A portion of this work was supported by NIH Grant HE-10549.

REFERENCES

1. H. G. Flynn, in Physical Acoustics Vol. I, Pt. B, W. P. Mason, Ed., Academic Press Inc., New York, 1964, p. 57.

2. M. S. Plesset, in Cavitation in Real Liquids, R. Davies, Ed. Elsevier Publishing Company, Amsterdam, 1964, p. 1.

3. H. S. Fogler, Chem. Engrg. Sci. 24, 1034 (1969).

4. W. J. Yang and H. C. Yeh, A.I.Ch.E.J. 12, 927 (1966).

5. K. S. Chan and W. J. Yang, J.A.S.A. 46, 205 (1968).

6. A. G. Frederickson, "Principle and Applications of Rheology" Prentice Hall, Englewood Cliffs, N.J. (1964).

7. H. S. Fogler and J. D. Goddard, Phys. Fluids 13, 1135 (1970)

8. I. Tanasawa and W. J. Yang, J. Appl. Phys. (to be published).

FIGURE CAPTIONS

Figure 1. Mechanical analogue of the (A) gas pressure, (B) viscous, and (C) viscoelastic effects in a gas-filled, oscillating bubble. The mass represents the effect of fluid inertia.

Figure 2. Dimensionless radius-time curves for various values of the ratio of elastic modulus to the amplitude of the pressure surge.

Figure 3. Effect of the Deborah number (fluid relaxation time/ Rayleigh collapse time) on bubble motion.

Figure 4. Maximum value of the first rebound radius as a function of the Deborah number for various values of $G_o/\Delta P$.

Figure 5. Effect of elastic modulus on bubble motion induced by acoustic pressure waves.

Figure 6. Effect of Deborah number on bubble motion induced by acoustic pressure waves.

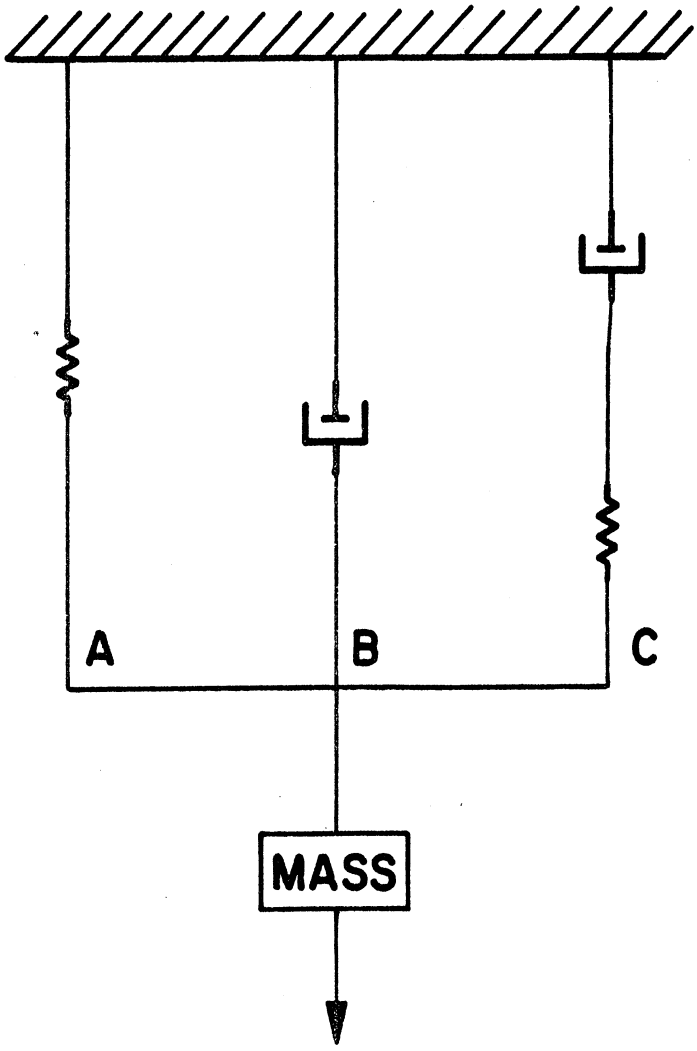

Figure 1

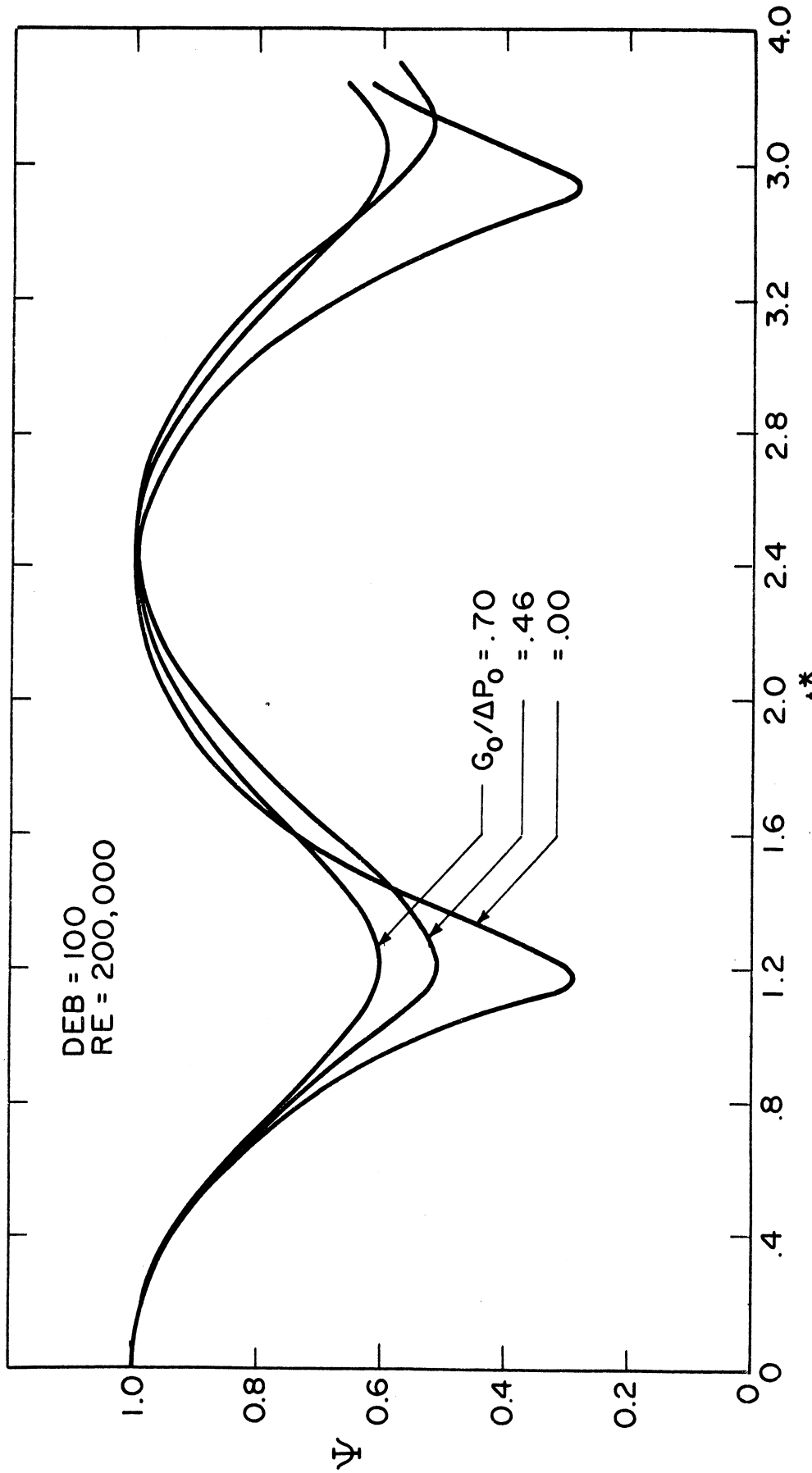
DEB = 100
RE = 200,000
$G_o/\Delta P_o$ = .70
= .46
= .00
Ψ
t*
0
.4
.8
1.2
1.6
2.0
2.4
2.8
3.2
3.0
4.0
0.2
0.4
0.6
0.8
1.0

Figure 2

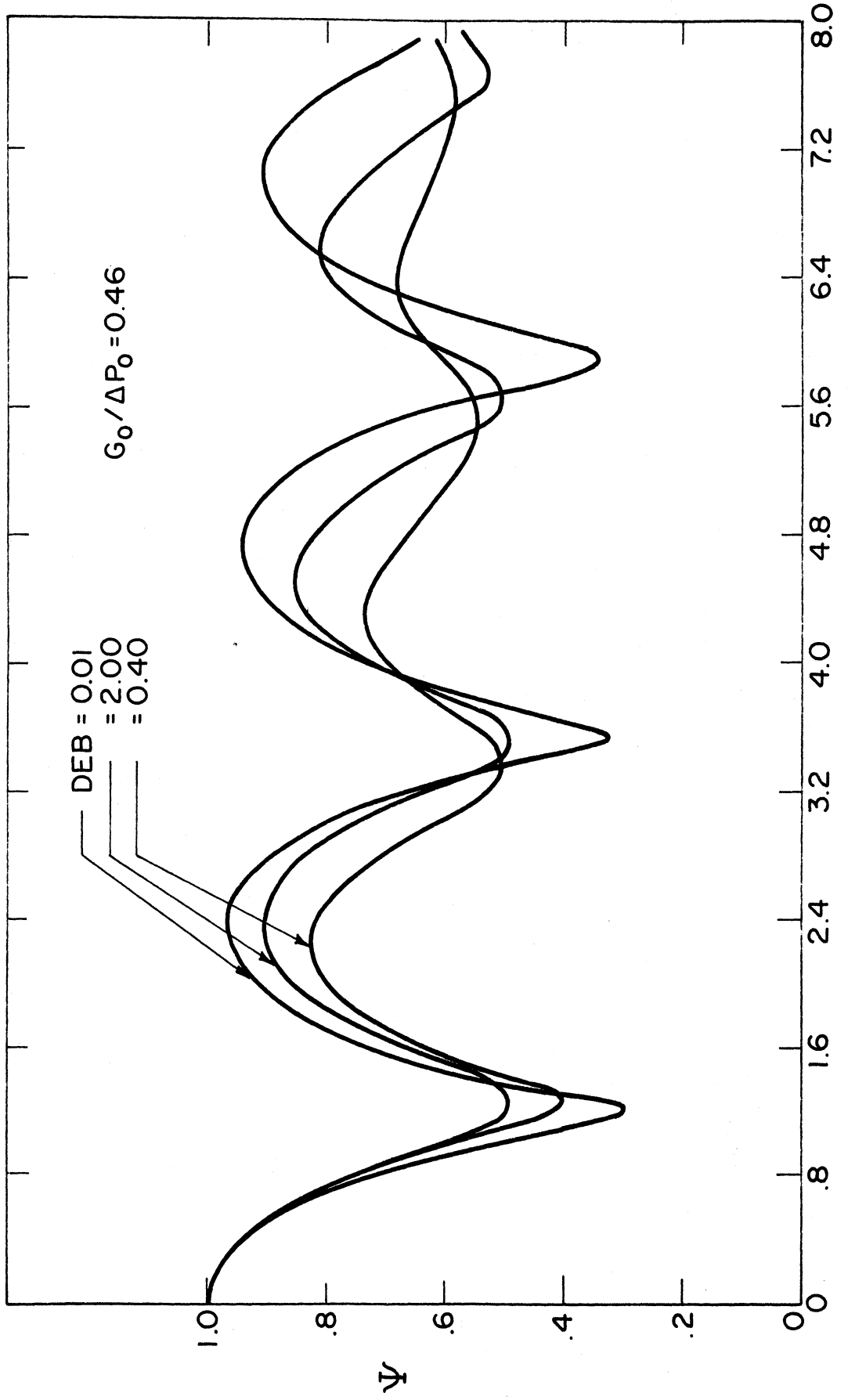
DEB = 0.01
= 2.00
= 0.40
$G_o/\Delta P_o = 0.46$
Ψ
t*
0
.2
.4
.6
.8
1.0
.8
1.6
2.4
3.2
4.0
4.8
5.6
6.4
7.2
8.0

Figure 3

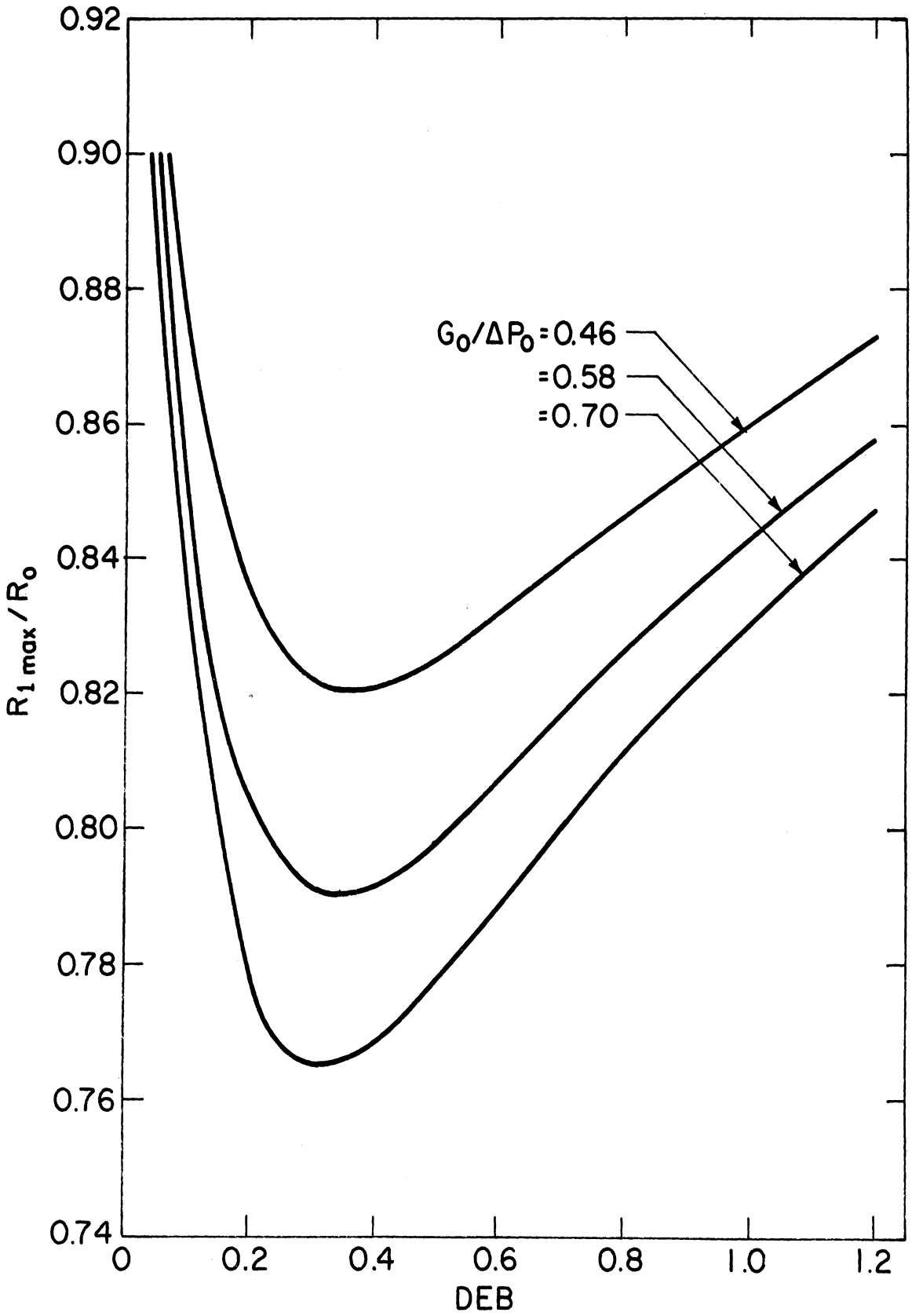
0.92
0.90
0.88
0.86
0.84
0.82
0.80
0.78
0.76
0.74
$R_{1\,max}/R_o$
$G_o/\Delta P_o$ = 0.46
= 0.58
= 0.70
0
0.2
0.4
0.6
0.8
1.0
1.2
DEB

Figure 4

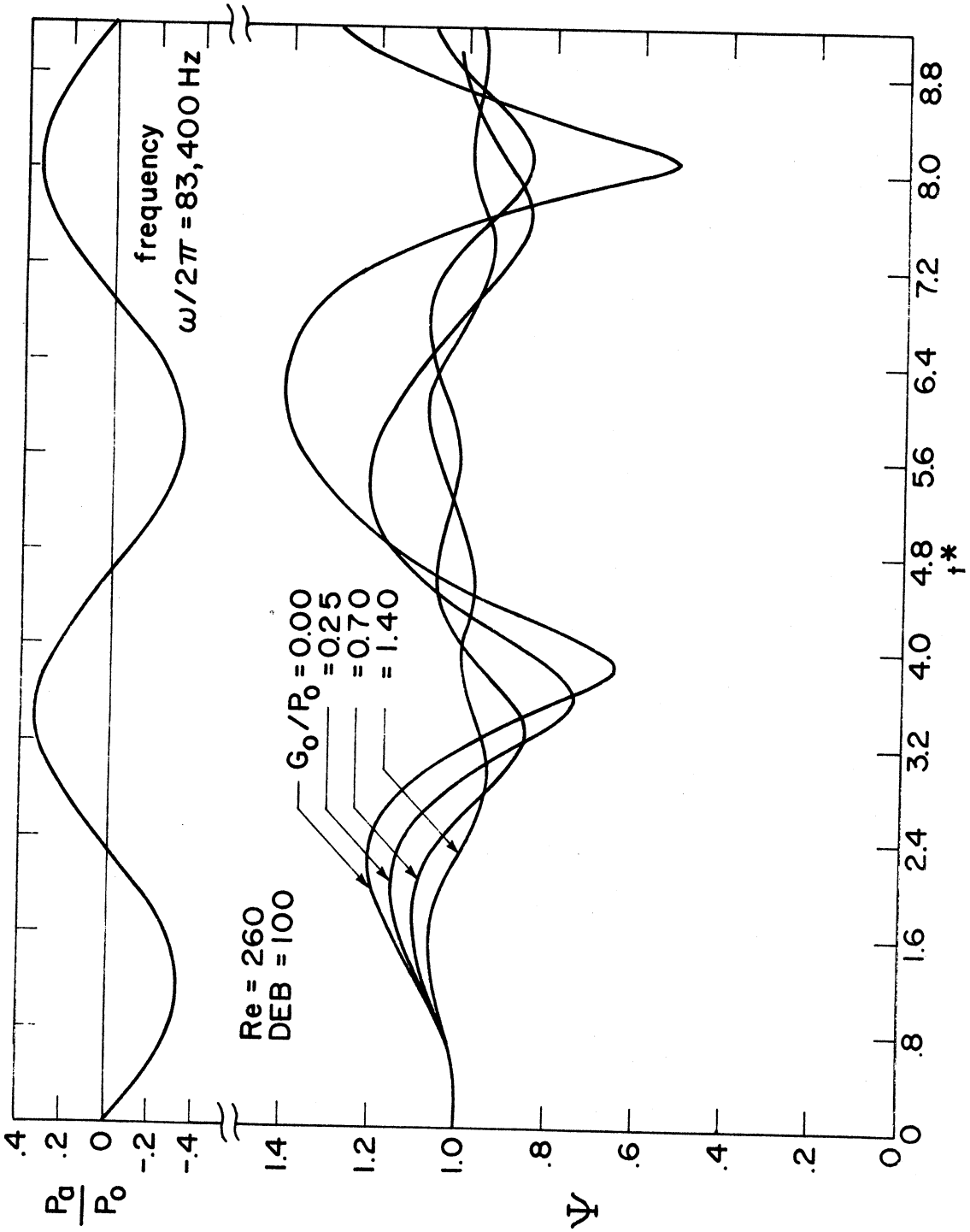
frequency
ω/2π = 83,400 Hz
Re = 260
DEB = 100
G₀/P₀ = 0.00
= 0.25
= 0.70
= 1.40
Pa/P₀
Ψ
t*
.4
.2
0
-.2
-.4
1.4
1.2
1.0
.8
.6
.4
.2
0
.8
1.6
2.4
3.2
4.0
4.8
5.6
6.4
7.2
8.0
8.8

Figure 5

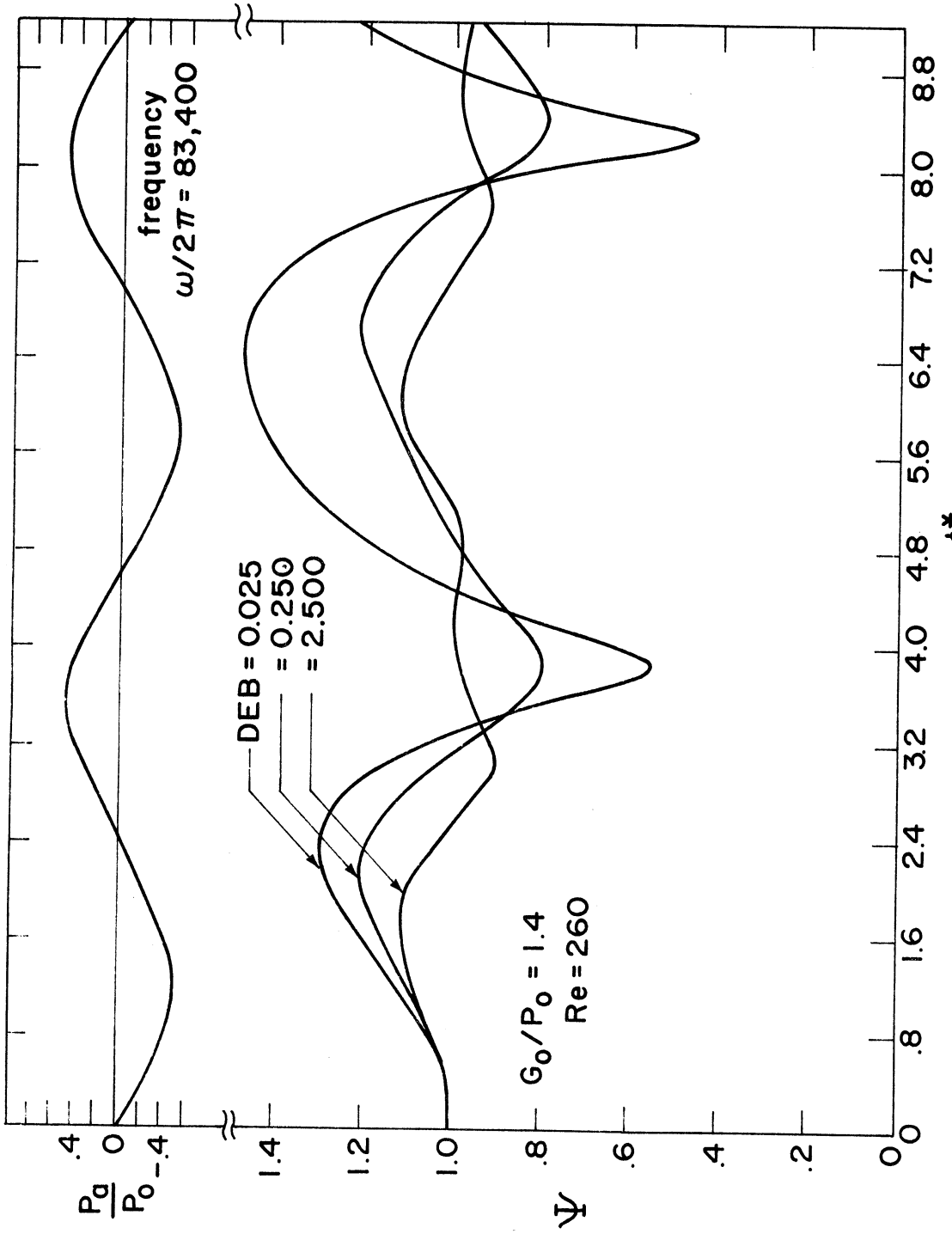

Figure 6

SECTION VI

Personnel

PERSONNEL

H. S. Fogler is an Assistant Professor in the Division of Chemical Engineering. He has worked on the application of ultrasonic waves to chemical reaction and physical transport systems for the past eight years. M. L. Cadwell is in his last year of study for the Ph.D. degree. His thesis topic is ultrasonic gas absorption. V. K. Verma is a fourth year graduate student and K. Lund a third year graduate student in the Division of Chemical Engineering. W. Franklin entered graduate school in September. Mr. Crittenden is currently completing the requirements for a B.S. degree in Chemical Engineering.